METAL(LOID) LIBERATION FROM ALASKAN COAL COMBUSTION PRODUCTS AS A FUNCTION OF TIME IN VARIOUS AQUEOUS MEDIA

BY

Kyle P. Milke, B.S.

A Thesis Submitted in Partial Fulfillment of the Requirements

for the Degree of

Master of Science

in

Chemistry: Environmental

University of Alaska Fairbanks

December 2018

APPROVED:

Dr. Jennifer J. Guerard, Committee Co-Chair
Dr. Sarah M. Hayes, Committee Co-Chair
Dr. Thomas P. Trainor, Committee Member
Dr. Thomas K. Green, Chair
Department of Chemistry & Biochemistry
Dr. Leah Berman, Interim Dean
College of Natural Science and Mathematics
Dr. Michael Castellini,
Dean of the Graduate School

Abstract

Little is known about the fate and potential toxicity of metal(loid)s that could be leached from coal combustion products by a (sub-)Arctic environment. Several potentially toxic elements are enriched in coal combustion products relative to the average crustal abundance including As, Cu, Se, and Sb. The overarching goal of this project is to examine the release of these and other metal(loid)s from early stage coal ash and fly ash from the University of Alaska Fairbanks (UAF) power plant and identify transformations in the presence of aqueous environmental media. Bioaccessibility experiments performed indicate that early stage coal ash and fly ash contain bioaccessible Cr, As, Se, Sb, and Pb. Bioaccessible concentrations of these commonly known toxic metal(loid)s were found to exceed EPA drinking water and freshwater regulations.

Early stage coal ash and fly ash was reacted with 18 MΩ H_2O (control) or simulated rainwater to quantify metal(loid) liberation as a function of time. Leachate pH increased to *ca.* 12.5 within the first hour. Some metal(loid)s quickly reached the maximum measured concentration and consistently decreased in concentration with time such as Ba, Pb, and Zn, while other metal(loid)s increased in concentration with increased reaction time (e.g., Al, V, and Cr). Leaching behavior of between early stage coal ash and fly ash may be controlled by total initial concentrations present in the two ashes, differences in particle size, dissolution and precipitation reactions, and heterogeneity of metal(loid) distribution within the particles.

Early stage coal ash and fly ash were also reacted with reconstituted dissolved organic matter solutions to simulate possible environmental interactions. It was found that for some elements (e.g., Ca), dissolved organic matter did not affect the mobility. Other metal(loid) mobilities were affected by the presence of dissolved organic matter, such as that of Sb, As, Zn, Se, Mo, and V. Some metal(loid) concentrations decreased while others increased with increasing dissolved organic carbon concentrations. Through these experiments, we have obtained a quantitative understanding of the kinetic controls of metal(loid) release from coal ash leaching with various aqueous media. Results from these experiments can help to improve storage and remediation processes for coal combustion products in an effort to protect human and the ecosystem health.

Table of Contents

List of Figures

Page

List of Tables

Page

Acknowledgments

I would like to acknowledge and thank the following people who have supported me, not only during the course of this project, but throughout my M.S. degree.

Firstly, I would like to express my gratitude to my committee members, Dr. Jennifer J. Guerard, Dr. Sarah M. Hayes, and Dr. Thomas P. Trainor for their support, guidance, and insight throughout this research project and my academic career.

I would like to thank undergraduates Kiana Mitchell, David Warner, and Jacob Sterle for assistance with lab work, data collection, and data processing. Also, UAF URSA, BLaST, and INBRE for funding this research project, me, and these undergrads throughout the years.

Lastly, I would like to thank all of my close friends and family. You all have encouraged me and believed in me over the years and helped me to focus on what has been a hugely rewarding and enriching experience.

Chapter 1 Introduction

Coal currently accounts for approximately one-third of electricity generation in the U.S. (ACAA, 2017). As of 2016, 45.3%, 44.4%, 10%, and 0.2% of coal burned in the U.S. is sub-bituminous, bituminous, lignite, and anthracite coal respectively (U.S. EIA, 2017). Anthracite coal is the highest rank of coal that contains the lowest moisture content and highest carbon content (86-97%) relative to other coal types (U.S. EIA, 2011). Lignite coal is the lowest rank of coal that contains the highest moisture content and lowest carbon content (25-35%) (U.S. EIA, 2011). Bituminous coal (45-86% carbon) and sub-bituminous coal (35-45% carbon) are ranked in between anthracite coal and lignite coal (U.S. EIA, 2011).

Sub-bituminous coal is mined from the Usibelli Coal Mine near Healy, Alaska and supplies much of the coal burned in Alaska's interior. Sub-bituminous coal is characterized by high Ca and low S content producing a strongly alkaline ash (Izquierdo and Querol, 2012). Healy coal has mass fractions of 29% moisture, 7% ash, 0.20% sulfur, and an energy content of 17,572.8 kJ kg^{-1} (7,560 btu/lb). Ashed Healy coal is predominantly composed of 44.4% SiO_2, 19.1% CaO, and 18% Al_2O_3, with elements expressed as oxides (Usibelli Coal Mine, 2015).

1.1 Coal combustion products

Coal combustion products (CCPs) remain after coal is combusted and consist of multiple fractions (**Figure 1.1**) (ACAA, 2017). Fly ash is classified for its suitability for reuse. For example, Class C fly ash can be used in cement production, and Class F is less desirable for this application (U.S. DOT, 2016). Class C fly ash (FA) typically contains a sum of SiO_2, Al_2O_3, and Fe_2O_3 that is $\geq$ 50% by mass when expressed as oxides. CaO content, which typically distinguishes the classes of FA, is *ca*. 30% to 40% for sub-bituminous class C FA (Chancey et al., 2010). Fly ash contains thin walled aluminosilicate air filled spheres known as cenospheres (Żyrkowski, 2014).

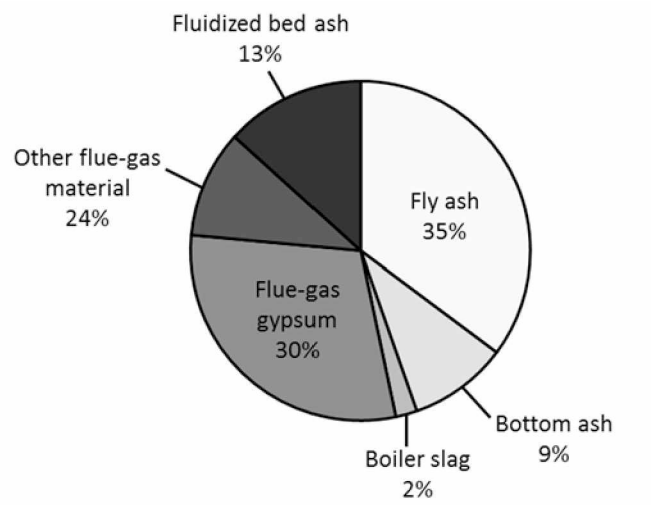

Figure 1.1 Fraction of coal combustion products produced in 2016 in the U.S. Total tonnage: 97,456,920.7 U.S. tons (ACAA, 2017).

From a set of published fly ash characteristics (**Table 1.1)**, class C fly ash ranges from 0.4-3.66 mass % carbon.

Table 1.1 Comparison of fly ash characteristics from literature. LOI = loss on ignition. Mineralogy = Qtz = Quartz (SiO2), Hem = Hematite (α-Fe_2O_3), Mul = Mullite ($3Al_2O_3 \bullet 2SiO_2$), Anh = Anhydrite ($CaSO_4$).

Study	Coal type	Ash type	Surface area (m^2/g)	LOI (%)	pH	CaO (%)	SiO_2 (%)	Al_2O_3 (%)	SO_3 (%)	Fe_2O_3 (%)	MgO (%)	Mineralogy
Akar et al., 2012	Lignite	C	0.175	-----	13.2	38.24	20.79	17.26	12.8	7.17	4.66	Qtz., Hem., Anh.
Koukouzas et al., 2011	Bituminous	C	17.9	15.6	-----	10.79	36.02	21.96	2.89	5.08	1.23	-----
Church et al., 1995	Sub-bituminous	C	-----	0.4	-----	27.9	40.71	16.31	0.44	6.95	-----	-----
Rivera et al., 2015	Bituminous	F	3.95	5.34	9.2	7.4	43.6	48	1.6	12.1	2.02	Qtz., Hem., Anh., Mul.

Coal combustion products such as FA, can be recycled in various industries including asphalt, land reclamation, construction, and agriculture (Izquierdo and Querol, 2012), as well as waste water treatment (Kalyoncu, 2001). In 2016, 97.5 million tons of CCPs were produced in the U.S., of which only *ca*. 56% were recycled (ACAA, 2017). Excess CCPs are stored in stockpiles and landfills where they may be transformed or dispersed in the surficial environment by: mass transport of particulates via surface water, precipitation of secondary phases, release into pore waters, or sorption/co-precipitation (U.S. EIA, 2011).

1.2 Environmental impacts of accidental coal combustion product releases

Stockpiles and leaching ponds that are used for the storage of CCPs have the potential to release these materials into the environment. Two such instances where this has occurred on a large scale are the Kingston CCP spill in Tennessee in 2008 (EPA, 2016) and the Duke Energy CCP spill in North Carolina in 2014 (EPA, 2017), both of which have since been classified as superfund sites. The Kingston power plant had a structure malfunction that led to *ca*. 1,306,000 tons of CCPs being released from a leaching pond into the Emory River (Ruhl et al., 2010). One day after the spill, levels of several metal(loid)s were found to be above Tennessee Water Quality Criteria for surface waters in some samples, including: Sb, Be, Cd, Cr, Pb, and As (EPA, 2009). Elevated concentrations of metal(loid)s in surface waters were found downstream but were typically below Environmental Protection Agency (EPA) maximum contaminant levels (MCLs) with the exception of As in areas of restricted water exchange (Ruhl et al., 2009). Transported CCPs that eventually dried caused a need for dust control mechanisms and air quality measurements in the area. Total cleanup costs were *ca*. $1,178,000,000 (EPA, 2014).

In 2014, the Duke Energy Steam Station had a malfunction that resulted in 39,000 tons of CCPs being spilled into the Dan River (EPA, 2017). Elevated concentrations of total metal(loid)s in surface waters *ca*. two weeks after the spill were found downstream. However, these were also typically below EPA ecological risk screening levels (ERSLs) with the exception of Cu and Pb, which were attributed to the non-dissolved fraction, since dissolved metal(loid) concentrations

did not exceed the ERSL values (EPA, 2014). Damage costs for the Duke Energy spill were estimated to be *ca*. $295,000,000 (Dennis, 2015).

Rivera et al. (2015) has shown that although the majority of metals released from the coal ash during the Kingston, TN spill were below EPA MCLs, a significant amount of metals were still released into adjoining river systems. It was found that roughly 550, 88, 48, 44, 38, 28, 21, 5, and 4 metric tons of Sr, Mn, Cu, Zn, As, Cr, Pb, U, and Se, respectively, were associated with an estimated 380,000 m^3 of residual ash left in the river systems (Rivera et al., 2015). These residual metals have the potential to cause long-term effects.

Extreme spill events such as these show that CCPs may come into contact with surface waters and cause elevated levels of metal(loid)s in aquatic systems, which may have the potential to affect both humans and aquatic life. Further, transported particles deposited in stream channels may continue to release toxic metal(oid)s for decades to come. These spills highlight the importance for better understanding of CCP metal(loid) interactions with the environment.

Thus, there is evidence that several metal(loid)s do get transported when the CCPs are spilled in the environment (Ruhl et al., 2010) and therefore they potentially come into contact with environmental phases. However, since the (sub-)Arctic is an entirely different ecosystem from those previous spills which occurred in the Eastern U.S., and CCPs are heavily compositionally varied based on their source and combustion process, the specific interactions with the environment for CCPs in Alaska are unknown.

1.3 Toxicity characteristic leaching procedure and synthetic precipitation leaching procedure

The EPA regulates using toxicity characteristic leaching procedures (TCLPs) and synthetic precipitation leaching procedures (SPLPs) to determine the mobility of organic and inorganic analytes present in liquid, solid, and multiphase wastes (EPA, 1992; EPA, 1994). Toxicity characteristic leaching procedures are commonly performed on FA to determine if appropriate regulatory levels are exceeded (Kim and Hesbach, 2009). The SPLP assesses the weathering of a

contaminant by an acidic rain (NJ DEP, 2013). Both protocols utilize a batch equilibrium leaching in which contaminants are partitioned between solids and an extraction solution. The results of the SPLP leaching are considered to be an estimate of field leachate concentrations while the TCLP leaching is designed to simulate the solvent properties of municipal waste leachates in a landfill, both of which are then compared against the appropriate criteria (NJ DEP, 2013; Kimmell et al., 2001). However, these experiments are not necessarily representative of long-term weathering processes in the environment.

1.4 Previous coal combustion product leaching studies

In addition to TCLP and SPLP methods, previous studies have examined the leachability of Class F and Class C FA metal(loid)s using jar, long-term batch, serial batch, and column leaching methods (Akar et al., 2012; Neupane and Donahoe, 2013; Koukouzas et al., 2011; Church et al., 1995; Khodadoust et al., 2011; Georgakopoulos et al., 2002). Typical leachates used include distilled water and simulated rainwaters. The majority of leaching studies involving FA measure relative cumulative mass leached and metal(loid) release as a function of time (Neupane and Donahoe, 2013).

To our knowledge, very limited literature is available on the leaching characteristics of Alaskan CCPs. Church et al. (1995) used FA that came from the Usibelli Coal Mine near Healy, Alaska. They investigated the effects of compaction, freezing and thawing, curing, and cement stabilization on metal(loid) leaching in order to identify toxic elements that may be released from the FA under (sub-)Arctic field conditions, and identify column leaching trends of the major and minor elements that make up the FA. The Healy coal FA samples consistently passed the TCLP test, with dissolved metal(loid) concentrations typically below 10% of the MCLs.

However, there are also some limited studies on sub-bitumunous CCP leaching from other locations. Neupane and Donahoe (2013) evaluated the leachability of alkaline FA samples derived from sub-bituminous Powder River Basin coal and several acidic FA samples from

Eastern Bituminous coals using long-term batch leaching experiments. They also report some crystalline phases along with a small amount of unburned carbon.

While these studies do provide an analysis of the physical/mineralogical and leaching properties of FA, they cannot accurately represent all types of FA. The composition of FA is not only dependent on the coal source but also combustion, pollution control, and handling processes (Neupane and Donahoe, 2013). These studies also do not evaluate CCP metal(loid)-organic matter interactions that would inevitably be encountered in surficial aquatic environments.

1.5 Metal(loid)-organic matter interactions

To our knowledge, CCP metal(loid)-organic interactions have been relatively unexplored. It has been shown that CCP-metal(loid)s leach into the environment, therefore they potentially come into contact with dissolved organic matter (DOM). Dissolved organic matter is a heterogenous mixture of organic compounds ubiquitous in surface waters and present in rather high concentration in interior Alaska compared to more temperate ecosystems (Guerard et al., 2009; Stevenson, 1982; Dittmar and Stubbins, 2014). It is defined as the organic matter fraction in solution that passes through a 0.45 μm filter (Stevenson, 1982). Dissolved organic matter can be derived from microbial activity, aquatic material, and the decomposition of organic materials, which can include soil organic matter and plant residues (Schwarzenbach et al., 2017; Wright and Reddy, 2009). The composition of DOM can be affected by both terrestrial and microbial inputs; therefore, it has been characterized along a spectrum of terrestrial to microbial derived DOM (Guerard et al., 2009; Stevenson, 1982; Dittmar and Stubbings, 2014; Schwarzenbach et al., 2017). Dissolved organic matter fractions can be operationally defined into three general categories: humic acids (higher molecular weight, water insoluble at pH < 1), fulvic acids (lower molecular weight, water soluble at most pHs), and humin (insoluble at all pHs) (Schwarzenbach et al., 2017). DOM typically contains humic and fulvic acids among other organics (Schwarzenbach et al., 2017).

DOM has the ability to control metal(loid) speciation, metal(loid) solubility, alter surface charges of particles, sorb to mineral surfaces, and interfere with mineral dissolution/ precipitation reactions (Aiken et al., 2011). The various functional groups present in a DOM molecule define its reactivity with metal(loid)s in natural waters (Aiken et al., 2011). Some common functional groups present in DOM are ketones, aldehydes, phenols, amines, thiols, quinones, and carboxylic acids (**Figure 1.2**) (Dittmar and Stubbins, 2014). These groups are mostly negatively charged at high pH, and thus expected to interact specifically with other charged ions in solution. Since CCP metal(loid)-DOM interactions in the (sub-)Arctic have been relatively unexplored, the effects of this type of interaction on the environment are unknown (Mutschlecner et al., 2018).

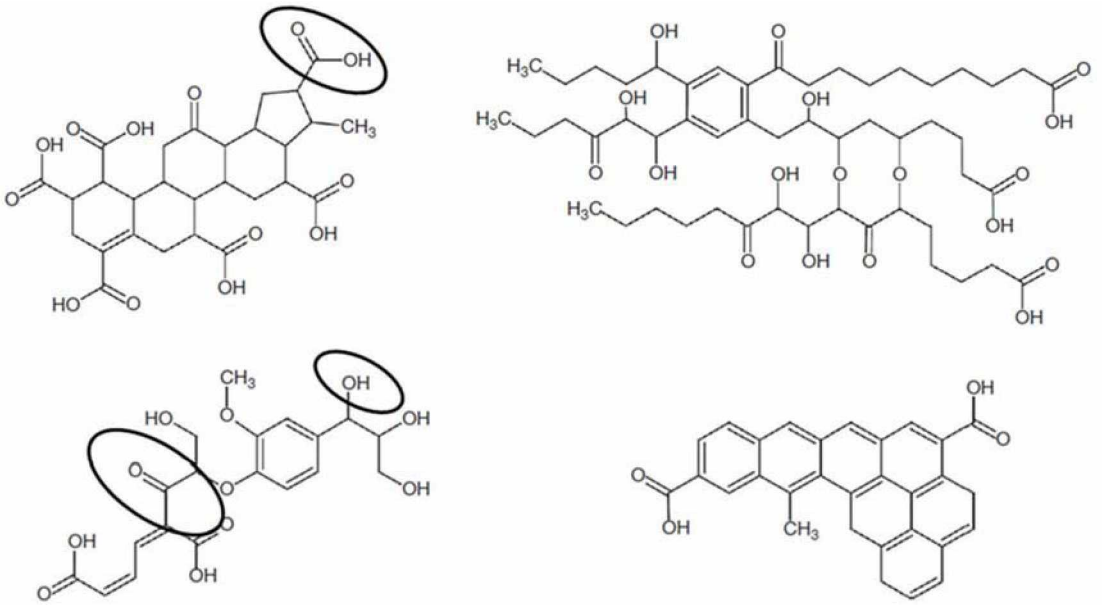

Figure 1.2 Hypothetical molecular structures proposed to be present in DOM. Dissolved organic matter can consist of millions of different compounds (Dittmar and Stubbins, 2014). Some reactive functional groups such as alcohols, carboxylic acids, and carbonyls have been circled (Dittmar and Stubbins, 2014).

Having knowledge of the way certain metal(loid)s react with DOM allow us to make predictions of how the CCP metal(loid)s might react with the DOM. CCP metal(loid) interactions with DOM are complicated by the fact that the metal(loid)s are not already freely dissolved, and so it is predicted that their interactions are coupled to their dissolution and precipitation (Schwarzenbach et al., 2017).

There have been many studies of metal(loid) mobility and speciation in the presence of DOM (e.g. Kalbitz and Wenrich, 1998; Temminghoff et al., 1997; Xiao et al., 2013; Waite and Morel, 1984; Haque et al., 2007). Metal(loid)s that are commonly elevated in CCPs and have been studied include: Al, As, Ca, Cr, Cu, Fe, Mn, Mo, Pb, Sb, Se, V, and Zn. Many studies have examined the sorption of some of these metal(loid)s to DOM over a range of pH (Temminghoff et al., 1997; Waite and Morel, 1984). Previous metal(loid)-DOM binding studies can provide insight into the behavior of CCP metal(loid)-DOM interaction

Several elements seem to mobilize in a DOM-dependent manner. Dissolved organic matter influence on the mobilization of Cr, Hg, Cu, and As in polluted wetland soils was studied by Kalbitz and Wenrich (1998). It was found that Cr, Hg, Cu, and As mobility was positively correlated with DOM. Complexation with DOM and solubility control of elements in a sandy soil was studied by Weng et al. (2002). It was found that DOM-complexed species are generally more significant for Cu and Pb than for Cd, Zn, and Ni. Copper mobility in a Cu-contaminated sandy soil as affected by pH and solid and DOM was studied by Temminghoff et al. (1997). It was found that at lower pH only 30% of Cu in solution was Cu bound to DOM but at higher pH 99% of Cu in solution was Cu bound to DOM. Selenium is a commonly known toxic element and micronutrient and little is known about its interactions in (sub-)Arctic environments (Pokrovsky et al., 2018). However, a recent study of Se in permafrost regions provided some insight into interactions between it and DOM (Pokrovsky et al., 2018). Selenium exhibited a linear relationship with dissolved organic carbon (DOC) concentration during two of the seasons. This suggests that increasing DOC promotes the leaching Se. It is suggested that the mobilization in watersheds occurs as organic and organo-Fe, Al colloids, most likely with reduced and elemental forms of Se (Pokrovsky et al., 2018). This can provide some insight into the CCP Se-DOM leaching results.

There are also several elements whose mobilization is not DOM-dependent. It has been observed that Cd and Zn mobility do not depend on DOM concentration (Kalbitz and Wenrich,

1998). However, their mobilization is dependent on other factors such as soil pH and mobile element content in the soil (Kalbitz and Wenrich, 1998). Weng et al. (2002) also observed that the DOM complexation with Cd and Zn is not very significant, in addition to Ni.

Iron is another metal commonly studied when looking at metal(loid)-DOM binding because of its abundance and its role in photochemical and redox shuttling processes (Poulin et al., 2014; Davidson et al., 2003; Strathmann, 2011). Humic substances contain a range of ligand functional groups that have free electron pairs that can be donated to Fe and other metal(loid)s to form coordination complexes (Yamashita and Jaffe, 2008). Important Fe-complexing groups are oxygen-, nitrogen-, and sulfur-containing functional groups (Yamashita and Jaffe, 2008). Carboxylates and phenolates are the most abundant of these (Yamashita and Jaffe, 2008). Organic molecules containing multiple Lewis base donor atoms in their structure can form multidentate complexes with Fe ions (Yamashita and Jaffe, 2008). The nature and extent of Fe ion complexation is dependent upon solution conditions, most notably pH and ligand-metal(loid) ratio (Yamashita and Jaffe, 2008).

Dissolved organic matter's ability to interact with metal(loid)s is dependent upon the functional groups and ligands that comprise it, which are unique in (sub-)Arctic environments compared those of other regions of the world (Mutschlecner et al., 2018). These groups have the potential to alter the apparent solubility of CCP metal(loid)s or interfere with DOM's basic functions such as redox shuttling in the water column (Davidson et al., 2003). Studying CCP metal(loid)-DOM interactions in Alaska can help to fill a gap in the current knowledge of CCP metal(loid)-DOM interactions in other systems of the world.

1.6 This study

Little is known about the fate and toxicity risk of metal(loid)s from CCPs in the (sub-)Arctic environment. The (sub-)Arctic environment is a particular region of interest due to its high carbon content and unique DOM composition all of which affect the interactions metal(loid)s will undergo in the environment (Mutschlecner et al., 2018). Coal combustion product

interactions with surficial aqueous environments will also depend on the physical and chemical properties of the CCPs (e.g., surface area, particle size, porosity, carbon content, etc.). Alaskan coal and combustion methods produce unique CCP chemistry, which warrants additional study (Izquierdo and Querol, 2012).

This study focuses on the potential for environmental release of metal(loid)s of potential concern from CCPs from the University of Alaska Fairbanks (UAF) power plant. The physical and chemical properties of sampled CCPs were extensively characterized in conjunction with long term (up to 3 month) batch leaching experiments under a variety of conditions. The leaching experiments reacted FA and early stage coal ash (ESCA) with >18 MΩ H_2O, simulated rainwater, and DOM solutions. This work provides a foundation and key insight that can be used to guide the management and mitigation of future environmental impacts of CCPs in high-latitude environments.

Chapter 2 Site Description

The Usibelli Coal Mine near Healy, AK is the only operating coal mine in Alaska and supplies 6 power plants in interior Alaska, including the UAF Heat and Power Plant in Fairbanks. It has produced sub-bituminous coal since 1943, with current production at 1.2-2 million tons of coal per year (Usibelli Coal Mine, 2015).

2.1 Travelling Grate Combustion

The UAF Atkinson Heat and Power Plant was built in 1962 and currently uses a stoker boiler system, sometimes also referred to as travelling grate combustion (**Figure 2.1**), which comprises the majority of coal-fired watertube boilers for commercial applications (EPA, 1998; Ward, 2018). The UAF powerplant was chosen for this study due to ease-of-access to CCP samples and its (sub-)Arctic location.

Coal-fired boiler classifications are based on the type, fuel, and method of construction. Boiler types, used to produce steam that provides both heat and electricity at UAF, are identified by their heat transfer method, which can be watertube, firetube, or cast iron. Watertube is the most common type of heat transfer method used in boiler systems (EPA, 1998). Types of coal-fired boilers that have been used are pulverized coal, cyclone, stoker, fluidized bed, and handfed (EPA, 1998).

When coal arrives at the power plant, it is crushed into 2 in. diameter chunks, which are then fed through a hopper. The feeder then distributes the coal chunks along the boiler grate. As the coal burns, it falls through the grate, while the ash that remains on the grate goes down to the ash pit where bottom ash is collected. The flue gases that are produced travel out of the furnace chamber and first encounter the cinder reinjection hopper. Many power plants have removed this mechanism because of mechanical problems (Ward, 2018). Heavy particles of ash and coal embers fall out of the flue gas stream and into the cinder reinjection hopper. The cinder ash is then reintroduced into the furnace via a set of lances and over-fire air. Over-fire air is part of an overall system to reduce NO_2emissions (Ward, 2018). Over-fire air provides

turbulence for the mixing of volatiles and air for combustion (Ward, 2018). Ash remaining in the flue gases after passing through the cinder reinjection hoppers encounters the cyclone separators. Any ash that remains entrained in the flue gas is then carried to the baghouse. The baghouse is the final stage of particulate capture and filters out the finest ash known as FA (Ward, 2018).

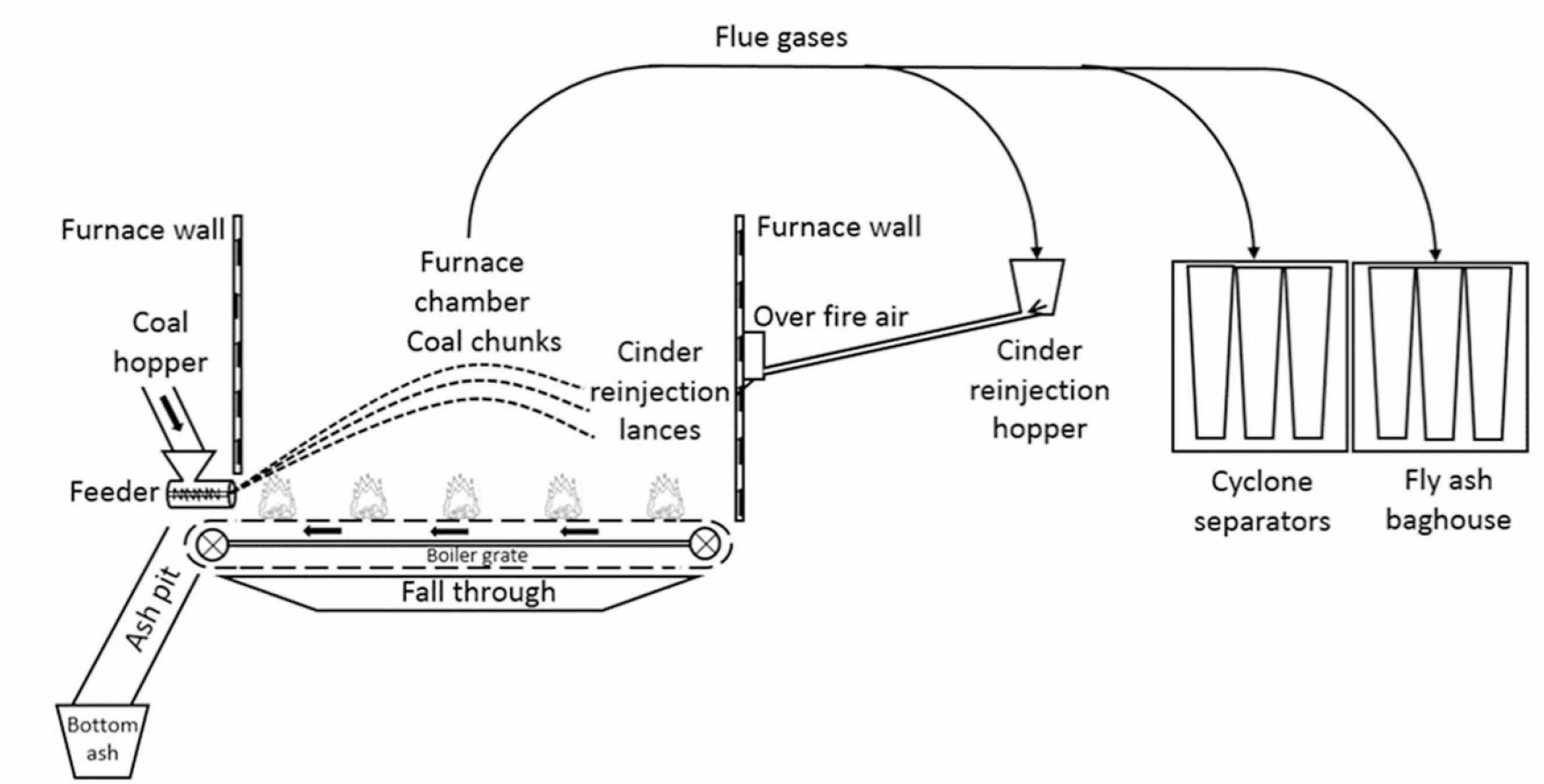

Figure 2.1 Schematic of travelling grate coal combustion process (Ward, 2018).

Chapter 3 Methods

3.1 Sample collection, preparation, and preservation

Dried ESCA was collected in spring 2014 from the UAF power plant and stored in a covered metal container at room temperature (O'Neil, 2015). Fly ash was collected in spring 2017 from baghouse ash hoppers at the UAF power plant. The ESCA was homogenized using an 8000D Dual Mixer/Mill (SPEX SamplePrep; Metuchen, NJ) due the particles' size heterogeneity. The ground sample was then placed in an acid washed 2 gallon HDPE bucket. The FA was placed in two acid washed 5 gallon buckets and sealed. Samples from the two buckets were homogenized using a large acid washed HDPE bag. The homogenized FA samples were then placed back in the acid washed 5 gallon buckets and stored at room temperature.

3.1.1 Dissolved organic matter collection, isolation, and storage

Organic matter samples were either fulvic acid or PPL (polystyrene polymer) extracts. Suwannee river fulvic acid (SRFA) and Pony Lake fulvic acid (PLFA) have been extensively characterized (USGS, 1994; Cawley et al., 2013). To obtain (sub-)Arctic DOM, 20 L of lake water was collected in spring 2016 from interior Alaska in a discontinuous permafrost area and filtered and isolated (Dittmar et al., 2008; Gagne et al., In prep.).

3.2 Chemicals and reagents

Ultrapure deionized (DI) water, with resistance greater than 18 MΩ, was obtained from a Milli-Q water system (Thermo Scientific, Waltham, MA). Methanol (ACS/HPLC, lot=DP032) was purchased from Honeywell Research Chemicals (Muskegon, MI). All acids used were trace metal grade (Omnitrace or Ultrex) and purchased from Millipore Sigma (Burlington, MA). All inductively coupled plasma-mass spectrometry (ICP-MS) standards were purchased from Agilent Technologies (Santa Clara, CA). Suwannee River fulvic acid and PLFA were obtained from the International Humic Substances Society (IHSS). Sodium nitrate (99%, lot=D06Y030), calcium chloride dihydrate (99%, lot=H13Z020), sodium sulfate (99%, lot=A16Z009), and glycine (99%, lot=10179965) were purchased from Alfa Aesar (Ward Hill, MA). Sodium citrate dihydrate

(99%, lot=1007575) was purchased from Ricca Chemical Company. Ammonium chloride (99%, lot=0000130546), and magnesium sulfate heptahydrate (99%, lot=517083) were obtained from Avantor (Radnor, PA). Sodium bicarbonate (99%, lot=139426), sodium chloride (99%, lot=3096C500), and sodium carbonate (ACS, lot=0624C514) were purchased through VWR (Radnor, PA). Sodium dihydrogen phosphate monohydrate (99%, lot=166285204) and sodium fluoride (99%, lot=20805EB) were purchased through Sigma Aldrich (St. Louis, MO). Potassium nitrate (99%, lot=EWR5894) was obtained through Wako Chemicals (Richmond, VA). Sodium azide (99%, lot=B0142014) was purchased through Acros Organics (Belgium, WI).

3.3 Wavelength dispersive X-ray fluorescence and multi-acid digestion

For wavelength dispersive X-ray fluorescence (WD-XRF) analysis performed at UAF Advanced Instrumentation Laboratory (AIL), *ca.* 7 grams of sample was ground in a ball mill with *ca.* 8 mL of polyvinyl alcohol as a binder and pressed into a pellet under *ca.* 20,000 psi for *ca.* 2 minutes . Analyses were performed using a PANalytical Axios WD-XRF (Westborough, MA) equipped with a 150 µm collimator, a LiF 220 crystal, and a scintillation detector. Analyses were performed to quantify the following elements: Al, As, Au, Ba, Bi, Br, Ca, Cl, Cr, Cu, F, Fe, Ga, Ge, K, Mg, Mn, Mo, Na, Nb, Ni, P, Pb, Rb, S, Sb, Se, Si, Sr, Ti, V, W, Y, Zn, and Zr.

Solid-phase total carbon (TC) was analyzed at the Cold Regions Research and Engineering Laboratory (CRREL, Fairbanks, AK) using a TOC-L analyzer (Shimadzu; Columbia, MD) equipped with a Solid Sample Combustion Unit (SSM-5000A). A 5-point external calibration was performed using anhydrous dextrose (BDH). Quality control checks were performed using potassium hydrogen phthalate every 10 analyses, and samples were run in triplicate. The values measured by TC were used to normalize the elemental values obtained from the WD-XRF method.

In order to better quantify elements that were near or below detection limit (BDL) using WD-XRF, samples of ESCA and FA were sent out for multi-acid digestion analysis at AGAT Laboratories (Calgary, AB). Samples were dissolved in a Teflon vessel with hot HCl, HNO_3, HF,

and $HClO_4$ and then filtered. The residue was then fused with Na_2O_2 and NaOH and quenched in the original filtrate. Samples were then analyzed for Ag, Al, As, Ba, Be, Bi, Ca, Cd, Ce, Co, Cr, Cs, Cu, Dy, Er, Eu, Fe, Ga, Gd, Ge, Hf, Ho, In, K, La, Li, Lu, Mg, Mn, Mo, Nb, Nd, Ni, P, Pb, Pr, Rb, S, Sb, Sc, Se, Sm, Sn, Sr, Ta, Tb, Te, Th, Ti, Tl, Tm, U, V, W, Y, Yb, Zn, and Zr by inductively coupled-optical emission spectrometry (ICP-OES) and ICP-MS.

For samples sent to AGAT Laboratories, major elements were analyzed by WD-XRF. The sample was fused with lithium metaborate/lithium tetraborate flux and the glass disk was then put into the WD-XRF. Major elements analyzed for include Al_2O_3, BaO, CaO, Cr_2O_3, Fe_2O_3, K_2O, MgO, MnO, Na_2O, P_2O_5, SiO_2, SrO, TiO_2, and V_2O_5.

AGAT Laboratories also analyzed for total sulfur and total carbon by combustion followed by infrared detection on LECO (Laboratory Equipment Corporation) instrumentation. Weighed sample was mixed with an accelerator and heated by induction furnace to oxidize sulfur to SO_2 and carbon to CO_2. Moisture and dust were removed and SO_2 and CO_2 are measured by a solid-state infrared detector.

3.4 Brunauer-Emmett-Teller surface area analysis

Samples were sent out for specific surface area determination but will not be completed in time for this thesis.

3.5 Environmental scanning electron microscopy

Samples were prepared for analysis using environmental scanning electron microscopy (ESEM) by affixing grains to a stub using carbon tape. The sample was coated with Ir using a Denton Vacuum Desk V (Denton Vacuum, Moorestown, NJ) sputter coater to a thickness of *ca.* 2 nm. The sample was then placed in a FEI Quanta 200 ESEM (FEI Company, Hillsboro, OR) under high vacuum mode ($<1.0x10^{-4}$ torr). Current (10-30 kV), spot size (2-5), and working distance (5-11 mm) varied. Average particle sizes were measured by taking images of random areas of CCP samples and putting them into Image J. Using the ruler tool, the width and length or diameter

of *ca.* 100 particles of each type were measured for the ESCA particles, FA mineral aggregates, and FA cenospheres (Żyrkowski, 2014). X-ray mapping of specific particles was performed using an energy dispersive IXRF Systems Model 550i X-ray detector (IXRF Systems, Austin, TX).

3.6 Solid-state ^{13}Carbon nuclear magnetic resonance

Solid-state cross-polarization magic angle spinning (CP-MAS) ^{13}C nuclear magnetic resonance (NMR) was used to characterize the organic components of the CCPs. *ca.* 2 grams of CCP were washed with hydrofluoric acid to remove paramagnetic metals (e.g. Fe and Co) (Ehlers et al., 2010). The samples were then diluted 2:1 with KBr to avoid arcing and packed in 80 µL zirconium rotors. A Bruker Avance III 600 MHz spectrometer (Billerica, Massachusetts) at 150 MHz ^{13}C frequency, using a Bruker 4 mm MAS probe to analyze the samples. 40K scans were collected using a spin rate of 15 kHz. Spectra were collected using the multiple cross-polarization method to be nearly quantitative (Johnson and Schmidt-Rohr, 2014). The spectra were processed using Topspin 3.5.7. Phasing, line broadening, and linear baseline corrections were applied to the spectra. To determine the percentages of various functional groups in the TOC composition the spectra were integrated between the corresponding chemical shift regions (Johnson and Schmidt-Rohr, 2014).

3.7 Fly ash and early stage coal ash leaching

In order to assess the extent and rate of metal(loid) leaching from the CCP samples, batch leaching experiments were performed. Two grams of FA or ESCA was placed in an acid washed 50 mL Nalgene™ polypropylene centrifuge tube with 40 mL of the selected leachate, covered with parafilm (open system experiments) or a cap (closed system experiments), and then placed on an end-over-end rotator at 8 rpm (Barnstead International, Dubuque, IA) for constant agitation (Neupane and Donahoe, 2013). Leachates included >18 MΩ H_2O (control) (open and closed system), simulated rain water (open system), and reconstituted DOM solutions (closed system), described further below (Koch et al., 1986).

Triplicate samples were sacrificed at 13 time points: 0 hr (method blank), 1 hr, 12 hr, 1 d, 2 d, 3 d, 5 d, 7 d, 10 d, 14 d, 21 d, 28 d, and 3 mo. Upon collection, samples were centrifuged at 15,000 revolutions min^{-1} (26,892 RCF) for 15 minutes using a Sorvall RC 5B Plus Superspeed Centrifuge (Dupont Company, Wilmington, DE) and the supernatant was then filtered through acid washed polypropylene 0.45 µm filters (Acrodisc GHP) and stored at room temperature prior to analysis. The solid residue was then rinsed with 20 mL of DI water and centrifuged at 15,000 revolutions min^{-1} (26,892 RCF) for 15 minutes. This second supernatant was then decanted and discarded. Solid residue was frozen and freeze-dried using a FreeZone Plus 12 Liter Cascade Console Freeze Dry System (Labconco; Kansas City, MO). Freeze-dried samples were then placed in acid washed LDPE scintillation vials for long-term storage a room temperature.

3.8 Synthetic precipitation leaching procedure

Synthetic precipitation leaching was performed according to the EPA method 1312. Briefly, DI H_2O was titrated with a solution of 60% concentrated sulfuric acid and 40% concentrated nitric acid by weight to a pH of 5.01. 1 L of the resulting solution was added to 1 L new HDPE Nalgene™ bottles containing 50 g of FA or ESCA. Experiments were performed in triplicate with reagent and DI H_2O method blanks. The bottles were then sealed and placed on a rotator (Associated Design and Manufacturing Company, Lorton, VA) at 30 rpm for 18 hours at room temperature (*ca.* 23°C). The samples were allowed to settle 2 hours prior to filtration. Supernatant splits for cation analysis were collected using acid-washed syringes, 0.2 um polypropylene filters (Acrodisc GHP; washed with 15 mL of 1M HNO3 followed by 60 mL DI water rinse), and falcon tubes. Samples were acidified to pH <2 using concentrated Ultrex grade HNO_3, 5 drops were added to ESCA and 9 drops were added to FA. Supernatant splits were also collected for pH, electrical conductivity (EC), alkalinity, and anions which were filtered using new, non-acid washed, 0.45 um hydrophilic polyethersulfone filters (Acrodisc Supor), syringes, falcon tubes, and 60 mL HDPE Nalgenes™. The pH, EC, and alkalinity of the supernatants were measured immediately. Cation and anion aqueous samples were then refrigerated until analysis by ICP-MS or ion chromatography (IC), respectively. Ion chromatography was performed using

standard methods by the U.S. Geological In-House Operational and Research Chemistry Laboratory. Alkalinity titrations were performed using phenolphthalein and total alkalinity determination by digital titration (Hach Company, 2018).

3.9 Physiological based extraction tests

To assess bioaccessibility of the metals in the ESCA and FA physiological based extraction tests (PBETs) were performed that mimicked gastric and lung biological conditions (Plumlee et al., 2014; Bauer et al., 2007; EPA, 2017). Physiological based extraction tests were performed with ground unreacted ESCA and FA, in addition to ESCA that had been reacted with DI H_2O for 1 hr, 24 hr, and 3 mo, and then freeze-dried.

Simulated gastric fluid (SGF) was prepared by making a 30.0300 g L^{-1} glycine solution in DI H_2O (EPA, 2017). Omnitrace HCl was used to adjust the pH of the SGF to pH= 1.5. The simulated lung fluid (SLF) was a modified Gambles solution prepared making an ammonium chloride (535.41 mg L^{-1}), magnesium chloride dihydrate (0.213 g L^{-1}), sodium chloride (6.7821 g L^{-1}), sodium bicarbonate (1.768 g L^{-1}), sodium carbonate (0.6295 g L^{-1}), sodium citrate dihyrdate (59.028 mg L^{-1}), glycine (0.4512 g L^{-1}), sodium sulfate (0.1793 g L^{-1}), calcium chloride (29.035 mg L^{-1}), and sodium dihydrogen phosphate monohydrate (166.59 mg L^{-1}) solution in DI H_2O (Bauer et al., 2007). Omnitrace HCl was used to adjust the pH of the SLF to pH= 7.4. The PBET solutions were preheated to 37˚C prior to initiating the experiments.

PBETs were initiated by adding 33.333 $\pm$ 0.0005 mL of SGF or 20.000 $\pm$ 0.0005 mL of SLF to a 50 mL HDPE Nalgene™ containing 0.333 $\pm$ 0.0005 g of ESCA or FA for SGF PBETs and 0.200 $\pm$ 0.0005 g of ESCA or FA for SLF PBETs. All experiments were performed in triplicate and conducted in an incubator shaker chamber (Lab-Line Instruments Inc., Melrose Park, IL) maintained at 37˚C. The pH of the SGF samples was measured after 10, 30 and 45 minutes, to make sure the physiological pH did not change, in necessary, the pH was readjusted with HCl. SGF and SLF experiments were terminated after 1 hr and 24 hr, respectively. After extraction, the samples were centrifuged 3,900 rpm (2,050 RCF), and the supernatant was filtered using

0.2 µm polypropylene filters (Acrodisc GHP) into 50 mL acid washed falcon tubes. The filtered supernatant was diluted 2x with Omnitrace 2% HNO_3 in preparation for ICP-MS analysis. The acidified supernatant was stored in the refrigerator (4°C, dark) for *ca.* 12 hours prior to analysis.

3.10 Elemental analysis of aqueous samples

An Agilent 7500 ce ICP-MS (Santa Clara, CA) was used to measure metal(loid) concentrations in supernatant solutions, including: Al, Sb, As, Ba, Bi, Cd, Ca, Cr, Co, Cu, Fe, Pb, Mn, Mo, Se, and V. External calibration was performed at the beginning of each ICP-MS run for every element (0.01-2000 ppb). In addition, appropriate internal standards were added in line throughout the analysis (Ge, Y, Sc, Rh, and Ir). Calibration checks and calibration blanks were measured every *ca. 10* samples. Further, appropriate method blanks, acid blanks and reference standards (SLRS-5 riverine water and NIST 1640a trace elements in natural water systems) were analyzed with each batch of samples.

3.11 Statistical analysis

In order to compare whether concentrations were statistically different or similar between the experiments JMP® Pro Version 13.2.1 was used. A student's t-test was performed on sets of leachate concentrations for each metal(loid) with a p-value of <0.05. Statistical analysis was performed to compare metal(loid) concentrations between the 1 hr, 7 d, and 3 mo time points. Statistical analysis was also performed to compare unreacted and reacted ESCA samples for physiological based extraction tests. Linear regressions were fitted to DOM trends by adding a linear trendline and displaying both the R^2 and equation of the line in Microsoft Excel. Outlier tests were performed for certain data points using a Grubbs' test for outliers.

3.12 Coal combustion product-dissolved organic matter interactions

Dissolved organic matter batch experiments were performed with ESCA and FA to simulate surface water interactions with CCPs. Dissolved organic matter solutions were prepared using SRFA, PLFA, and Goldstream Valley organic matter extract (GSE) from Fairbanks, Alaska. Suwannee River fulvic acid is terrestrially derived and PLFA is microbially derived (USGS, 1994;

Cawley et al., 2013). A stock solution of each DOM was prepared in DI H_2O in varying concentrations (0, 5, 10, 20, 50, 100 mg carbon L^{-1}). 40 mL of each DOM solution was reacted with 2 g of FA or ESCA in acid washed 50 mL centrifuge tubes for 7d, in duplicate. CCP samples were reacted in a closed system due to sample limitations. The centrifuge tubes were covered in foil to avoid photochemical reactions and continuously agitated on an end-over-end rotator, centrifuged, and filtered with 0.45 µm GHP filters. The supernatant was then diluted 2:1 with 2% HNO_3 in preparation for analysis by ICP-MS. The following elements were analyzed for: As, Ca, Cd, Co, Cr, Fe, Mn, Mo, Sb, Se, Te, V, and Zn.

3.13 Geochemical modeling

Geochemical modeling was performed with Visual MINTEQ 3.1 (EPA Environmental Research Laboratory, Athens, GA). Geochemical modeling was performed for Al, Ca, Cr, Fe, Zn, As, Se, Ba, and Pb. Ionic strength was fixed for these calculations and 0.01 mg L^{-1} NaCl was added to the model solution to help charge balance the calculation. CO_2 was made a fixed species at 0.00038 atm. Each metal(loid) was modeled individually and possible solid phases were added to the system individually as an infinite solid phase. A pH sweep was then performed with the output being the log total dissolved metal(loid) concentration. Log total dissolved metal(loid) concentration was then plotted vs. pH and leaching data points were plotted for comparison. Points above the log total dissolved metal(loid) concentrations are considered to be supersaturated with respect to the infinite solid phase indicating that the formation of the solid is thermodynamically favored, points below are considered to be undersaturated indicating that the formation of the solid is not thermodynamically favored, and points on the line are saturated indicating a potential equilibrium with the solid phase, if it is present.

Chapter 4 Results

4.1 Physiochemical properties

4.1.1 Elemental composition

Elemental composition of ESCA and FA were measured both at UAF and by AGAT, a contract laboratory (**Table 4.1** and **Table 4.2**). AGAT also measured two FA standard reference materials (SRM; NIST 2691 and NIST 1633a; **Table 4.1**). Comparing AGAT data with the certified and provisional values from NIST, most elements are within 10-15% difference, except when the element being measured occurs at a low concentration, near the detection limit of the technique. When comparing the AGAT data with UAF data, roughly two-thirds of the elements for the ESCA are >15% different, while roughly half of the elements for the FA are >15% different (**Table 4.2**). For the remainder of this thesis, any WD-XRF values reported will be from the AGAT Laboratory analysis, unless otherwise noted.

Total carbon analysis revealed that the ESCA contained *ca*. 28 $\pm$ 1 wt.% carbon and the FA contained *ca*. 18.6 $\pm$ 0.1 wt.% carbon (**Table 4.1** and **Table 4.2**). Elemental analysis shows that the sum of CaO, SiO_2, Al_2O_3, S, Fe_2O_3, and organic carbon account for 94 $\pm$ 2 wt.% and 87 $\pm$ 1 wt.% of the ESCA and FA, respectively. After C, the most abundant elements are Ca and Si, which are present at 21.6 $\pm$ 0 wt.% CaO and 26.9 $\pm$ 0 wt.% CaO, and 26.0 $\pm$ 0.4 wt.% SiO_2 and 18 $\pm$ 1 wt. % SiO_2 in ESCA and FA, respectively.

Major element concentrations for ESCA and FA are below the Healy coal concentrations for SiO_2, Al_2O_3, S, K_2O, TiO_2, and BaO, and are above for S, MgO, P_2O_5, CaO, and Fe_2O_3. Early stage coal ash MnO concentrations are below Healy coal concentrations while FA are above. The FA has lower concentrations of Na_2O, Al_2O_3, SiO_2, P_2O_5 TiO_2, and BaO compared to the standard reference material NIST SRM2691 and higher concentrations of S, K_2O, Fe_2O_3, and MnO (**Table 4.1**). All FA minor and trace element concentrations were $\geq$20 wt.% different from the NIST SRM 2691 values with the exception of Ga for samples analyzed at UAF.

Table 4.1 Elemental composition of ESCA and FA by AGAT contract laboratory.

Elements	Early Stage Combustion Ash	Fly Ash	SRM NIST 2691			SRM NIST 1633a		
			Meas. Value	Cert. Value[a]	% Dif.[b]	Meas. Value	Cert. Value[a]	% Dif.[b]
Element (wt.%)								
C	28 ± 1	18.6 ± 0.1	0.09			2.77		
S	0.554 ± 0.001	2.12 ± 0.08	0.849	0.83	2	0.158	0.18	-12
Al_2O_3	10.5	11.4 ± 0.2	18.3	18.54	-1	27.2	27.02	1
BaO	0.4 ± 0.01	0.55 ± 0.02	0.7	0.66	6	0.14	0.17	-18
CaO	21.6	26.9	25.5	25.81	-1	1.54	1.55	-1
Cr_2O_3	0.01	0.02	<0.01	0.01		0.03	0.03	0
Fe_2O_3	7.1 ± 0.2	9.78 ± 0.01	6.29	6.32	0	13.5	13.44	0
K_2O	0.55	0.64 ± 0.02	0.41	0.41	0	2.26	2.26	0
MgO	3.455 ± 0.007	5.25 ± 0.01	5.22	5.17	1	0.75	0.75	0
MnO	0.11	0.36 ± .01	0.02	0.03	-33	0.02		
Na_2O	0.29 ± 0.01	0.17 ± 0.03	1.45	1.47	-1	0.16	0.23	-30
P_2O_5	0.14 ± 0.01	0.12 ± 0.01	1.15	1.17	-2	0.4		
SiO_2	26.0 ± 0.4	18 ± 1	36.2	36.01	1	48.8		
SrO	0.21 ± 0.01	0.27 ± 0.01	0.37	0.32	16	0.09	0.1	-10
TiO_2	0.46 ± 0.01	0.43 ± 0.01	1.53	1.5	2	1.39	1.33	5
V_2O_5	0.03 ± 0.01	0.03	0.04			0.05	0.05	0
LOI	27.9 ± 0.6	21.7 ± 0.1	0.31	0.23	35	3.45		
Element (mg kg^{-1})								
Al	5.7 ± 0.04	6.28	9.81	9.81	0	14.8	14.3	3
Ca	15.2 ± 0.3	19.00	17.6	18.45	-5	1.19	1.11	7
Fe	4.59 ± 0.09	6.38 ± 0.02	3.99	4.42	-10	8.85	9.4	-6
K	0.47	0.54 ± 0.01	0.36	0.34	6	1.95	1.88	4
Mg	2.08 ± 0.01	3.18 ± 0.04	3.13	3.12	0	0.47	0.455	3
P	0.045 ± 0.007	0.04	0.53	0.51	4	0.17		
S	0.52 ± 0.02	1.82 ± 0.02	0.77	0.83	-7	0.16	0.18	-11
Ti	0.265 ± 0.007	0.24	0.85	0.9	-6	0.82	0.8	2
Ag	0.5 ± 0.1	2.10	1.4			1.3		
As	11	124.5 ± 0.7	25	30	-17	163	145	12
Ba	3300 ± 200	4320 ± 20	6120	5900	4	1330	1500	-11
Be	1.9 ± 0.1	3.05 ± 0.07	4.2	8	-48	13.7	12	14
Bi	0.4 ± 0.2	3.0 ± 0.2	0.8			1.1		
Cd	0.40	5.8 ± 0.2	1.1			1.1	1	10
Ce	42.6 ± 0.8	69 ± 1	103			165	180	-8
Co	23.7 ± 0.1	27.4 ± 0.6	26.4	26	2	47.8	46	4
Cr	82 ± 4	85	58	68	-15	185	196	-6
Cs	1.65 ± 0.07	4.9 ± 0.3	1.2	1	20	9.7	11	-12
Cu	114.5 ± 0.7	840 ± 20	192			116	118	-2
Dy	4.08 ± 0.09	6.23 ± 0.03	8.1			14		
Er	2.38 ± 0.02	3.6 ± 0.1	4.82			7.91		
Eu	1.58 ± 0.03	2.31 ± 0.05	3.04	2	52	3.7	4	-8
Ga	15.8 ± 0.4	36 ± 2	30.5			59	58	2
Gd	4.8 ± 0.1	7.62 ± 0.06	9.56			16.8		

Table 4.1 (Cont'd): Elemental composition of ESCA and FA by AGAT contract laboratory.

Elements	Early Stage Combustion Ash	Fly Ash	SRM NIST 2691			SRM NIST 1633a		
			Meas. Value	Cert. Value[a]	% Dif.[b]	Meas. Value	Cert. Value[a]	% Dif.[b]
			Element (mg kg^{-1})					
Ge	BDL	0.2	0.1			2.5		
Hf	2.95 ± 0.07	3.2	9	10	-10	6.9	8	-14
Hg	1.06 ± 0.07	3.6 ± 0.1	0.08	0.0578	38	0.188	0.16	18
Ho	0.86 ± 0.04	1.30 ± 0.02	1.68			2.88		
In	BDL	0.40	<0.2			<0.2		
La	21.6 ± 0.2	33.4 ± 0.4	56.2			78.2		
Li	16.00	23.5 ± 0.7	47			207		
Lu	0.36 ± 0.01	0.49 ± 0.01	0.71			1.07		
Mn	770 ± 20	2670 ± 10	148	200	-26	177	179	-1
Mo	6.5 ± 0.1	11.4 ± 0.3	8.9			31.9	29	10
Nb	7.00	7.4 ± 0.1	32.1			27.8		
Nd	20.05 ± 0.07	32.6 ± 0.4	46.2			75.4		
Ni	75 ± 3	125	52	53	-2	121	127	-5
Pb	15 ± 1	140 ± 10	35.8	29	23	67.8	72.4	-6
Pr	4.9 ± 0.1	7.9 ± 0.1	11.8			18.9		
Rb	23.4 ± 0.5	34 ± 1	18.6			142	131	8
Sb	3.8 ± 0.2	27 ± 2	2.5			6.9		
Sc	15.55 ± 0.07	17.6 ± 0.1	24.6	24	3	38.5	40	-4
Se	BDL	22	13	17	-24	11	10.3	7
Sm	4.35 ± 0.07	7.1	9.1			15.8		
Sn	2.0 ± 0.9	8.0 ± 0.3	3.1			5.9		
Sr	1640 ± 30	2160	2990	2700	11	803	830	-3
Ta	0.50	0.5	1.9			1.9		
Tb	0.69 ± 0.04	1.08 ± 0.01	1.37			2.46		
Te	0.10	0.65 ± 0.07	0.9			0.2		
Th	7.40	11.8 ± 0.4	23.4	26	-10	24.3	24.7	-2
Tl	0.20	2.3 ± 0.1	0.6			5.3	5.7	-7
Tm	0.37 ± 0.01	0.51 ± 0.01	0.72			1.12		
U	3.28 ± 0.01	4.28 ± 0.06	7.75			9.27	10.2	-9
V	152 ± 1	160 ± 3	232			322	297	8
W	1.7 ± 0.2	8.0 ± 0.4	2.7			5.8		
Y	26.6 ± 0.6	40.7 ± 0.1	53			91.4		
Yb	2.40	3.35 ± 0.07	4.6			7.4		
Zn	25.00	237 ± 8	96	120	-20	232	220	5
Zr	108 ± 6	114 ± 2	341			254		

[a] Certified values obtained from NIST certificates. Underlined values are provisional values.

[b] Percent difference = [(measured value- certified value) divided by the certified value] *100 percent.

Table 4.2 Comparison of UAF and AGAT elemental composition.

Element	Avg. Crust. Abun.	UAF ESCA	AGAT ESCA	% Dif.[b]	UAF FA	AGAT FA	% Dif.[b]	Healy Coal[c]
Element (wt.%)								
TC	-----	27.2 ± 2	28 ± 1	3	17.5 ± 0.3	18.6 ± 0.1	6	70[d]
TS	-----	-----	0.554 ± 0.001		-----	2.12 ± 0.08		0.3
Na_2O	3.27	0.18 ± 0.02	0.30 ± 0.01	48	0.2 ± 0.1	0.17 ± 0.03	7	0.3
MgO	2.48	1.7 ± 0.1	3.460 ± 0.007	70	5.2 ± 0.1	5.25 ± 0.01	1	3.1
Al_2O_3	15.4	6.6 ± 0.1	10.5 ± 0	46	9.15 ± 0.07	11.5 ± 0.2	23	18
SiO_2	66.6	16.5 ± 0.3	26.0 ± 0.4	45	13.3 ± 0.2	18 ± 1	31	44.4
P_2O_5	0.15	0.045 ± 0.001	0.140 ± 0.007	103	0.048 ± 0.0008	0.120 ± 0.007	86	0.07
S	0.0062	1.82 ± 0.03	0.50 ± 0.02	114	3.84 ± 0.03	1.80 ± 0.02	72	2
K_2O	2.8	0.52 ± 0.01	0.55 ± 0	6	0.663 ± 0.03	0.64 ± 0.02	4	1.2
CaO	3.59	15.5 ± 0.2	21.6 ± 0	33	25 ± 0.3	26.9 ± 0	7	19.1
Fe_2O_3	11.2	13.5 ± 0.2	7.1 ± 0.1	62	19.1 ± 0.1	9.78 ± 0.01	65	7
TiO_2	0.64	0.44 ± 0.01	0.46 ± 0.01	5	0.41 ± 0.01	0.43 ± 0.01	6	0.8
MnO	0.1	0.092 ± 0.001	0.11 ± 0	18	0.340 ± 0.005	0.360 ± 0.007	6	0.16
BaO	0.07	0.310 ± 0.003	0.40 ± 0.01	25	0.460 ± 0.008	0.56 ± 0.02	20	0.57
Element (mg kg^{-1})								
Cl	370	500 ± 200	-----		340 ± 20	-----		
V	97	160 ± 10	152 ± 1	4	180 ± 40	160 ± 3	10	
Cr	92	450 ± 50	82 ± 4	138	200 ± 60	85 ± 0	81	
Ni	47	60 ± 20	75 ± 3	14	124 ± 4	125 ± 0	1	
Co	17.3	-----	23.7 ± 0.1		-----	27.0 ± 0.6		
Cu	28	134 ± 8	115.0 ± 0.7	15	880 ± 20	840 ± 20	5	
Zn	67	39 ± 3	25 ± 0	44	272 ± 5	237 ± 8	14	
Ga	17.5	15.2 ± 0.3	16.0 ± 0.4	5	36 ± 1	36 ± 2	0	
Ge	1.4	2.1 ± 0.5	< 0.1 ± 0		8.0 ± 0.4	0.2 ± 0	190	
As	4.8	19 ± 3	11 ± 0	54	138 ± 4	125.0 ± 0.7	10	
Se	0.09	7 ± 8	< 5 ± 0		16 ± 2	22 ± 0	32	
Br	1.6	25 ± 1	-----		68.0 ± 0.7	-----		
Rb	84	30 ± 2	23.0 ± 0.5	27	41 ± 1	35 ± 1	17	
Sr	320	1580 ± 20	1640 ± 30	4	2090 ± 20	2160 ± 0	3	
Y	21	28 ± 4	27.0 ± 0.6	3	35.0 ± 0.5	40.7 ± 0.1	15	
Zr	193	90 ± 10	108 ± 6	13	90 ± 20	114 ± 2	24	
Nb	12	8 ± 3	7 ± 0	13	9 ± 2	7.4 ± 0.1	16	
Mo	1.1	9 ± 1	6.5 ± 0.1	32	11 ± 2	11.4 ± 0.3	5	
Sb	0.4	12 ± 1	3.8 ± 0.2	101	34 ± 3	27 ± 2	24	
Te	-----	-----	0.1 ± 0		-----	0.70 ± 0.07		
W	1.9	3 ± 2	2 ± 0.2	36	4 ± 4	8.0 ± 0.4	69	
Au	-----	7 ± 1	-----		-----	-----		
Pb	17	40 ± 2	15 ± 1	92	392 ± 2	143 ± 10	93	
Bi	0.16	5.92 ± 0	0.5 ± 0.2	169	6 ± 3	3.0 ± 0.2	71	

[a] Average crustal abundances from upper crust values (Rudnick and Gao, 2003).

[b] Percent difference = [(UAF value- AGAT value) divided (mean of UAF and AGAT values)] *100 percent.

[c] Healy coal values from Usibelli Coal Mine website (Usibelli Coal Mine, 2015).

[d] Carbon content present in Healy Coal, not ashed sample.

The most abundant minor elements (defined as occurring at concentrations of 100-10,000 mg kg^{-1}) in both the FA and ESCA were Sr 2160 $\pm$ 0 mg kg^{-1} and 1640 $\pm$ 30 mg kg^{-1}, respectively. Copper was also found to be in high concentrations in the FA (840 $\pm$ 20 mg kg^{-1}) but not the ESCA (115.0 $\pm$ 0.7 mg kg^{-1}). The FA contained higher concentrations of minor elements and trace elements (defined as occurring at concentrations <100 mg kg^{-1}) relative to ESCA.

Enrichment factor plots for the elements measured relative to average crustal abundance are shown in **Figure 4.1 A** for major elements and **Figure 4.1 B** for selected minor and trace elements (Rudnick and Gao, 2003). The majority of major elements show similar depletion or enrichment trends for the FA and ESCA. Sulfur present in the FA is the only major element with an enrichment factor >100. A little over half of the minor and trace elements are enriched for both the ESCA and FA (**Figure 4.1 B**). Some of the elements with the highest enrichment factor in both the ESCA and FA are potentially toxic, including: As, Cu, and Sb. Chromium, another commonly known toxic metal(loid), is depleted in both CCP samples studied. Selenium present in the FA is the only trace element with an enrichment factor >100. Lastly, there are several elements (Zn, Ga, and Pb) that are enriched in the FA but depleted in the ESCA.

4.1.2 Particle morphology

Particle size and morphology was assessed using ESEM. ESCA particles are typically porous in appearance with a wide range of sizes. A representative particle is shown in **Figure 4.2 A**. The length of the smaller axis ranged from 179 µm to 629 µm (average= 350 $\pm$ 99 µm; median= 347 µm) and the longer axis ranged from 242 µm to 950 µm (average= 516 $\pm$ 151 µm; median= 518 µm). An X-ray analysis of these particles demonstrates that it is primarily composed of Ca, S, Si, Al, Fe, and Mg (**Figure 4.2 A**). Presence of Ir in the X-ray map of all particles is from coating the particles in Ir in order to analyze them under high vacuum mode on the ESEM and is not actually present in the particle. The average particle size of the ESCA is much larger than the FA particles, which has important potential implications for specific surface area and thus for mineral weathering and metal(loid) mobility.

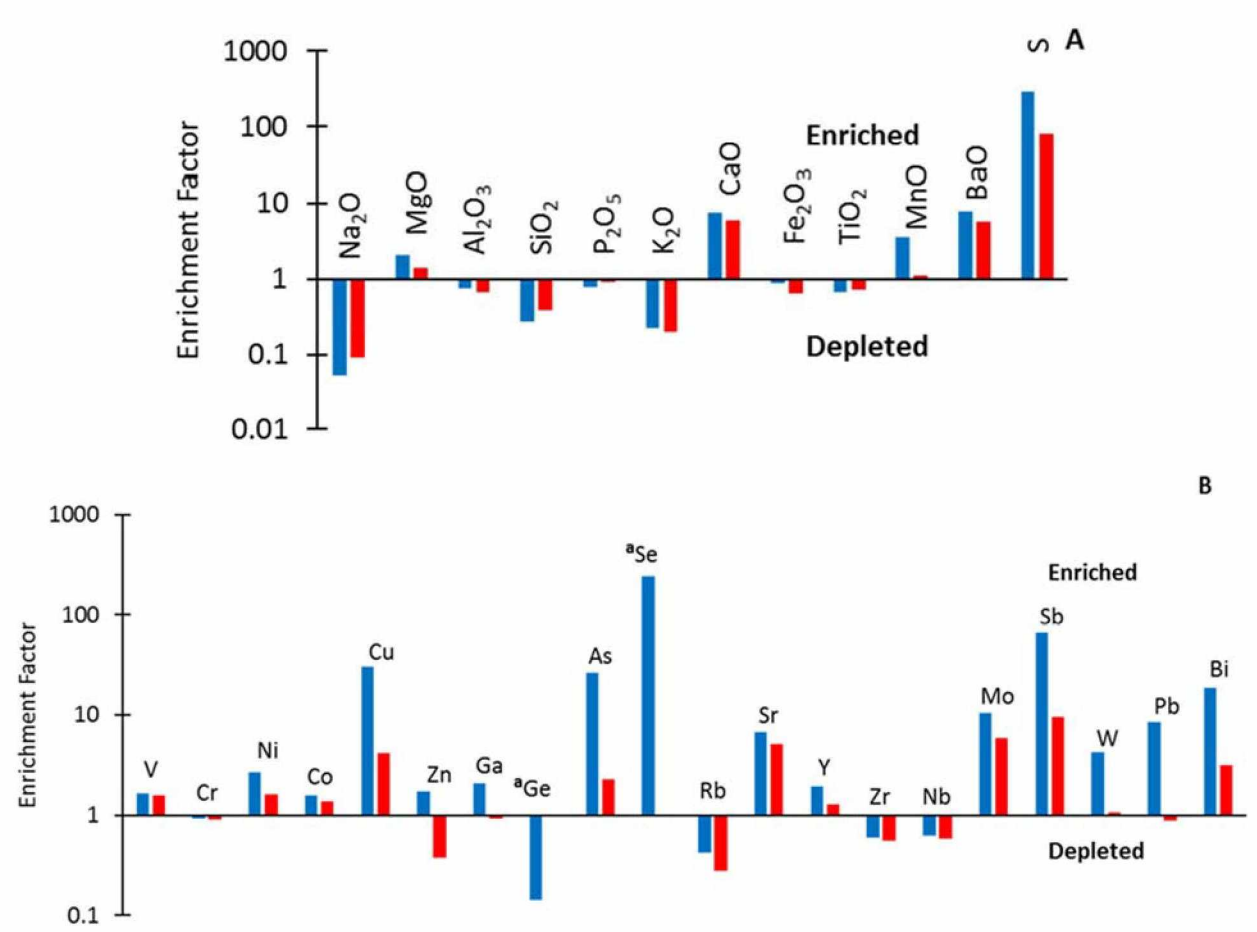

Figure 4.1 Elemental enrichment factors. Early stage coal ash (red) and FA (blue). [a]AGAT ESCA value was below detection limit.

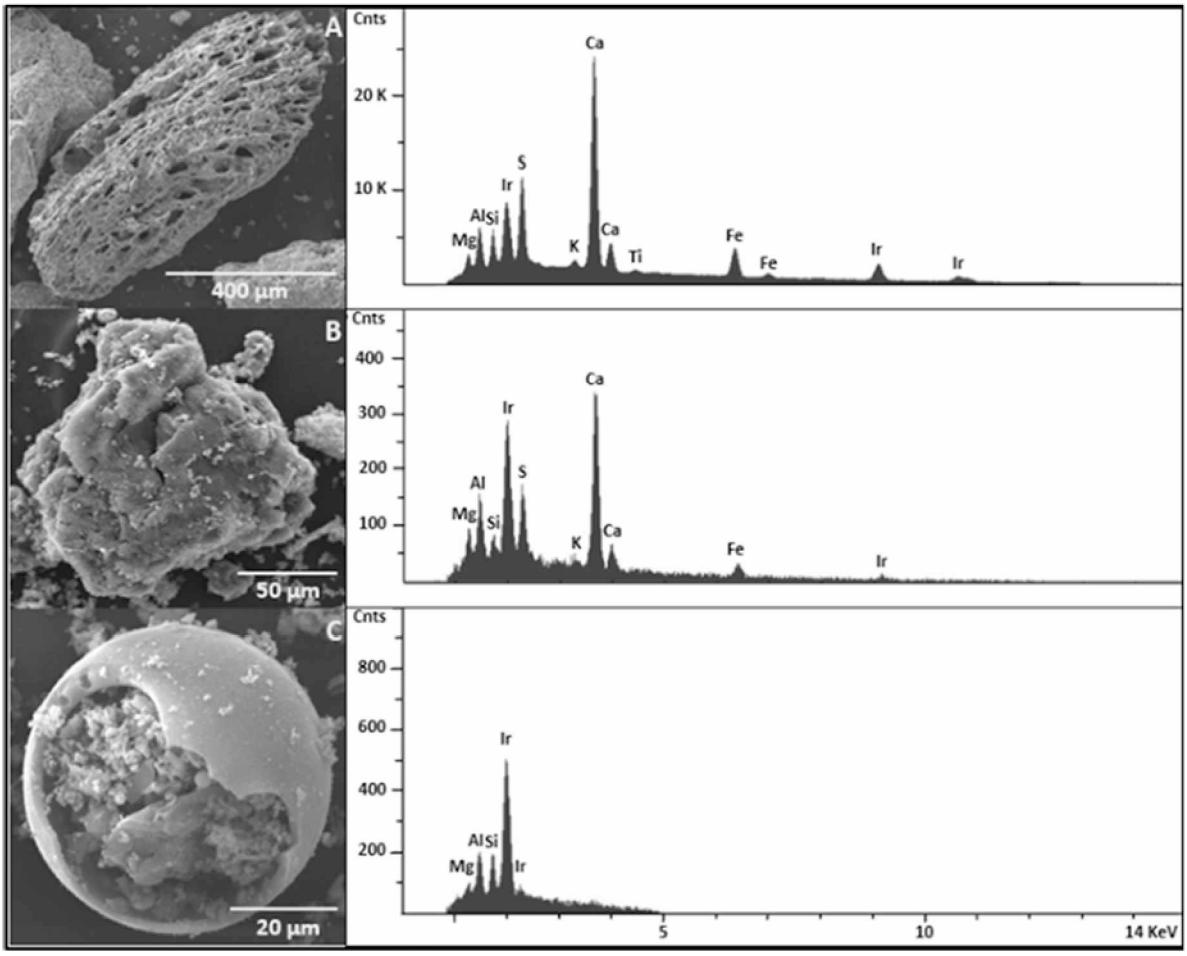

Figure 4.2 Scanning electron microscopy of coal combustion product particles. a) Early stage coal ash porous particle. b) Fly ash mineral aggregate. c) Fly ash cenosphere.

The majority of FA particles are typified by one of two morphologies: mineral aggregates and cenospheres. Mineral aggregates with ranged in size from 7.0 µm to 80.5 µm (average= 18.8 $\pm$ 10 µm; median= 16.1 µm) on the shorter axis and 9.6 µm to 97.2 µm (average= 29.2 $\pm$ 15 µm; median= 25.9 µm) on the longer axis. A typical FA mineral aggregate is shown in **Figure 4.2 B**. X-ray analysis of these particles (**Figure 4.2 B**), shows that they are primarily made of Ca, S, Si, Al, Mg, and Fe, which is consistent with other major elements reported in FA samples in this and other studies (Akar et al., 2012; Neupane and Donahoe, 2013; Koukouzas et al., 2011; Church et al., 1995). A second typical morphology is cenospheres that ranged in diameters from 1.9 µm to 46 µm (average= 7.50 $\pm$ 7 µm; median= 5.17 µm). The majority of cenospheres observed had mineral aggregates that nucleated on the surface and also particles present on the interior of the cenosphere (**Figure 4.2 C**) with heterogenous

metal(loid) concentrations. X-ray analysis of these particles (**Figure 4.2 C)** shows that they are primarily made of Si, Al, and Mg. Żyrkowski et al. (2014) reports FA cenospheres as being aluminosilicate glasses with some crystalline phases such as quartz, mullite, and calcite.

4.1.3 Organic composition

Solid-state CP-MAS ^{13}C NMR spectra (**Figure 4.3**) were obtained for ESCA and FA in order to quantify the percentages of various functional groups present in each of the samples (**Table 4.3**). The organic composition of the CCPs was primarily composed of oxygenated aliphatic carbons, including ethers and alcohols, followed by alkyl substituted aromatic carbons, other aliphatic carbons, phenolic carbons, carboxylic acids, and carbonyls (**Table 4.3**). Fly ash contained more aliphatic carbons relative to ESCA (16% and 22% in ESCA and FA respectively), while ESCA contains more alkyl substituted aromatics (26% and 30% in ESCA and FA, respectively). None of the other integration regions are substantially different <3%. Early stage coal ash contains higher percentages of functional groups with the exception of oxygenated aliphatic carbons and aliphatic carbons.

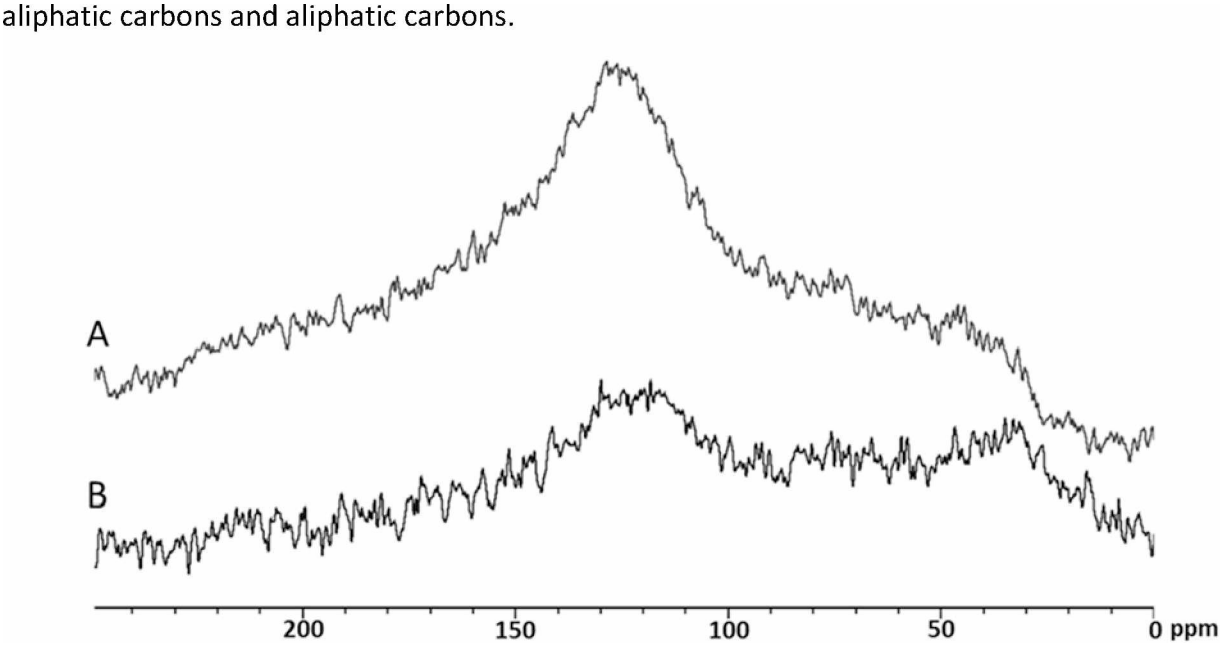

Figure 4.3 Solid-state ^{13}C nuclear magnetic resonance spectra. a) Early stage coal ash spectrum. b) Fly ash spectrum.

Table 4.3 Early stage coal ash and fly ash organic functional groups. Spectra integrated between the corresponding chemical shift regions similar to those used in Cawley et al. (2013).

Functional groups	Integration region (ppm)	FA %	ESCA %
Aliphatic carbons	0-60	22.5	16.3
Oxygenated aliphatic carbons	60-110	33.1	30.6
Alkyl substituted aromatics	110-140	25.7	30.2
Phenolic carbons	140-160	8.6	10.0
Carboxylic acids	160-190	6.8	7.8
Carbonyls	190-230	3.3	5.2

4.2 Synthetic precipitation leaching procedure

Synthetic precipitation leaching procedure metal(loid) concentrations can be seen in **Table 4.4**, and the majority of elements analyzed were below detection limit (BDL). No elements detected exceeded Environmental Protection Agency Freshwater Criteria Maximum Concentrations (EPA FW CMCs) or Environmental Protection Agency Drinking Water Maximum Contaminant Levels (EPA DW MCLs) with the exception of Pb in the FA (EPA, 2018). The highest concentrations observed in both the ESCA and FA were for Ca. Typically metal(loid)s leached from one CCP or the other, but not both, the exceptions being Se, Mo, and Pb. Synthetic precipitation leaching procedure values can be seen plotted on the leaching graphs in the following sections.

Table 4.4 Synthetic precipitation leaching procedure results.

Element (mg L^{-1})	ESCA	SD	Fly ash	SD	EPA DW MCL	EPA FW CMC
Ca	204	2	571	3	N/A	N/A
(µg L^{-1})						
V	17.5	0.2	BDL	BDL	N/A	N/A
Cr	3.37	0.2	BDL	BDL	100	[a]570
Mn	BDL	BDL	3.17	0.4	N/A	N/A
Fe	BDL	BDL	BDL	BDL	N/A	N/A
Co	BDL	BDL	0.21	0.02	N/A	N/A
Cu	BDL	BDL	4.13	0.4	1300	N/A
Zn	BDL	BDL	3.26	1	N/A	N/A
As	0.21	0.1	BDL	BDL	10	340
Se	1.80	0.04	0.77	0.04	50	N/A
Mo	20.1	0.2	6.00	1	N/A	N/A
Pb	0.08	0	29.4	0.9	[b]15	65

[a]EPA FW CMC for Cr (III). EPA FW CMC for Cr (VI) is 16 µg L^{-1}.
[b]EPA DW MCL action level.
Environmental Protection Agency Drinking Water Maximum Contaminant Level (EPA DW MCL).
Environmental Protection Agency Freshwater Criteria Maximum Concentration (EPA FW CMC).

4.3 Leaching experiments

The degree of leaching over the 7 d and 3 mo time periods for the elements measured varied with respect to element, leachate, and CCP. Percent leached was determined as the concentrations found in the supernatants divided by the initial concentrations in the unreacted samples, times 100. For FA-18, FA-RW, and ESCA-RW, for the 7 d time point, Ca had the highest percentage leached out of all metal(loid)s listed with the exception of Ba for FA-RW and Mo for ESCA-RW (**Table 4.5**). For FA-RW, ESCA-18, and ESCA-RW, for the 3 mo time point, Ca had the highest percentage leached out of all metal(loid)s listed with the exception of Ba and Mo for FA-RW, Mo for ESCA-18, and Mo for ESCA-RW (**Table 4.5**). Highest percentages leached between the 7 d and 3 mo time points varied between experiment and element, there was no discernable trend.

Table 4.5 Percent leached of elements for 7 d and 3 mo time points.

	FA-18		FA-RW		ESCA-18		ESCA-RW	
% leached	7 d	3 mo	7 d	3 mo	7 d	3 mo	7 d	3 mo
Ca	3.7E-01	9.8E-05	3.4E-01	1.0E-01	BDL	1.5E-01	1.9E-01	1.0E-01
Ba	4.1E-01	1.7E-01	4.6E-01	1.7E-01	1.8E-02	1.1E-02	1.2E-01	6.3E-02
Al	3.6E-03	3.4E-02	9.3E-04	N/A	BDL	BDL	3.9E-03	1.3E-02
Fe	2.0E-05	8.2E-05	1.7E-04	3.7E-05	BDL	BDL	5.6E-05	3.8E-05
Pb	2.7E-02	1.9E-03	1.8E-02	2.6E-03	BDL	BDL	BDL	BDL
V	2.6E-04	1.1E-03	2.3E-03	9.1E-04	1.1E-02	2.4E-02	2.4E-03	1.0E-02
Mo	1.1E-01	1.1E-01	1.0E-01	1.1E-01	3.2E-01	3.4E-01	2.3E-01	4.0E-01
Cr	BDL	BDL	1.0E-04	8.1E-04	7.0E-04	2.0E-02	2.2E-05	7.6E-03
Cu	1.8E-03	2.3E-05	7.3E-04	8.3E-05	BDL	BDL	BDL	2.4E-05
Zn	1.8E-03	1.9E-03	3.5E-03	1.0E-03	BDL	BDL	BDL	BDL
Se	6.0E-03	8.8E-03	7.3E-03	7.9E-03	N/A	N/A	N/A	N/A
Mn	3.9E-05	1.3E-05	1.6E-05	4.3E-06	3.1E-06	BDL	BDL	BDL
Sb	3.3E-03	3.2E-03	2.6E-03	2.9E-03	8.9E-03	4.6E-02	5.8E-03	5.8E-03
Co	4.9E-03	1.4E-03	4.5E-03	1.7E-03	9.3E-04	5.9E-04	2.2E-03	1.4E-03
As	2.2E-04	2.4E-04	2.5E-04	1.0E-04	1.5E-03	8.2E-04	5.0E-04	5.0E-04
Te	6.2E-03	BDL	2.2E-02	1.1E-02	BDL	BDL	BDL	BDL
Bi	BDL	5.3E-05	3.7E-04	3.3E-05	BDL	BDL	BDL	BDL

[a]N/A: Result was inconclusive for unreacted solid sample, so percent leached could not be calculated.
[b]BDL: Concentration in supernatant was below detection limit, so percent leached could not be calculated.

4.3.1 pH trends with time

The pH of the FA was higher than ESCA for each experiment at all time points (**Figure 4.4**). Prior to initiating the experiments, the >18 MΩ H_2O and simulated rainwater solutions had pHs of *ca.* 7 and *ca*. 6.5, respectively. Within the first hour of leaching, the pH increased to an average of 12.18 $\pm$ 0.05 for all ESCA samples and an average of 12.73 $\pm$ 0.06 for all FA samples. A maximum pH of 12.31 $\pm$ 0.01 for the ESCA >18 MΩ H_2O closed system (ESCA-18 C) was observed at the 24 hr time point. A maximum pH of 12.56 $\pm$ 0.01 and 12.54 $\pm$ 0.03 for the ESCA rainwater (ESCA-RW) and ESCA >18 MΩ H_2O open system (ESCA-18 O) was observed at 14 d and 21 d, respectively. A maximum pH of 12.93 $\pm$ 0.00 and 12.86 $\pm$ 0.01 was reached at 14 d and 21 d for the FA >18 MΩ H_2O (FA-18) and FA rainwater (FA-RW) samples, respectively. The pH decreased toward the end of the experiment for all open experiments (after the 21 d time point). Early

stage coal ash samples ended at an average pH of 12.1 ± 0.2 at 3 mo. FA samples ended at an average pH of 12.44 ± 0.04 at 3 mo.

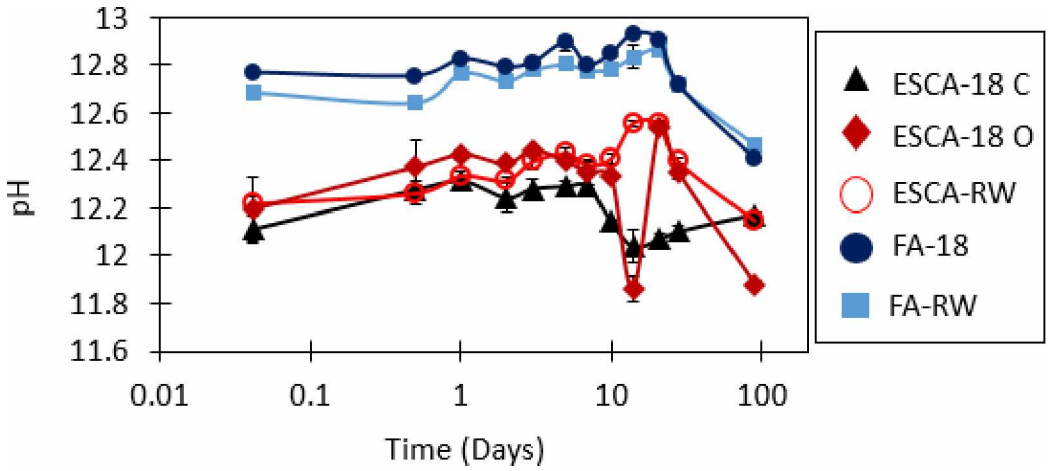

Figure 4.4 Trends in leachate pH with time.

4.3.2 Calcium leaching trends

Calcium concentrations observed in the FA leachates were higher by about a factor of 2 than the ESCA leachates, even though Ca content in the CCPs are relatively similar (21.6 wt.% CaO and 26.9 wt.% CaO for ESCA and FA, respectively). Calcium concentration trends in time were similar for all experiments and similar in shape to the pH trends observed (**Figure 4.5**). Fly ash Ca concentrations increased from 573.4 ± 12.3 mg L^{-1} to 645.7 ± 13.8 mg L^{-1} and 575.8 ± 7.6 mg L^{-1} to 712.9 ± 13.2 mg L^{-1} between 1 hr-7 d for the FA-RW and FA-18 experiments, respectively. Starting at day 7 and day 10, Ca concentrations sharply decreased to 197.1 ± 17.2 mg L^{-1} and 0.19 ± 0.01 mg L^{-1} for the FA-RW and FA-18 experiments, respectively. Fly ash leached Ca concentrations at 1 hr were statistically similar to one another regardless of the leachate. Early stage coal ash Ca concentrations appear to remain steady until 14 d at which point it decreased slightly. Fly ash Ca concentrations were similar to, and lower in the case of FA-18, than ESCA at the last time point (t=90 d). Calcium measured in the SPLP solutions were very similar to the concentrations measured for the FA and slightly lower for the ESCA.

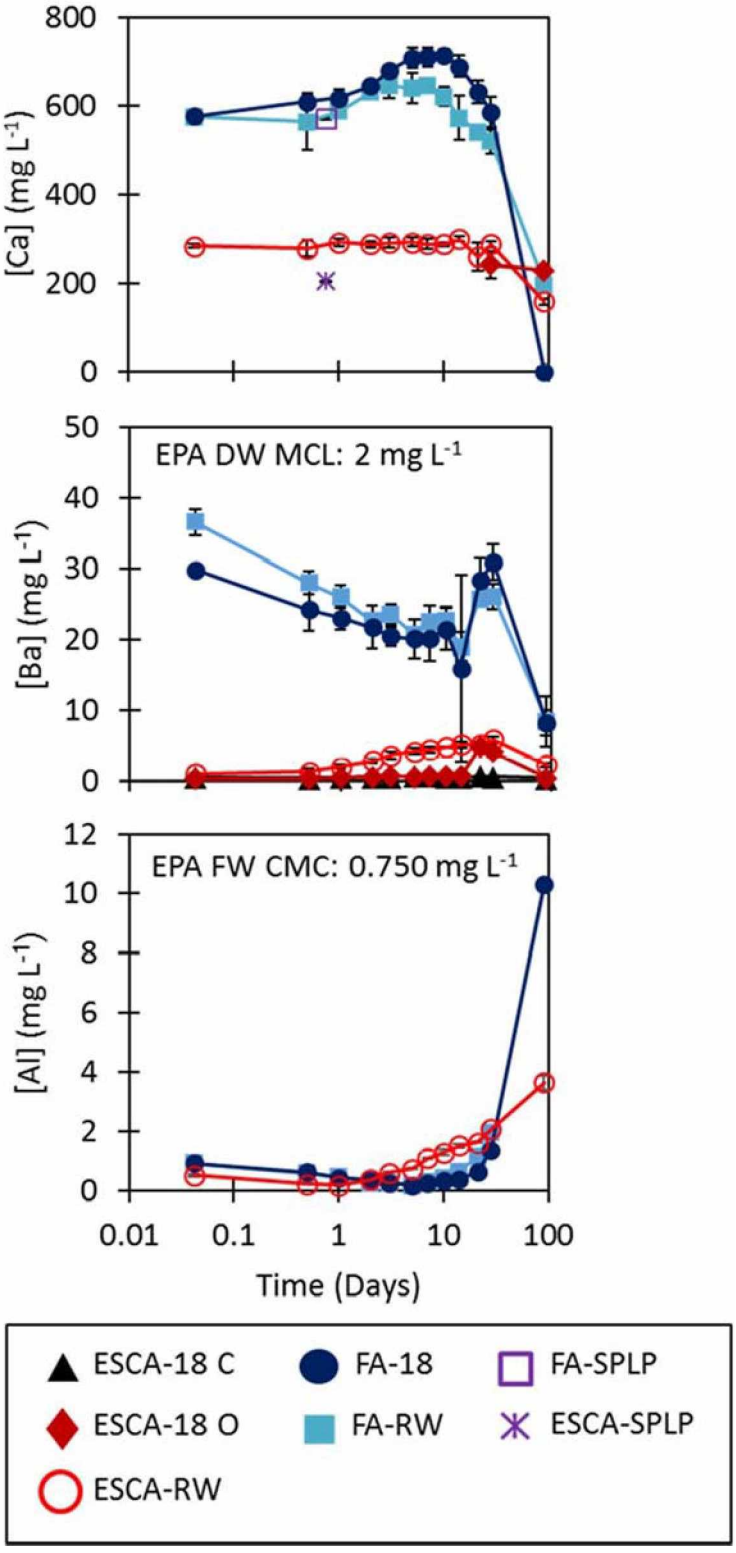

Figure 4.5 Major element (Ca, Ba, and Al) leaching results. Calcium concentrations for ESCA-18 C and most of ESCA-18 O are not presented because they were above the calibration curve for the ICP-MS run (2000 µg L^{-1}). Early stage coal ash-18 O 21 d-28 d samples are presented

Figure 4.5 (Cont'd) because they were run on Flame AA. Aluminum concentrations for ESCA-18 C and ESCA-18 O are not presented because they were above the calibration curve for the ICP-MS run (above 100 μg L^{-1}). 14 d-28 d ESCA-RW and FA-RW were ≥20% different from National Institute of Standards (NIST) reference. Environmental Protection Agency Drinking Water Maximum Contaminant Level (EPA DW MCL). Environmental Protection Agency Freshwater Criteria Maximum Concentration (EWP FW CMC).

4.3.3 Barium leaching trends

Barium leached concentrations were higher in the FA experiments than for the ESCA experiments even though Ba concentrations in the CCPs were similar (0.4 wt.% BaO and 0.55 wt.% BaO in ESCA and FA, respectively). Barium concentrations exceeded the EPA DW MCL for all fly ash time points, 1 d-3 mo for ESCA-RW, and 21 d-28 d ESCA-18 O experiments (**Figure 4.5**). ESCA-18 C Ba concentrations were invariant with time (0.5 ± 0.1 mg L^{-1} average Ba), while ESCA-RW Ba concentrations steadily increased from 1.04 ± 0.02 mg L^{-1} Ba at day 1 to 5.8 ± 0.4 mg L^{-1} Ba at 28 d, at which point they decreased close to the concentrations observed at the 1 hr time point. Similarly, ESCA-18 O Ba concentrations increased to 4.7 ± 0.4 mg L^{-1} Ba at 21 d and then decreased close to the starting concentrations (0.34 ± 0.07 mg L^{-1} Ba). Fly ash Ba concentrations (initially 36.6 ± 1.9 mg L^{-1} and 29.9 ± 0.5 mg L^{-1} for FA-RW and FA-18, respectively) decreased from 1 hr-14 d before they increased to 28 d and then decreased dramatically at 90 d to a final concentration of *ca.* 8 mg L^{-1}. Ba concentrations for the 7 d and 3 mo time points were statistically similar for both FA experiments, and the ESCA-18 O and ESCA-18 C experiments.

4.3.4 Aluminum leaching trends

Fly ash leached Al concentrations started slightly higher than ESCA leached Al concentrations and ended much higher even though both CCPs started with similar concentrations of Al (FA 11.4 wt.% Al_2O_3 and 10.5 wt.% Al_2O_3 in FA and ESCA, respectively) (**Figure 4.5**). Aluminum concentrations exceeded EPA Freshwater Criterion Maximum Concentrations (EPA FW CMCs; [Al] > 0.75 mg L^{-1})[64] for the 1 hr time points for both FA experiments and then fell below EPA FW CMC levels. Until after 21 d and 28 d for the FA-RW and FA-18 experiments, respectively, at which time it increased dramatically to more than 10 times the EPA FW CMC. Environmental

Protection Agency FW CMC levels were exceeded for ESCA-RW after 5 d. There was not an observable increase in leached Al concentrations for ESCA or FA until 2 d and 7 d respectively. It was determined that FA 1 hr and 7 d concentrations were statistically similar regardless of the leachate.

4.3.5 Iron leaching trends

Unlike most metals, Fe exhibited different behavior between the experiments with the same CCP (**Figure 4.6**). Initial Fe concentrations in the ESCA and FA before leaching were similar (7.13 wt.% Fe_2O_3 and 9.78 wt.% Fe_2O_3, respectively). Early stage coal ash-RW and FA-RW leaching trends appear to be similar, albeit at different concentrations, with relatively consistent concentrations until day 10 (12.3 ± 1.3 μg L^{-1} and 54.8 ± 1.8 μg L^{-1} for ESCA-RW and FA-RW, respectively), after which there is a slight increase in measured Fe followed by a dramatic decrease at day 90. Fly ash-18 exhibits a different trend and at much lower concentration than that of the FA-RW, in which concentrations of Fe are relatively consistent at ca. 7 μg L^{-1} until day 5, followed by a slight decrease and then a marked increase at day 90. Concentrations for 1 hr, 7 d, and 3 mo time points were not statistically similar for either CCP.

4.3.6 Lead leaching trends

Fly ash-18 Pb concentrations exceeded EPA FW CMCs levels for the 1 hr time point and FA-18 and FA-RW Pb concentrations exceeded EPA DW TT ALs for all time points except 3 mo. Lead concentrations in unreacted ESCA and FA were 15 mg kg^{-1} and 140 mg kg^{-1}, respectively. Lead concentrations were BDL for ESCA-18 C and ESCA-18 O time points and not analyzed in the ESCA-RW leachates (**Figure 4.6**). Lead concentrations were initially high (up to 70 μg L^{-1}) and decreased throughout the experiment to ca. 2.6 μg L^{-1} at 90 d. Lead concentrations for the FA experiments were statistically similar for the 3 mo time point, but statistically different for 7 d. Synthetic precipitation leaching procedure results appear to be in agreement with the simulated rainwater leaching results for both FA and ESCA.

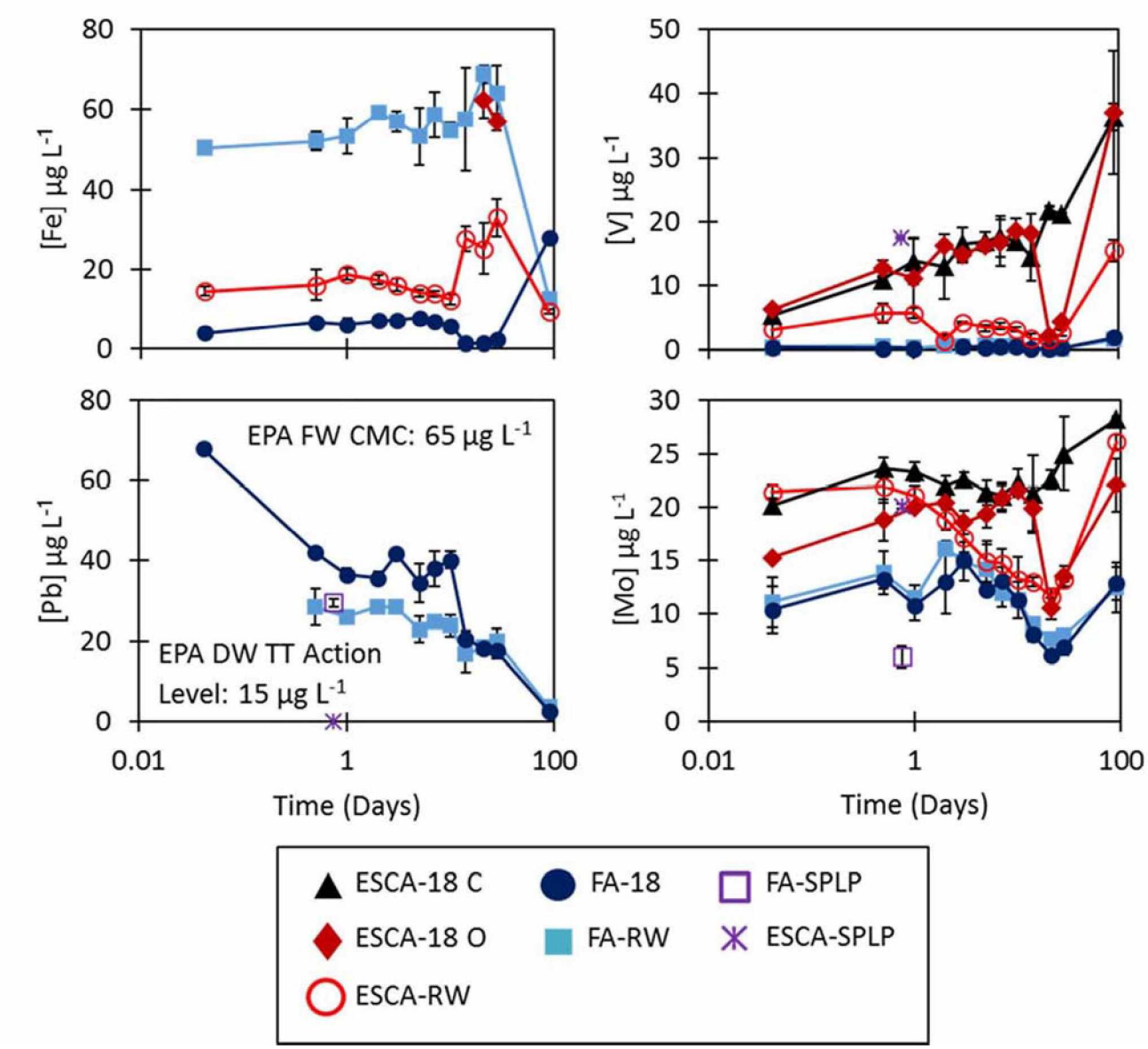

Figure 4.6 Iron, Pb, V, and Mo leaching results. Iron was not measured for ESCA-18 C experiments and was below detection limit for the majority of ESCA-18 O experiments. Lead concentrations were below detection limit for all ESCA-18 C and ESCA-18 O samples and were not analyzed for ESCA-RW. Lead concentrations were ≥20% different from National Institute of Standards (NIST) reference for 1 hr-10 d for FA-18. Vanadium concentrations were below detection limit for 2 d FA-18 and 14 d FA-RW samples. Environmental Protection Agency Freshwater Criteria Maximum Concentration (EPA FW CMC). Environmental Protection Agency Drinking Water Treatment Technique Action Level (EPA DW TT Action Level).

4.3.7 Vanadium leaching trends

Unlike many other elements, ESCA V leachate concentrations were higher than FA V in all experiments, despite the similar unreacted CCPs content (160 mg kg^{-1} and 152 mg kg^{-1}, respectively). ESCA-18 C experiments were typified by increasing V concentrations throughout the experiment (**Figure 4.6**). Early stage coal ash-18 O also increased but only until 14 d when there was a sharp decrease in V concentration until the last time point. Early stage coal ash-18 C and ESCA-18 O concentrations were statistically similar for 1 hr, 7 d, and 3 mo time points. ESCA-RW exhibited much lower V concentrations throughout the experiment, but had a similar increased concentration at the last time point. Fly ash V leached concentrations were low, sometimes BDL, and remained fairly constant until 28 d-3 mo where there was a slight increase in concentration. Fly ash-18 and FA-RW concentrations were statistically similar for 1 hr, 7 d, and 3 mo in addition to being statistically similar to the ESCA-RW 1 hr leached concentrations. Vanadium concentrations in SPLP leachates for the FA were BDL and higher than the ESCA-RW leachate concentrations.

4.3.8 Molybdenum leaching trends

Molybdenum leachate concentrations were higher in ESCA experiments relative to FA experiments (**Figure 4.6**), despite similar Mo contents in unreacted ESCA and FA (6.5 mg kg^{-1} and 11.4 mg kg^{-1}, respectively). Almost all experiments exhibit an increase in Mo concentration between 1 hr and 12 hr, then the ESCA-18 C, ESCA-RW, and FA samples decrease while ESCA-18 O continues to increase to day 10. Small fluctuations are observed between timepoints until day 21, at which time a minimum concentration is reached for all experiments. Concentrations then increase again until day 90, at which time all concentrations are slightly higher than at 1 hr. Fly ash experiment leached Mo concentrations are statistically similar for 1 hr and 7 d. Leached ESCA-RW Mo concentrations were statistically similar to FA experiments for the 7 d time point. Leached Mo concentrations for FA-RW and ESCA-18 O experiments were statistically similar for the 3 mo time point. Synthetic precipitation leaching procedure Mo concentrations were below both the ESCA-RW and FA-RW leached Mo concentrations.

4.3.9 Chromium leaching trends

Leached Cr concentrations were higher for ESCA than for FA, although total Cr concentrations were similar for ESCA and FA (82 mg kg^{-1} and 85 mg kg^{-1}, respectively). Leached Cr concentrations did not exceed EPA DW MCLs or FW CMCs during any of the experiments. Chromium leaching trends appeared to be similar to that of Al, albeit at lower concentrations, with initial low concentrations that increase with time (**Figure 4.7**). Early stage coal ash-18 C concentrations began to exponentially increase after 1 d. Early stage coal ash-18 O and ESCA-RW Cr concentrations decreased from 1 hr-28 d, and then sharply increased from 28 d-3 mo. The majority of FA Cr concentrations were BDL (*ca.* 0.7 µg L^{-1}). Chromium concentrations at 7 d were statistically similar for the FA-RW and ESCA-RW experiments. Chromium concentrations at 3 mo were statistically similar for ESCA-18 open and closed experiments. Synthetic precipitation leaching procedure Cr concentrations were higher than the ESCA-RW leached Cr concentrations, and were BDL for FA which is consistent with the near detection limit Cr concentrations for the FA-RW experiment.

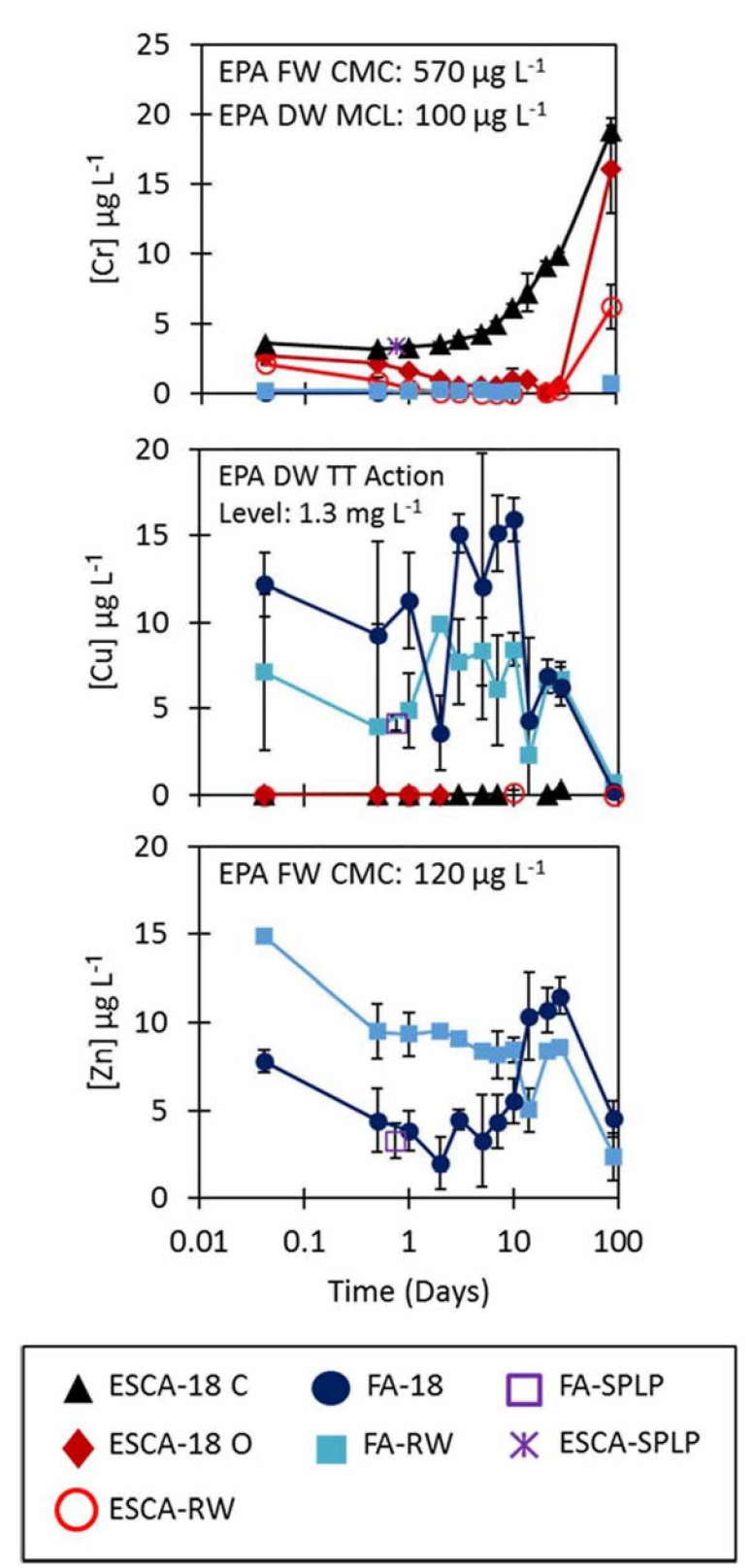

Figure 4.7 Chromium, Cu, and Zn leaching results. Chromium concentrations were ≥20% different from National Institute of Standards (NIST) reference for 1 hr-28 d for ESCA-18 C. Chromium concentrations were also below detection limit for 14 d ESCA-RW, 2 d-90 d FA-18,

Figure 4.7 (Cont'd) and 14 d-28 d FA-RW. Copper concentrations were below detection limit for 7 d-14 d for ESCA-18 C, 3 d-90 d for ESCA-18 O, 0.5 d for ESCA-RW, 2 d-7 d for ESCA-RW, and 14 d-28 d for ESCA-RW. Zinc concentrations were below detection limit for ESCA-18 C and ESCA-18 O and were not analyzed for ESCA-RW. Environmental Protection Agency Drinking Water Maximum Contaminant Level (EPA DW MCL). Environmental Protection Agency Freshwater Criteria Maximum Concentration (EPA FW CMC). Environmental Protection Agency Drinking Water Treatment Technique Action Level (EPA DW TT Action Level).

4.3.10 Copper leaching trends

The majority of time points for ESCA experiments were BDL, which is somewhat surprising since total concentrations of FA and ESCA are less than an order of magnitude different (840 mg kg^{-1} and 114.5 mg kg^{-1}, respectively). All leached Cu concentrations were below EPA Drinking Water Treatment Technique Action Levels (EPA DW TT AL)[64]. There is not a clear leaching trend for FA Cu leached concentrations, which ranged from 12.2 $\pm$ 1.8 µg L^{-1} to 0.18 $\pm$ 0.14 µg L^{-1} and 7.1 $\pm$ 4.5 µg L^{-1} to 0.69 $\pm$ 0.20 µg L^{-1} for the FA-18 and FA-RW, respectively. Fly ash experiments 1 hr and 3 mo concentrations were statistically similar (**Figure 4.7**). Leached Cu concentrations for the FA-SPLP were in agreement with those observed for the FA-RW experiment. Leached Cu concentrations for the ESCA-SPLP were BDL, which is consistent with the near detection limit concentrations of Cu leached during the ESCA-RW experiment.

4.3.11 Zinc leaching trends

In the unreacted CCPs, Zn contents were 25.00 mg kg^{-1} in ESCA and 237 mg kg^{-1} in FA. Zinc concentrations never exceeded EPA FW CMC values (**Figure 4.7**). Zinc concentrations were BDL in the ESCA-18 C and ESCA-18 O leachates and it was not analyzed for in the ESCA-RW leachate. Fly ash-RW Zn concentrations consistently decreased, similar to the trend seen for Pb. Zinc concentrations are lower for the FA-18 experiment than the FA-RW experiment, after 10 d, however, the Zn concentrations for the 3 mo time point are statistically similar. Leached Zn concentrations from the FA-SPLP were *ca.* 5 µg L^{-1} lower than those observed in the FA-RW experiment. Early stage coal ash-SPLP Zn concentrations were BDL, which is consistent with the BDL Zn concentrations in the ESCA-RW experiments.

4.3.12 Selenium leaching trends

Selenium leaching trends are unique in that there is only a small variation in concentrations for all experiments at all time points and all experiments have statistically similar concentrations for 1 hr, 7 d, and 3 mo time points (**Figure 4.8**). The exception to this is ESCA-18 C, which has a statistically lower concentration at 90 d. Selenium content of the unreacted CCPs were BDL and 16 mg kg^{-1} for ESCA and FA, respectively, and Se leachate concentrations do not exceed the EPA DW MCL. Leached Se concentrations for the ESCA-SPLP were in agreement with the results of the ESCA-RW experiment. Leached Se concentrations for the FA-SPLP were lower than those seen in the FA-RW experiment.

4.3.13 Manganese leaching trends

Manganese concentrations did not exceed 2 µg L^{-1} for any time points for any experiments, but were higher in the FA experiments relative to the ESCA experiments (**Figure 4.8**). Total Mn concentrations are somewhat lower in the ESCA relative to the FA, 0.11 wt.% MnO and 0.36 wt.% MnO, respectively. Manganese concentrations decreased slightly from 1 hr-12 hr for ESCA-18 O experiments and then exhibited little variation (range = 0.04 µg L^{-1} to 0.02 µg L^{-1}) for the remainder of the experiment. Manganese concentrations exhibited small variations (range= *ca*. 1 µg L^{-1} to 2 µg L^{-1}) for the FA experiments and do not exhibit a clear leaching trend. Fly ash leached Mn concentrations at 1 hr and 7 d were statistically similar regardless of leachate. Fly ash manganese concentrations appeared to decrease overall, they were lower at 3 mo than at 1 hr. Early stage coal ash-18 O leached Mn concentrations were determined to be statistically similar to FA-RW leached Mn concentrations for 1 hr and 7 d time points. Leached Mn concentrations from the FA-SPLP were *ca*. 2 µg L^{-1} higher than those observed in the FA-RW experiment.

4.3.14 Antimony leaching trends

The unreacted ESCA contains an order of magnitude less Sb than FA (3.8 mg kg^{-1} and 27 mg kg^{-1}, respectively). Early stage coal ash-18 O Sb concentrations decrease from 1hr-12hr and then steadily increase up to 3mo, while ESCA-18 C and ESCA-RW initially have lower concentrations,

but similarly exhibit a steady increase from 1hr-3mo, although it is less pronounced for the ESCA-RW (**Figure 4.8**). FA concentrations are higher at 1 hr for both experiments than that of the ESCA but end lower than the ESCA-18 C and ESCA-18 O experiments. Fly ash Sb concentrations end slightly lower than the 1hr time point. Early stage coal ash-18 O Sb concentrations are statistically similar to both FA experiment Sb concentrations at the 1hr and 3mo time points. Early stage coal ash-18 open and closed experiment Sb concentrations were statistically similar for the 1hr time point. Fly ash experiment Sb concentrations were statistically similar for the 1hr and 3mo time points. The Sb EPA DW MCL are never not exceeded.

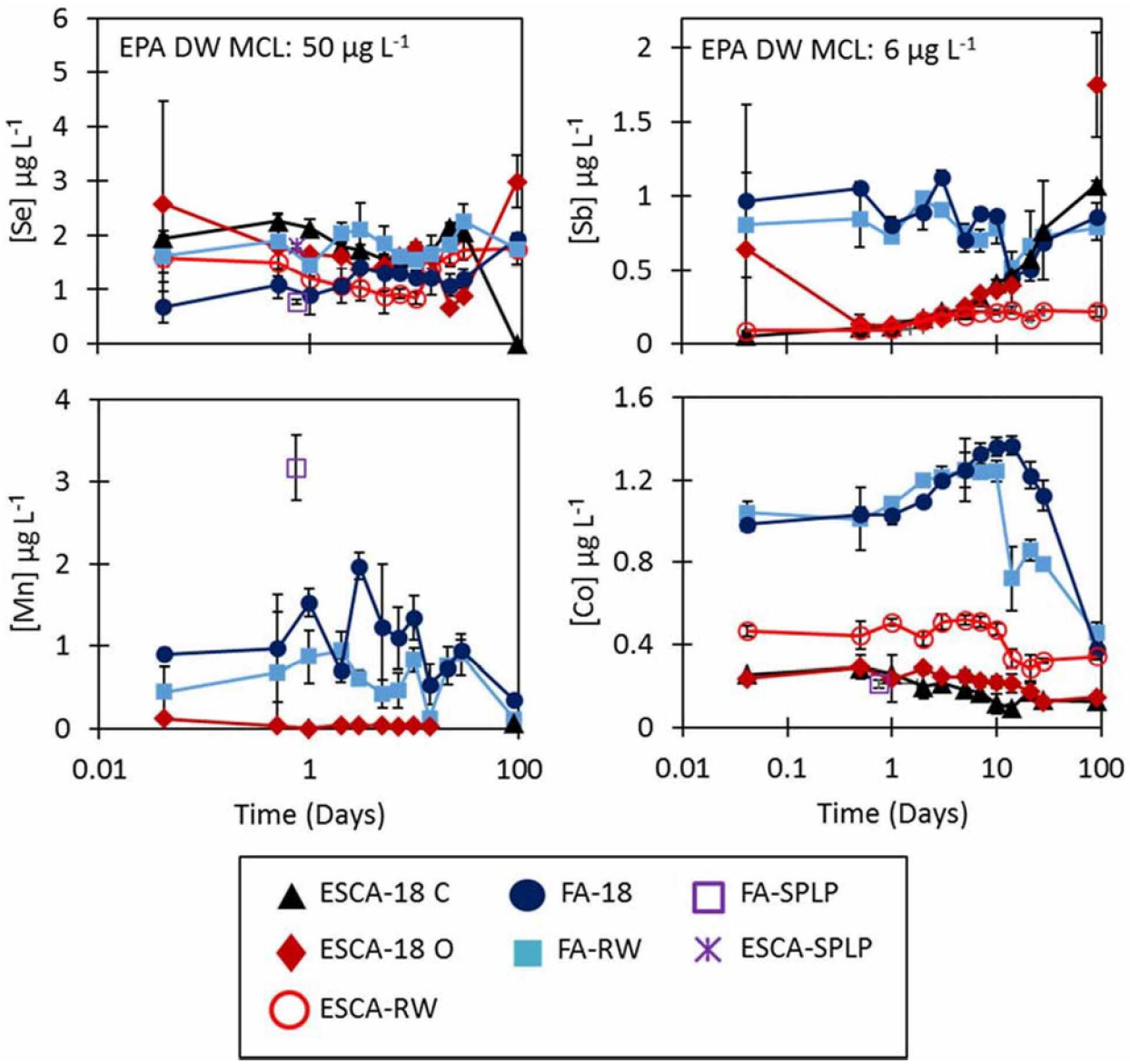

Figure 4.8 Selenium, Mn, Sb, and Co leaching results. Manganese concentrations for ESCA-18 C and ESCA-RW were below detection limit. Antimony concentrations were below detection limit for 21 d-28 d ESCA-18 O. Environmental Protection Agency Drinking Water Maximum Contaminant Level (EPA DW MCL).

4.3.15 Cobalt leaching trends

Cobalt leaching trends were similar to Ca, with measured leachate concentrations substantially lower for ESCA than for FA, despite similar amounts of Co in unreacted solids (23.7 mg kg^{-1} and 27.4 mg kg^{-1}, respectively). Early stage coal ash experiments were consistently *ca.* <0.5 µg L^{-1} for all experiments. Fly ash experiments were initially steady, increased slightly after 1 d, and showed a more significant decrease in Co concentrations after 14 d than the decrease seen in

ESCA experiments (**Figure 4.8**). Early stage coal ash-18 C and ESCA-18 O Co concentrations were statistically similar for 1 hr, 7 d, and 3 mo time points, while FA Co concentrations were statistically similar for 1 hr and 3 mo time points. Leached Co concentrations did not exceed 1.5 μg L^{-1} for either CCP. Leached Co concentrations for the FA-SPLP were *ca*. 1 μg L^{-1} lower than those observed in the FA-RW experiment. Leached Co concentrations for the ESCA-SPLP were BDL.

4.3.16 Arsenic leaching trends

Total As in the unreacted ESCA and FA were 11 mg kg^{-1} and 124.5 mg kg^{-1}, respectively. Arsenic concentrations did not exceed EPA FW CMCs or EPA DW TT ALs in any leachates (**Figure 4.9**). There is no discernable trend in As concentrations, similar to Se, and the majority of As concentrations were statistically similar for 1 hr, 7 d, and 3 mo time points with the exception of 3 mo FA-18 and FA-RW and 3 mo ESCA-18 C and ESCA-18 O. Leached As concentrations from the ESCA-SPLP were *ca*. 0.15 μg L^{-1} higher than those observed in the ESCA-RW experiment. Leached As concentrations from the FA-SPLP were BDL.

4.3.17 Tellurium leaching trends

Tellurium concentrations in unreacted ESCA and FA were low, 0.10 mg kg^{-1} and 0.65 mg kg^{-1}, respectively. Early stage coal ash-18 C and ESCA-18 O Te concentrations were BDL for all time points, and Te concentrations were not analyzed in the ESCA-RW (**Figure 4.9**). Several time points for FA-18 were also BDL. Tellurium concentrations remained steady in the FA-RW experiment with the exception of a slight increase after 10 d and then a decrease after 21 d. 3 mo Te concentrations were lower than 1 hr concentrations.

4.3.18 Bismuth leaching trends

Total concentrations of Bi in ESCA and FA were low (0.5 mg kg^{-1} and 3.0 mg kg^{-1}, respectively). Thus, it is not surprising that Bi concentrations were BDL for all ESCA-18 C and ESCA-18 O time points and the majority of time points for ESCA-RW and FA-RW (**Figure 4.9**). Interestingly, there is a spike of 0.5 μg L^{-1} for 7 d-21 d for the FA-RW. However, a Grubb's test for outliers was

performed and it was determined this point was a significant outlier. Further, Bi contamination is commonly due to the use of makeup by users, which is a possible source of the anomalous Bi (Rodushkin et al., 2010; Knight et al., 2017).

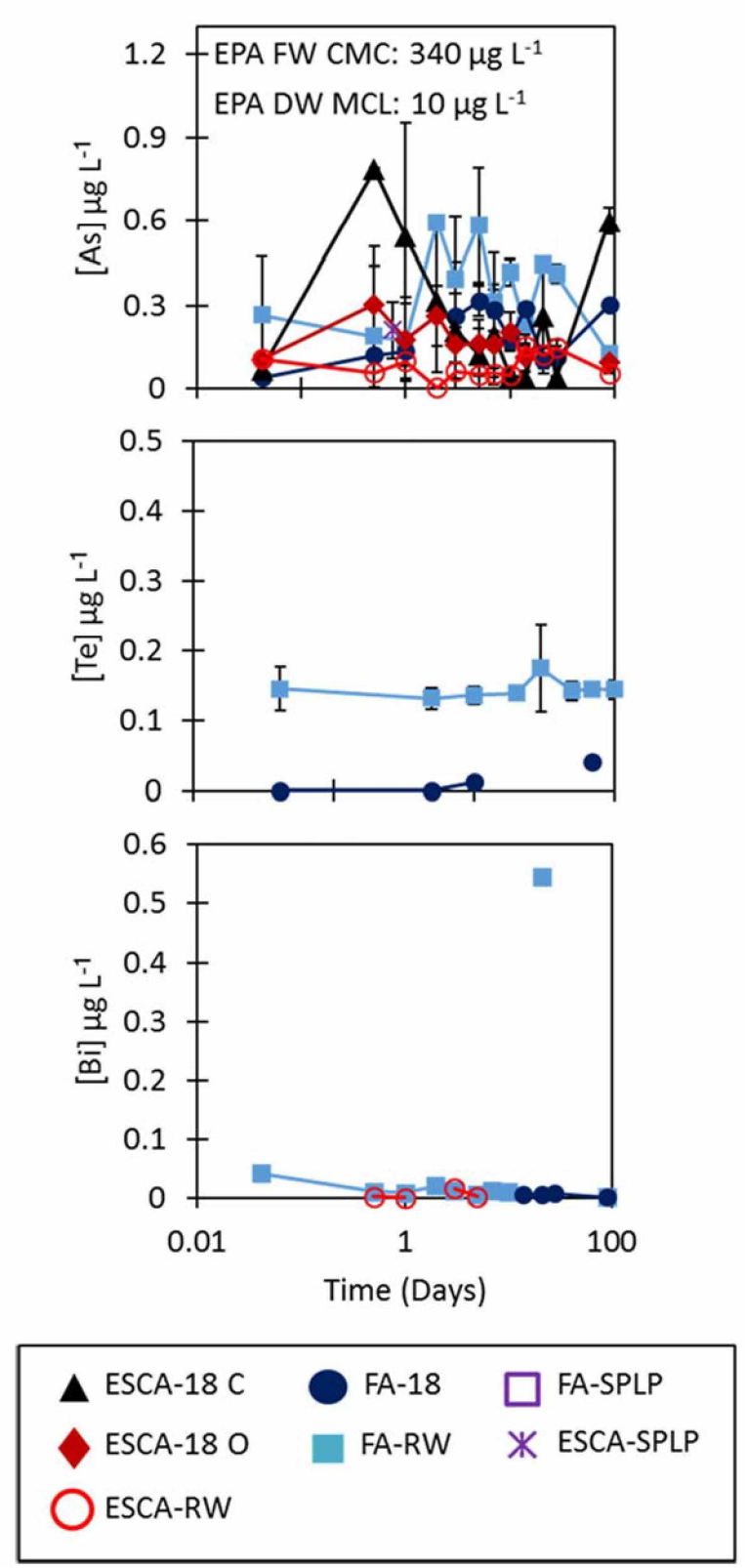

Figure 4.9 Arsenic, Te, and Bi leaching results. Arsenic concentrations were below detection limit for 21 d-28 d for ESCA-18 O and 2 d for FA-18. Tellurium concentrations were below detection limit for all ESCA-18 C and ESCA-18 O time points and was not analyzed for ESCA-RW.

Figure 4.9 (Cont'd) Tellurium concentrations were below detection limit for 1 hr-12 hr, 2 d-5 d, 10 d, and 90 d for FA-18. Bismuth concentrations were below detection limit for all ESCA-18 C and ESCA-18 O time points, 2 d ESCA-RW, 7 d-90 d ESCA-RW, 1 hr-10 d FA-18, 14 d FA-RW, and 28 d-90 d FA-RW. Environmental Protection Agency Drinking Water Maximum Contaminant Level (EPA DW MCL). Environmental Protection Agency Freshwater Criteria Maximum Concentration (EPA FW CMC).

4.4 Initial coal combustion product-dissolved organic matter leaching observations

Seven-day closed leaching experiments with CCPs in solutions of DOM isolates were used to assess the influence of dissolved organic carbon content and quality on metal(loid) release from CCPs. The color of the solutions was one of the most apparent changes before and after leaching. Before leaching, solutions were light yellow/brown in color, reflecting the initial color of the made-up solutions of DOM isolates. After 7 d of leaching, upon filtration of the supernatant, the solutions were observed to be colorless (UV/Vis absorbance was not run on these solutions to quantify the extent of color loss). This suggests that either the initially dissolved organic matter became associated with the solid phase during the experiment, through either sorption to CCP particles or aggregation, or that the DOM transformed so much as to alter its chromophoric properties to render it colorless.

The pH of all DOM solutions had increased when samples were harvested after 7 d (**Table 4.6**)**.** All DOM solutions started at roughly the same pH (**Table 4.6**). Early stage coal ash Suwannee River fulvic acid (SRFA) and ESCA Goldstream organic matter extract (GSE) leaching experiments ended at a pH of *ca.* 12.8., while the FA SRFA and FA GSE experiments ended at a slightly higher pH of 13.3. The pH of the ESCA Pony Lake fulvic acid (PLFA) and FA PLFA solutions ended at *ca*. 12.5. Final pH values are similar to those observed for the >18 MΩ H_2O and simulated rainwater leachates at 7 d (**Figure 4.4**).

Table 4.6 Starting pH measurements of DOM solutions. Pony Lake Fulvic Acid (PLFA); Suwannee River Fulvic Acid (SRFA); Goldstream Extract (GSE).

[DOC] mg C L^{-1}	PLFA	[a]SRFA	GSE
0	*ca* . 7	*ca* . 7	*ca* . 7
5	4.70	----	4.86
10	4.48	----	4.44
20	4.19	----	4.18
50	3.91	----	3.85
100	3.71	3.45	3.50

[a]pH was only measured with leftover DOM solution after leaching experiment was set up, and so for some SRFA samples, there was not enough volume left over to measure the pH except for the 100 mg C L^{-1} solution.

The degree of leaching over the 7 d period for the elements measured varied with respect to element and DOM isolate used. Percent leached was determined as the concentrations found in the supernatants divided by the initial concentrations in the unreacted samples, times 100. For both CCPs, Ca had the highest percentage leached out of all metal(loid)s listed with the exception of Mo for ESCA (**Table 4.7**). The percent leached metal(loid)s for FA were higher for Ca, Fe, Mn, Sb, As, Zn, and Co than for ESCA, but lower for Mo, Se, V, and Te than ESCA for nearly all of the DOM isolates (**Table 4.7**), which also correlated with overall trends in observed leachate concentrations between ESCA and FA experiments.

While Al, Ba, Cd, Cr, Cu, and Pb concentrations were reported for the experiments in section 4.3, these are not reported for the DOM experiments. Cadmium leachate concentrations were BDL for all DOM solutions at all carbon concentrations, and Cr leachate concentrations were BDL for nearly all DOM solutions at all carbon concentrations. The exceptions were for Cr in the presence of PLFA, where for ESCA, Cr leachate concentrations were above detection limits but < 0.1 µg L^{-1} up to 20 mg C L^{-1}, and above detection limit but < 0.015 µg L^{-1} for the lowest carbon concentration for FA. Aluminum and Ba were outside the upper limit of the calibration curve of 100 µg L^{-1}. Copper and Pb both failed calibration checks and could not be used quantitatively.

Total organic carbon analysis performed on the DOM solutions before leaching revealed the presence of slightly different carbon concentrations than 0, 5, 10, 20, 50, and 100 mg C L^{-1}.

Actual 100 mg C L^{-1} solutions contained 75.6 mg C L^{-1}, 90.5 mg C L^{-1}, and 94.2 mg C L^{-1} for the PLFA, SRFA, and GSE, respectively. However, for simplicity, these solutions will still be referred to as 0, 5, 10, 20, 50, and 100 mg C L^{-1}.

Table 4.7 Percent leached of elements for 100 mg C L^{-1} DOM solutions after 7 days. These are in order of highest to lowest leachate concentrations of the controls in section 4.3.

DOM Medium	PLFA		SRFA		GSE	
Ash Leached	ESCA	FA	ESCA	FA	ESCA	FA
Calcium	1.6E-01	3.5E-01	2.1E-01	3.5E-01	2.2E-01	3.5E-01
Iron	2.1E-04	4.7E-04	3.5E-04	4.7E-04	1.4E-04	3.0E-04
Vanadium	4.9E-03	2.3E-04	4.1E-03	1.9E-04	2.7E-03	1.9E-04
Molybdenum	5.7E-01	BDL	3.8E-01	9.5E-02	3.0E-01	6.7E-02
Cobalt	BDL	4.1E-04	1.8E-03	3.4E-03	1.3E-03	2.8E-03
Zinc	BDL	4.4E-03	BDL	3.6E-03	BDL	BDL
Selenium	N/A	BDL	N/A	1.0E-02	N/A	2.8E-03
Manganese	7.9E-06	1.0E-04	1.7E-05	7.2E-05	BDL	4.6E-05
Antimony	BDL	3.0E-03	BDL	2.3E-03	BDL	1.1E-03
Arsenic	BDL	2.0E-04	BDL	2.7E-04	BDL	BDL
Tellurium	1.2E-02	9.2E-03	3.9E-03	8.7E-03	1.2E-02	7.5E-03

[a]N/A: Result was inconclusive for unreacted solid sample, so percent leached could not be calculated.
[b]BDL: Concentration in supernatant was below detection limit, so percent leached could not be calculated.

4.4.1 Calcium-dissolved organic matter leaching

Calcium was present in the highest concentrations out of all the elements leached from the ESCA or FA for all DOM solutions (**Figure 4.10**). The highest ESCA Ca concentrations are observed for the GSE, while the lowest are observed for the PLFA. Leached Ca concentrations in the presence of FA are statistically similar for SRFA and GSE but not PLFA. While a higher concentration of leached Ca between the highest [DOC] and control (0 mg C L^{-1}) was observed for ESCA, overall Ca concentrations do not appear to have a strong dependence on carbon concentration for either CCP. In fact, Ca concentrations for FA for all DOM solutions are statistically similar for 5-20 mg C L^{-1}, while for ESCA, they are statistically similar for 5, 50, and 100 mg C L^{-1}. Early stage coal ash Ca concentrations are also statistically similar for 10-20 mg C L^{-1} but these concentrations are statistically different from those observed for 5, 50, and 100 mg C L^{-1}.

4.4.2 Iron-dissolved organic matter leaching

For Fe leached from ESCA in the presence of DOMs, SRFA displayed the highest leached iron concentrations compared to the other two isolates (**Figure 4.10**). For FA, both fulvic acids displayed the highest leached Fe concentrations overall. While there does not a appear to be a change in ESCA Fe leached for the SRFA solution for DOC concentrations up to ca. 20 mg C L^{-1} leached, Fe increases for the highest SRFA concentrations. However, in FA, SRFA Fe concentrations slightly decrease upon the addition of carbon. Both the PLFA and GSE solutions appear to show similar decreasing trends with increasing carbon concentrations for ESCA, but only GSE shows a decreasing trend with increasing [DOC] for FA.

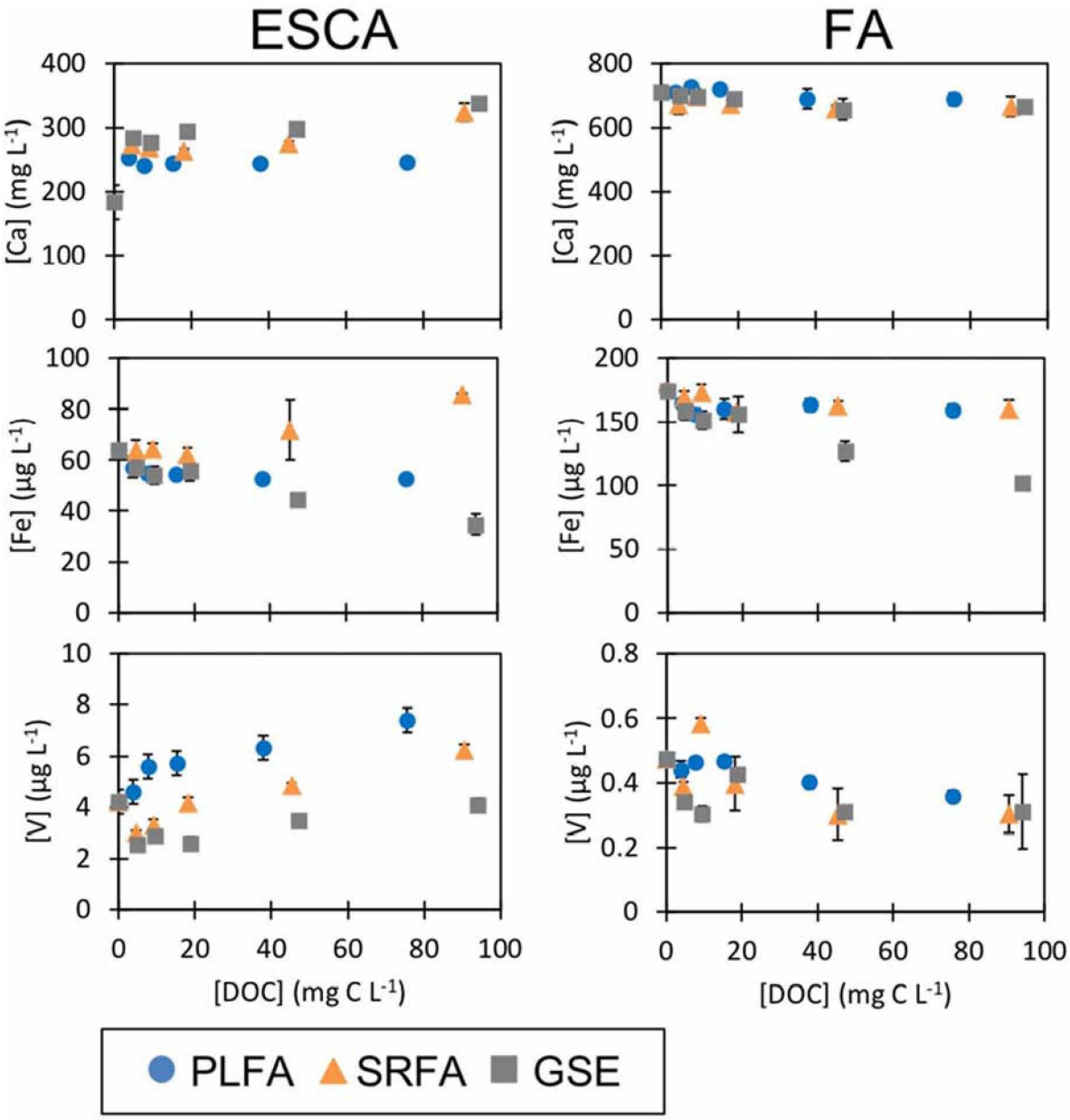

Figure 4.10 Seven-day leachate concentrations for Ca, Fe, and V for CCPs in the presence of DOM isolates.

4.4.3 Vanadium-dissolved organic matter leaching

The highest concentrations of ESCA V leached are seen in the PLFA, then SRFA, and lastly GSE. However, for FA, differences in V leachate concentrations between the isolates are less pronounced (**Figure 4.10**). Overall, ESCA V concentrations increase with increasing [DOC], with the exception of V leachate concentrations dipping below the control upon added SRFA and GSE. These increases with increasing [DOC] are not observed for the FA, where V leachate concentrations appear to decrease with increasing carbon concentrations.

4.4.4 Molybdenum-dissolved organic matter leaching

The highest concentrations of ESCA Mo leached are seen in the PLFA, then SRFA, and lastly GSE, while for the FA, highest Mo concentrations are seen in the SRFA, then GSE, and lastly PLFA (**Figure 4.11**). In fact, Mo concentrations for FA in presence of PLFA were BDL for [DOC] over 20 mg C L^{-1}. Overall, ESCA Mo concentrations appear to increase with increasing [DOC] for all isolates. However, for FA, increases with increasing [DOC] do not appear to be observed, and in the presence of PLFA, Mo sharply decreases with increasing [DOC].

4.4.5 Cobalt-dissolved organic matter leaching

Cobalt leachate concentrations appear to follow similar trends for both CCPs (**Figure 4.11**). SRFA and GSE yield the highest Co leachate concentrations, while PLFA yields the lowest leachate concentrations and a steadily decreasing trend with increasing [DOC], falling BDL for the highest mg C L^{-1} PLFA solution for ESCA. Cobalt concentrations for ESCA slightly decrease in SRFA and GSE at [DOC] up to 20 mg C L^{-1}, and then appear to increase slightly for SRFA and decrease slightly for GSE. However, for the FA, Co concentrations in SRFA and GSE initially drop at lower [DOC] and then remain steady with increasing [DOC].

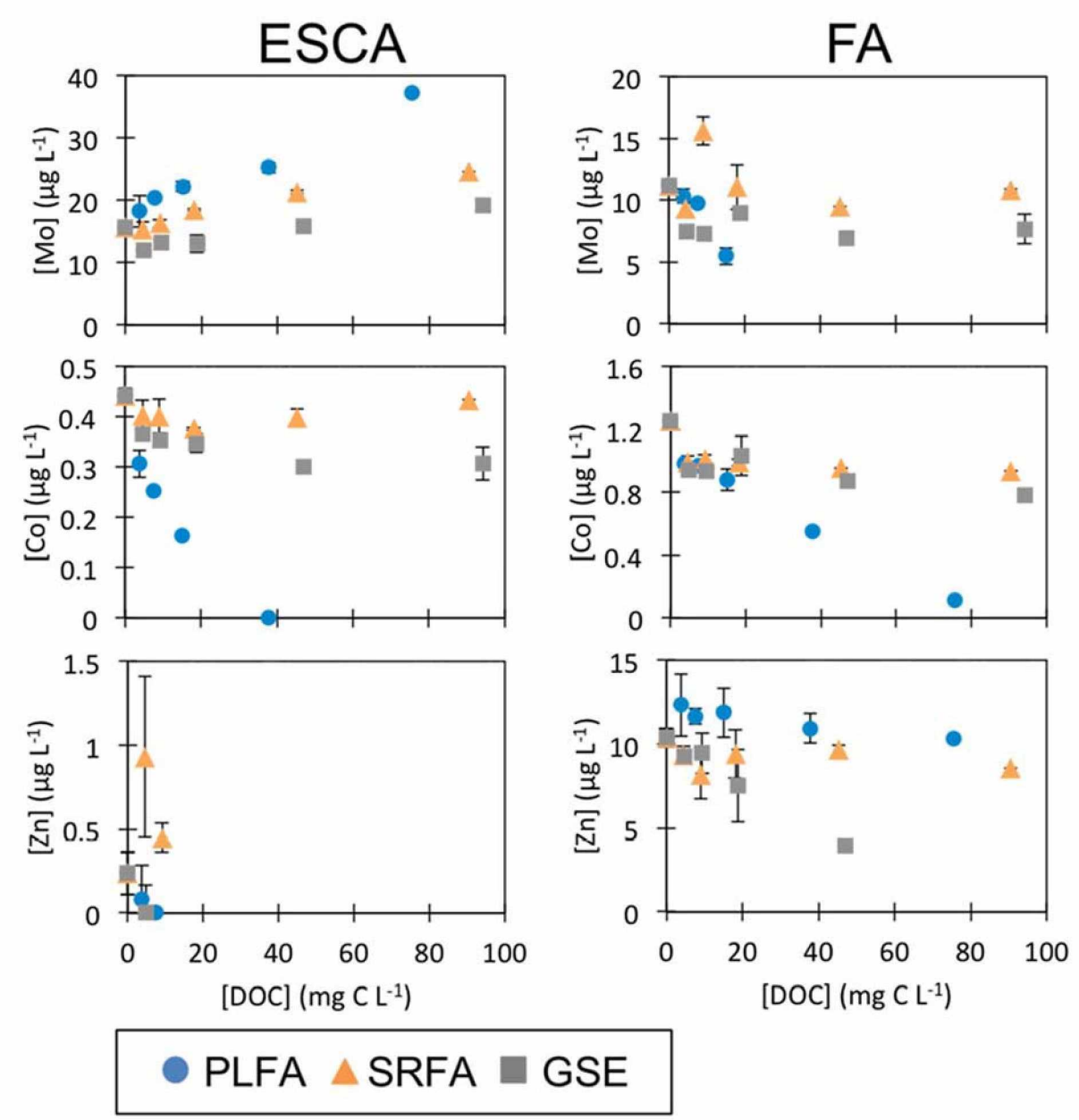

Figure 4.11 Seven-day leachate concentrations for Mo, Co, and Zn for CCPs in the presence of DOM isolates.

4.4.6 Zinc-dissolved organic matter leaching

All ESCA Zn concentrations were BDL for all DOM solutions above 20 mg C L^{-1} (**Figure 4.11**). Early stage coal ash Zn concentrations increase with increasing [DOC] initially for SRFA, but then decrease with increasing [DOC]. However, for the FA, measurable concentrations were detected for nearly all carbon concentrations. The highest Zn leachate concentrations for FA occur in the presence of PLFA. Zn leachate concentrations in PLFA appear to increase relative to

the control (0 mg C L^{-1}) upon carbon addition, but then decrease slightly with increasing carbon concentrations. Zinc leachate concentrations for FA in the presence of SRFA do not appear to show clear trends, but for GSE Zn leachate concentrations appear to decrease with increasing [DOC], falling BDL for 100 mg C L^{-1}.

4.4.7 Selenium-dissolved organic matter leaching

For ESCA, Se leachate concentrations were the highest in the presence of SRFA, then GSE, then PLFA, but differences could not be as easily identified for FA (**Figure 4.12**). Selenium leachate concentrations increase with increasing [DOC] for SRFA after an initial small decrease in presence of the lowest carbon concentration. Selenium leachate concentrations appear to increase for GSE for ESCA after an initial small decrease in presence of the lowest carbon concentration, and appear to decrease with increasing carbon concentration in the presence of PLFA, falling BDL above 20 mg C L^{-1}. Selenium leachate concentrations in PLFA showed similar trends for FA as well. However, FA Se leachate concentrations in the presence of SRFA and GSE show no discernable increases or decreases with carbon relative to the control.

4.4.8 Manganese-dissolved organic matter leaching

Leached concentrations of Mn for ESCA are not easily distinguishable between the DOM isolates (**Figure 4.12**). Slightly higher concentrations of Mn ESCA concentrations were leached by SRFA, then PLFA, and lastly GSE. For FA, PLFA displayed the highest Mn leachate concentrations upon addition of DOC, followed by SRFA and GSE. There is an overall decreasing trend in Mn leachate concentrations for ESCA for all DOM solutions, where the sharpest decrease is for the GSE solution which falls BDL above 20 mg C L^{-1}. The same pattern was not observed for the FA, where instead values dropped compared to the control but did not appear to vary with increasing [DOC].

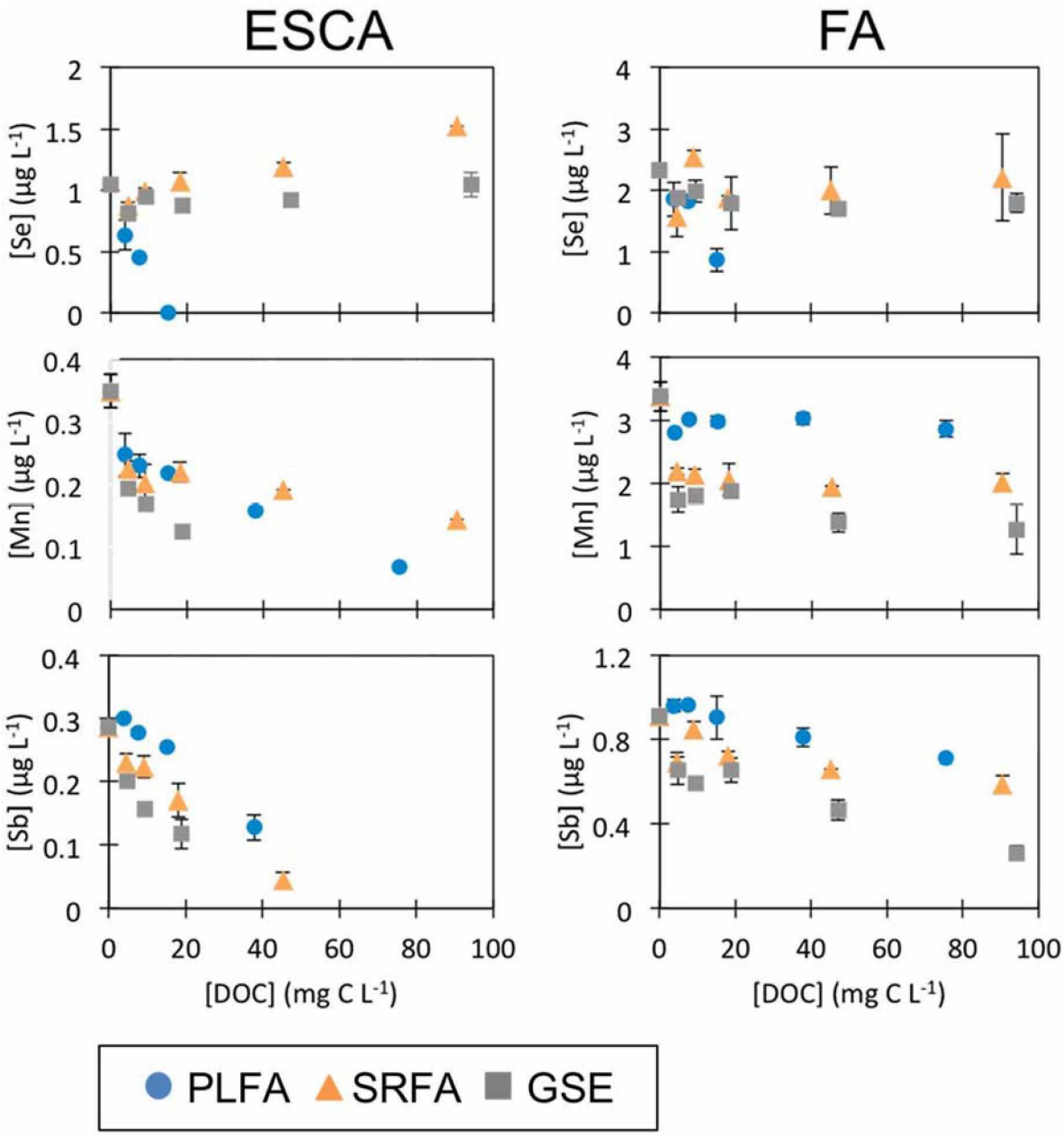

Figure 4.12 Seven-day leachate concentrations for Se, Mn, and Sb for CCPs in the presence of DOM isolates.

4.4.9 Antimony-dissolved organic matter leaching

For both ESCA and FA, Sb leachate concentrations were highest for PLFA, followed by SRFA and GSE (**Figure 4.12**). Decreases in Sb leachate concentrations with increasing [DOC] was observed for all DOM solutions in the presence of both CCPs, however decreases appeared to be sharper

for ESCA than FA. Antimony leachate concentrations for ESCA are BDL for [DOC] above 50 mg C L^{-1} for all DOM isolates.

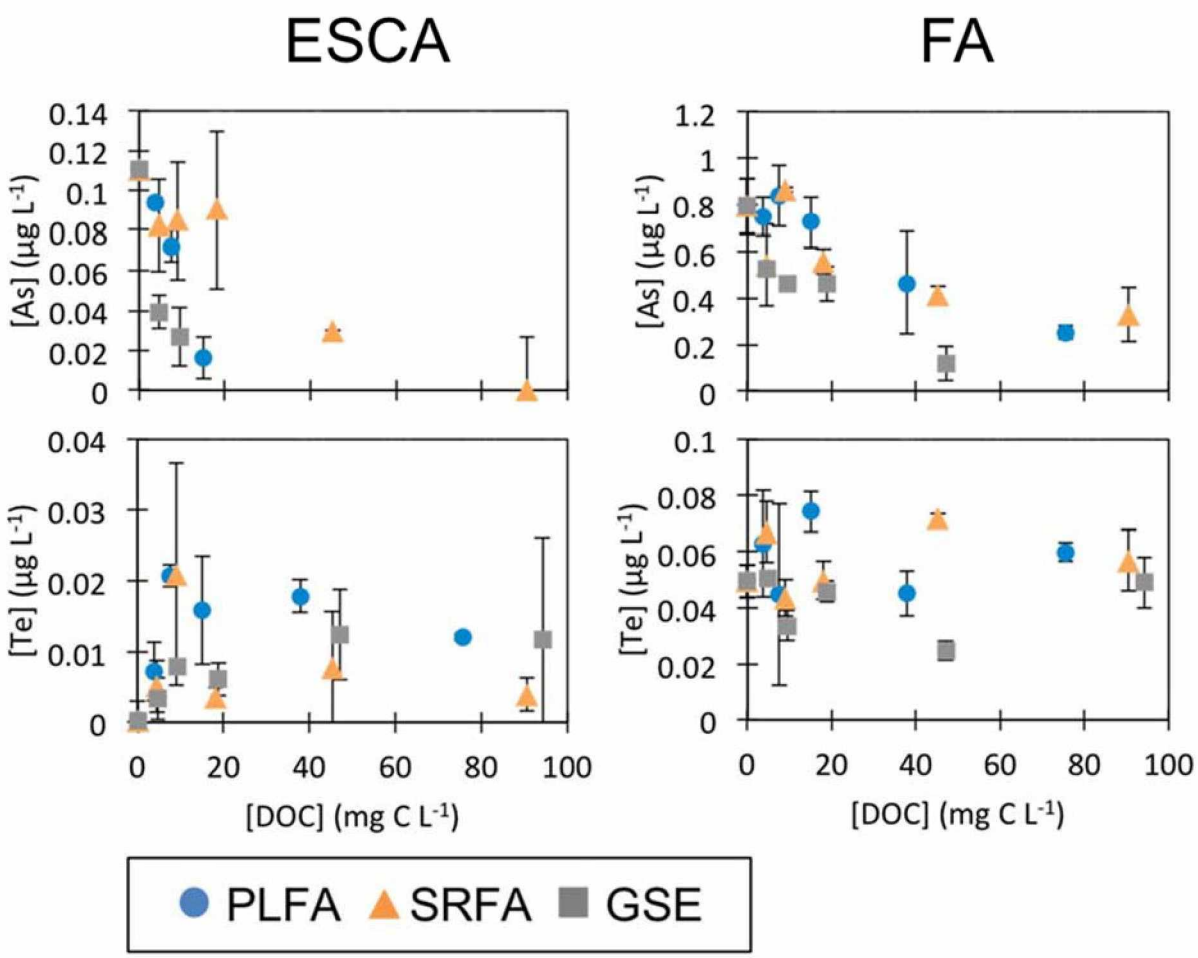

Figure 4.13 Seven-day leachate concentrations for As and Te for CCPs in the presence of DOM isolates.

4.4.10 Arsenic-dissolved organic matter leaching

Differences in As leachate concentrations with respect to DOM isolate were not pronounced for either ESCA or FA (**Figure 4.13**). Arsenic concentrations overall decreased upon increasing [DOC] for both CCPs for all DOM isolates, with ESCA As leachate concentrations falling BDL for PLFA and GSE above 20 mg C L^{-1}, while FA As leachate concentrations were BDL for only the highest carbon concentration of GSE. Higher concentrations of leached As were seen in the SRFA solutions for ESCA but not in FA.

4.4.11 Tellurium-dissolved organic matter leaching

Tellurium leachate concentrations were very low, and not able to observe differences between DOM isolates or trends with increasing [DOC], which may be due to the low leachate concentrations measured and their uncertainties (**Figure 4.13**).

4.5 Coal combustion product metal(loid) bioaccessibility

Physiologically-based extraction tests were performed on selected, potentially toxic elements (Cr, As, Se, Sb, and Pb). Supernatant concentrations of all five metal(loid)s exceeded EPA FW CMCs and EPA DW MCLs for unreacted CCPs, with the exception of the Cr concentrations for the unreacted ESCA in SLF. Further, higher concentrations of metal(loid)s were solubilized in SGFs relative to SLFs in most cases, which has been previously reported (Knight et al., 2017; Schaider et al., 2007). Bioaccessibility experiments were also performed on the residual solids from the ESCA leaching experiments using the 1 hr, 24 hr, and 3 mo time points.

4.5.1 Chromium bioaccessibility

The percent Cr liberated from unreacted SGF FA was higher than the amount liberated from any ESCA samples (**Figure 4.14**). The liberated fraction of all of the reacted ESCA solids were statistically similar to the unreacted ESCA liberated fraction. All SGF concentrations measured, and FA in SLF, exceeded EPA FW CMCs and EPA DW MCLs.

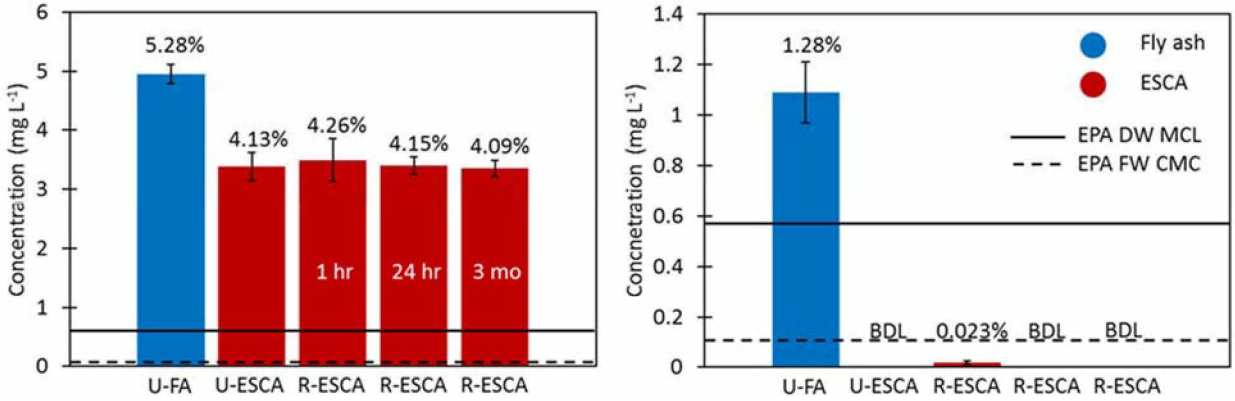

Figure 4.14 Chromium results of PBET extraction. Simulated gastric fluid (left) and simulated lung fluid (right). U: Unreacted; R: Reacted. Environmental Protection Agency Drinking Water

Figure 4.14 (Cont'd) Maximum Contaminant Level (EPA DW MCL). Environmental Protection Agency Freshwater Criteria Maximum Concentration (EPA FW CMC).

4.5.2 Arsenic bioaccessibility

Despite a substantially higher As concentration measured in the FA SGF supernatant, the percent As leached for unreacted FA was lower than that measured in the unreacted ESCA leached sample (11.14% and 16.95%, respectively; **Figure 4.15**). The SGF solubilized fraction was statistically similar for the unreacted, 1 hr, and 24 hr ESCA samples. Similarly, in the SLF, a higher concentration but lower fraction of As was liberated in the FA relative to any of the ESCA samples. The SLF solubilized fraction was statistically similar for the 1 hr, 24 hr, and 3 mo ESCA samples, but statistically different from the unreacted ESCA sample. All FA and ESCA samples exceed EPA FW CMCs and EPA DW MCLs.

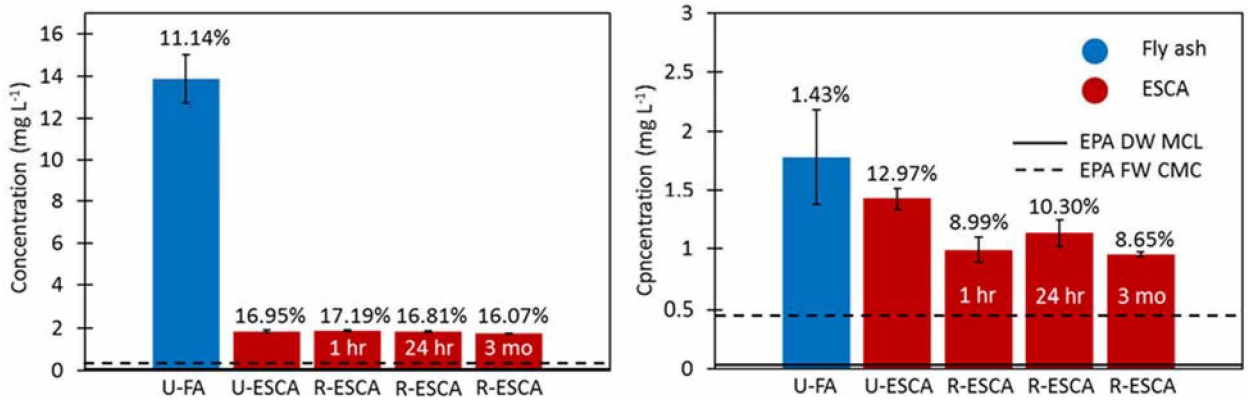

Figure 4.15 Arsenic results of PBET extraction. Simulated gastric fluid (left) and simulated lung fluid (right). U: Unreacted; R: Reacted. Environmental Protection Agency Drinking Water Maximum Contaminant Level (EPA DW MCL). Environmental Protection Agency Freshwater Criteria Maximum Concentration (EPA FW CMC).

4.5.3 Selenium bioaccessibility

The measured SGF and SLF supernatant concentrations of Se leached for FA was substantially higher than that of any of the ESCA samples (**Fig. 4.16**). Physiological based extraction tests of reacted ESCA solids in SGF were statistically similar for the 1 d, 3 mo, and unreacted samples, with the 1 d being the most bioaccessible. The reacted 1 hr, 24 hr, and 3 mo ESCA sample Se concentrations were statistically similar to the unreacted ESCA sample Se concentrations in the SLF. All PBET supernatant concentrations for FA and ESCA samples exceeded EPA DW MCLs.

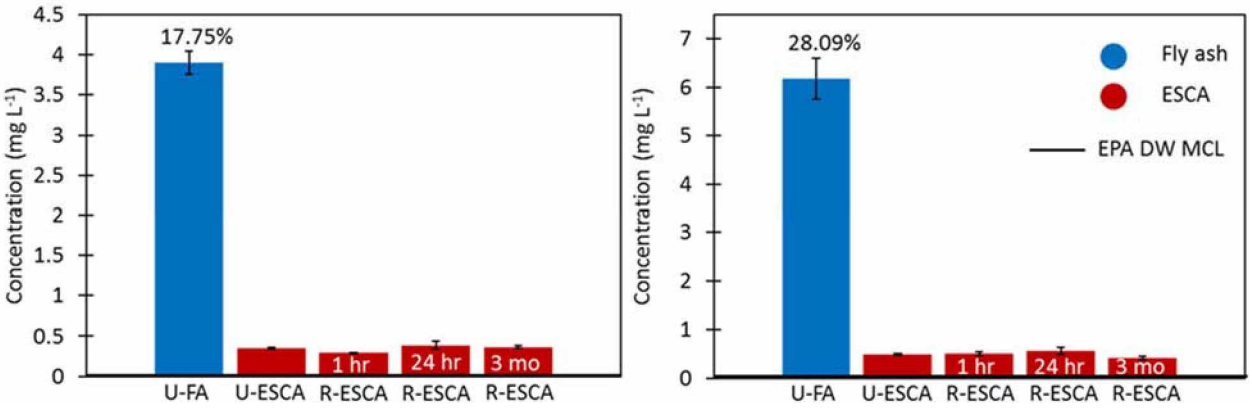

Figure 4.16 Selenium results of PBET extraction. Simulated gastric fluid (left) and simulated lung fluid (right). No percent leached values are displayed for ESCA because Se was below detection limit in the acid digestion analysis. U: Unreacted; R: Reacted. Environmental Protection Agency Drinking Water Maximum Contaminant Level (EPA DW MCL).

4.5.4 Antimony bioaccessibility

The measured concentration and percent Sb leached for FA was higher than that of any ESCA for the SGF and SLF with the exception of the 24 hr and 3 mo SLF samples (**Fig. 4.17**). The reacted ESCA SGF Sb concentrations are statistically similar to the unreacted ESCA SGF Sb concentrations. Only the 1 hr reacted ESCA SLF Sb concentrations are statistically similar to the unreacted ESCA SLF Sb concentrations. The FA and all ESCA samples exceeded EPA DW MCLs.

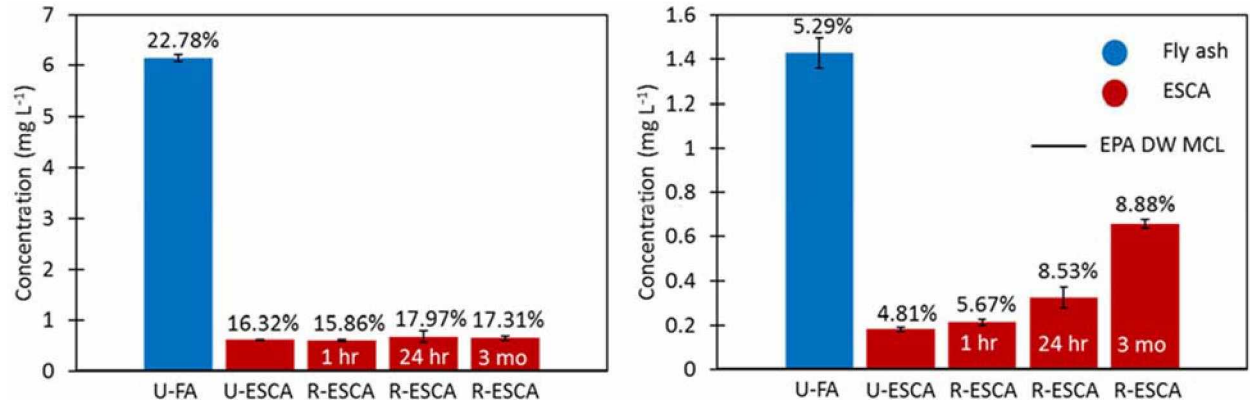

Figure 4.17 Antimony results of PBET extraction. Simulated gastric fluid (left) and simulated lung fluid (right). U: Unreacted; R: Reacted. Environmental Protection Agency Drinking Water Maximum Contaminant Level (EPA DW MCL).

4.5.5 Lead bioaccessibility

The percent Pb leached for unreacted FA was higher than of any ESCA sample (**Fig. 4.18**). Lead concentrations were BDL for all SLF supernatants. All Pb concentrations were statistically similar for unreacted and reacted ESCA samples. Unreacted FA and ESCA SGF samples exceeded EPA DW MCLs and EPA FW CMCs.

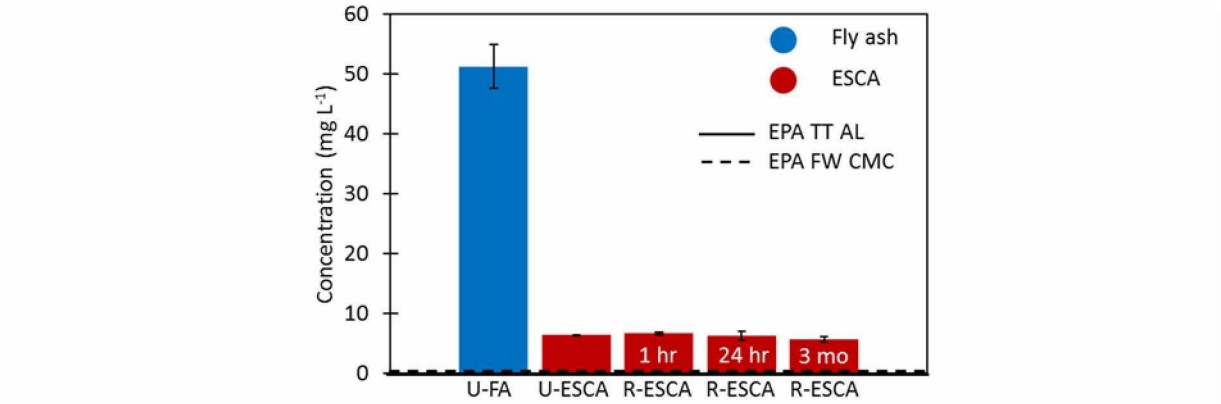

Figure 4.18 Lead results of PBET extraction. Simulated lung fluid results were below detection limit. U: Unreacted; R: Reacted. Environmental Protection Agency Treatment Technique Action Level (EPA TT AL). Environmental Protection Agency Freshwater Criteria Maximum Concentration (EPA FW CMC).

Chapter 5 Discussion

5.1 Physical and chemical characteristics of fly ash and early stage coal ash

Coal can contain more than 120 minerals, however, only *ca*. 33 of these are in most coal samples, and only *ca*. 8 are abundant enough to be considered major constituents (Schweinfurth, 2016). Some common major mineral constituents in coal include quartz (SiO_2), kaolinite ($Al_2Si_2O_5(OH)_4$), illite ($KAl_4(AlSi_7O_{20})(OH)_4$), montmorillonite ($(1/2\ Ca,Na)_{0.7}\ (Al,Mg,Fe)_4\ [(Si,Al)_4\ O_{10}\ ]_2\ (OH)_4 \cdot nH_2O$), chlorite ($(Mg,Al,Fe)_{12}[(Si,Al)_8\ O_{20}]\ (OH)_{16}$), pyrite ($FeS_2$), calcite ($CaCO_3$), and siderite ($FeCO_3$) (Schweinfurth, 2016). Sub-bituminous coal typically contains 35-45% C (U.S. EIA, 2011). However, the carbon compounds present are extremely complex and are not well understood (Schweinfurth, 2016). The physical and chemical characteristics of FA and ESCA are controlled by the combustion temperature, combustion process, and cooling rates present in the powerplant (Ward, 2018; Kutchko and Kim, 2006).

5.1.1 Carbon

Total carbon present in the UAF samples, 28 wt.% and 18.6 wt.% in ESCA and FA, respectively, are quite high compared to not only SRM 2691 and SRM 1633a (0.09 wt.% and 2.77 wt.% C) (**Table 4.1**) but also values reported by Neupane and Donahoe (2013) and Church et al. (1995) (approximated in **Table 1.1** as LOI and ranging from 0.4-15.6) (Akar et al., 2012; Koukouzas et al., 2011; Church et al., 1995; Rivera et al., 2015). The difference between the samples is most likely due to the FA being collected at the last stage of the combustion process, resulting in less un-combusted residual carbon. It is interesting to see that the UAF FA has a higher carbon content than the FA analyzed by Church et al. (1995). Church et al. (1995) analyzed a sample from the Healy, Alaska powerplant (built in 1967) that utilizes a pulverized coal firing system, and therefore, the coal that produced the sample, would be from the same source as the UAF coal (Usibelli Coal Mine, 2015; Church et al., 1995). However, this difference most likely comes from variances in the combustion processes between the UAF and Healy powerplants. High residual C content in CCPs, especially FA, can greatly affect it's uses in various projects such as

cement mixtures (Mohebbi et al., 2015). Since high C FA cannot be marketed as a cement mixture, it reduces the amount of CCP that is recycled, leaving more in stockpiles and landfills (Maroto-Valer et al., 2008). High residual C content particles exhibit porous, apolar, and aromatic surface (Schwarzenbach et al., 2017). These characteristics cause the particle to have a high affinity for many organic pollutants (Schwarzenbach et al., 2017). These characteristics may also play an important role in the lability of metal(loid)s from CCPs.

In high residual C CCPs, it is especially important to have an understanding of the organic functional groups present within the CCPs. Certain organic functional groups are capable of serving as sites of specific interactions, such as cation exchange, with other molecules or metal(loid)s (Dittmar and Stubbins, 2014). **Table 4.3** shows the presence of both carboxylic acids and phenolic carbons, by combining these percentages, we might be able to assume a proxy for the amount of black carbon in the samples (FA 34.3% and ESCA 40.15%) (Hayes et al., 2006). A higher black carbon content was expected in the ESCA compared to the FA not only because of the total carbon analysis, but also simply from the appearance of the two samples (ESCA is black while FA is grey). Black carbon potentially could inhibit metal(loid)s from being released from the CCPs (Inyang et al., 2015). Given the alkaline nature of the UAF CCP samples, it is expected that the functional groups present would be deprotonated and involved in cation binding (Schwarzenbach et al., 2017). Carboxylic acids are also present in both CCP samples, and when deprotonated complex with divalent metals such as Fe (Schwarzenbach et al., 2017). Carboxylic acids in the CCP particles could inhibit metal(loid)s from going into solution and they could also complex with metal(loid)s that were released into solution, therefore decreasing observable concentrations (Schwarzenbach et al., 2017).

5.1.2 Major elements

Elements with the highest enrichment relative to average crustal abundance include S, Ca, and Ba, in order of decreasing enrichment. Enrichment of S is not surprising because it volatilizes during the combustion process and can precipitate secondary minerals or redeposit on the surface of particles in addition to the UAF powerplant not utilizing any sulfur emission controls

(Iyer, 2002; Ward, 2018). CaO concentrations are enriched, which is a characteristic of the Class C FA. Aluminum and Si are both depleted relative to the average crustal abundances, despite composing a large mass fraction.

Some high mass fraction elements present in the UAF ash samples were Fe, Ca, S, Si, Al, and Mg. Quartz, mullite ($3Al_2O_3 \bullet 2SiO_2$), hematite (α-Fe_2O_3), and maghemite (γ-Fe_2O_3) are common constituents in FA (e.g., Neupane and Donahoe (2013); Akar et al. (2012); Koukouzas et al. (2011); Rivera et al. (2015); **Table 1.1**) and are possible source for the high observed Fe_2O_3, SiO_2, and Al_2O_3 content. Further, ESEM-observed elemental relationships are consistent with the major elements observed (**Figure 4.2**). The typical ESCA and FA mineral particles are composed of Mg, Al, Si, S, K, Ca, Fe, and potentially Ti (**Figure 4.2 A**). The cenosphere imaged is primarily composed of Mg, Al, and Si (**Figure 4.2 C**), which is consistent with the aluminosilicate glassy particle description in literature (Żyrkowski, 2014). Amorphous materials such as amorphous SiO_2 are metastable phases that are kinetically but not thermodynamically favored (Langmuir, 1997). Neupane and Donahoe (2013) suggest that these aluminosilicate phases would slowly undergo dissolution. High concentrations of MgO seen in the UAF FA and ESCA samples could be a result of magnesium oxide addition during the coal combustion process (Ward, 2018). The UAF powerplant adds magnesium oxide to the boilers in order to make it easier to remove boiler slag (Ward, 2018).

The ESCA particles appear to be porous, but larger than the FA particles. The smaller sizes of the FA particles mean they have a larger relative surface area (range= 0.175-17.9 $m^2 g^{-1}$), which has the potential to make them more reactive and influence metal(loid) leachability; this will be discussed further in another section. In addition, the FA particles appear to be associated with many micron-sized particles that may be highly reactive in the surficial environment, because they are present on the surface and readily available (Neupane and Donahoe, 2013). Metal(loid)s that are deposited on the surface of the FA particle could potentially leach much faster than the elements present within the particle matrix.

Further, it is common for cenospheres to have volatilized metal(loid) particles deposit on the surface during the cooling process (**Figure 4.2 C**) (Jegadeesan et al., 2007). Common volatilized metal(loid)s during the combustion process include Mn, Ba, V, Co, Cr, Ni, Ln, Ga, Nd, As, Sb, Sn, Br, Zn, Se, Pb, Hg, and S (Iyer, 2002). Less commonly volatilized metal(loid)s include Mg, Na, K, Mo, Ce, Rb, Cs, and Nb while Si, Fe, Ca, Sr, La, Sm, Eu, Tb, Py, Yb, Y, Se, Zr, Ta, Na, Th, Ag, and Zn are typically not volatile (Iyer, 2002). Some metals, such as Ca are hypothesized to be on the surface or in the aluminosilicate glass of the UAF fly ash particles, while other metals, such as Cr, Mo, and V are hypothesized to be present in the interior of these particles, causing a delayed dissolution. Leaching trends of these elements, and their concentrations within the particle will be discussed in further sections.

5.1.3 Solid phase equilibrium modeling of major elements

Due to the high concentrations of Ca, Al, Ba, and Fe and their possible roles in primary and secondary mineral formations, solid phase equilibrium modeling was performed (**Figure 5.1**). Calcium is oversaturated with respect to calcite and slightly undersaturated with respect to anhydrite ($CaSO_4$). Aluminum is oversaturated with respect to both diaspore (α-AlO(OH)) and gibbsite ($Al(OH)_3$), but undersaturated with amorphous $Al(OH)_3$. Barium is oversaturated with witherite ($BaCO_3$) but undersaturated with barite ($BaSO_4$). Lastly, Fe is oversaturated with respect to hematite and magnetite, but undersaturated with siderite for most samples. The implications of oversaturation and undersaturation with respect to these solid phases will be discussed further when talking about observed leaching trends.

5.1.4 Minor and trace elements

Potentially toxic minor and trace elements were found in the UAF FA and ESCA, and are commonly associated with CCPs, and is a primary motivation for this and other research efforts to understand potential transformation pathways in the surficial environment (**Table 4.1**) (Neupane and Donahoe, 2013; Church et al., 1995; Iyer, 2002). The FA typically contained higher concentrations of potentially hazardous metal(loid)s than the ESCA with the exception of Cr. Enrichment factors in excess of 10 were measured for Se, Sb, Cu, As, Bi, and Mo, in order of

decreasing enrichment for the FA (**Figure 4.1 B**).This may be due to the entrainment of metal(loid)-bearing particles, volatilization of these minor and trace elements during the combustion process that then partition, followed by condensation into particles or deposition on the surface of the FA particles as the flue gasses cool (Iyer, 2002).

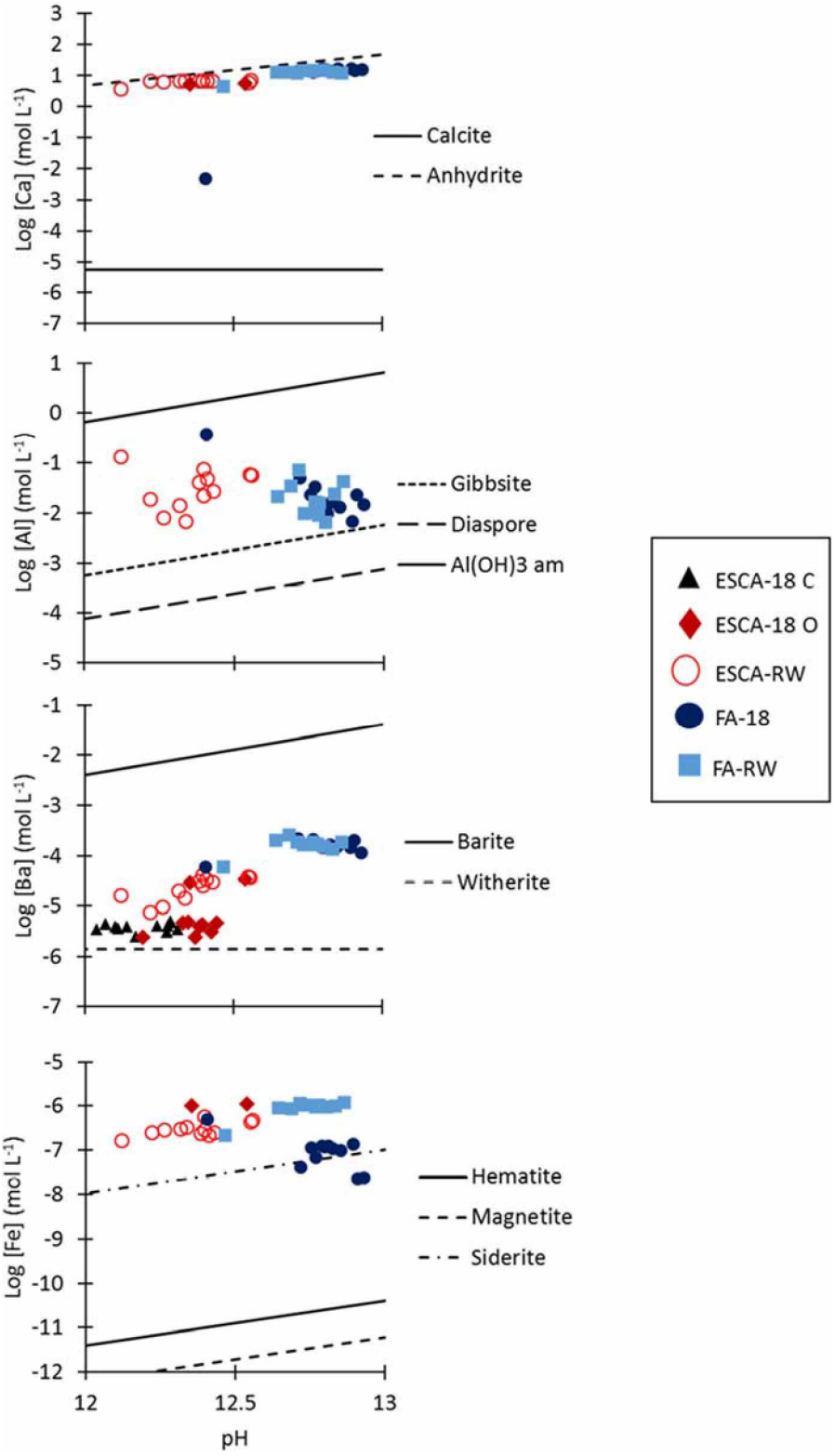

Figure 5.1 Solid phase equilibrium modeling of major elements. Modeling was performed in MINTEQ 3.1 as an open system with various possible solid phases.

5.1.5 Solid phase equilibrium modeling of minor and trace elements

A few minor and trace elements (Pb, Zn, and Cr) exhibited leaching trends of interest, and so solid phase equilibrium modeling was performed in order to hypothesize reasons for the observed trends (**Figure 5.2**). Both and Pb and Zn are undersaturated with respect to several common possible solid phases. Chromium was undersaturated with respect to $Cr(OH)_{2\ (s)}$ for most samples. The implications of undersaturation of these elements with respect to these possible solid phases will be discussed further when talking about observed leaching trends.

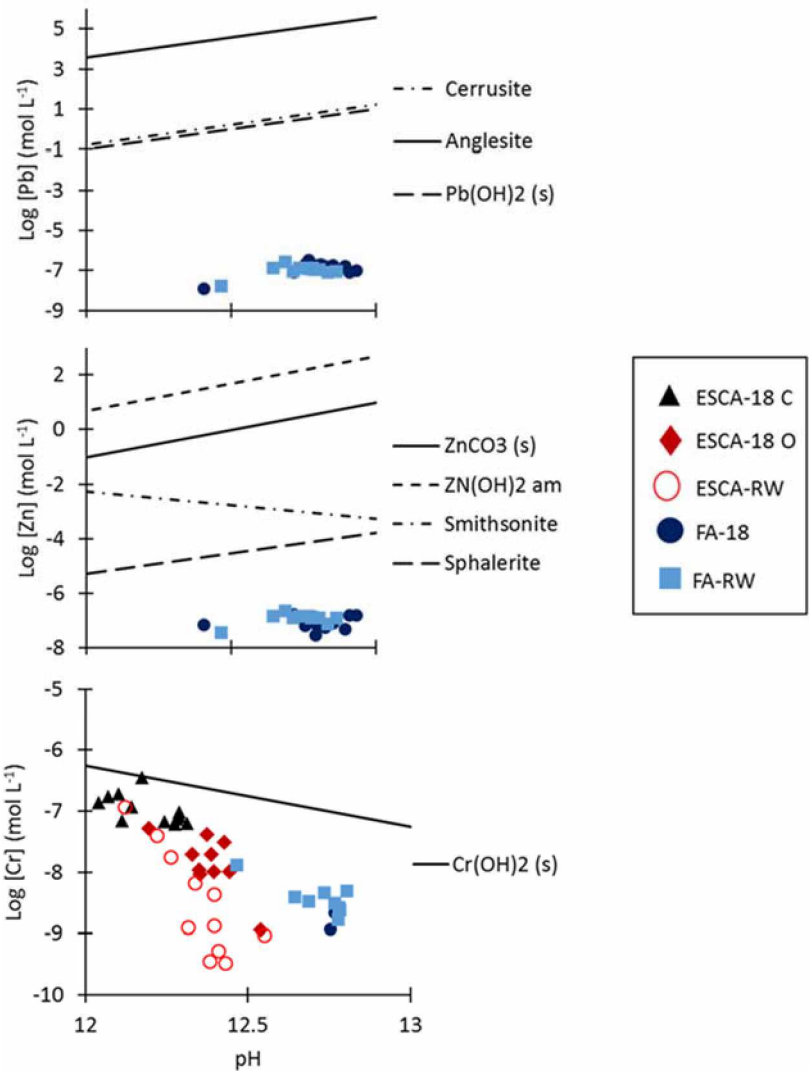

Figure 5.2 Solid phase equilibrium modeling of minor and trace elements. Modeling was performed in MINTEQ 3.1 as an open system with various possible solid phases.

5.2 Competing controlling processes

As with many aqueous systems, there are many processes occurring in solution at once during the CCP leaching experiments. These concurrent processes include: dissolution and precipitation reactions, sorption, differences in total initial concentrations, differences in CCP characteristics (surface area, particle size, organic moieties, and elemental composition), and heterogeneity of elemental distribution within the CCP particles. This makes the trends in the ESCA and FA leaching behaviors difficult to unambiguously attribute to a single process. However, it is possible to gain some insight into the factors controlling metal(loid) leaching behavior with the help of solid phase equilibrium modeling.

5.2.1 pH controls

There are a few possible reasons for the alkaline pH observed during the leaching experiments. Some literature suggests an alkaline pH can be caused by the dissolution of CaO and MgO: $CaO + H_2O \rightarrow Ca(OH)_2 \rightarrow Ca^{2+} + 2\ OH^-$ (Iyer, 2002). However, preliminary X-ray diffraction results of UAF ash samples do not indicate the presence of CaO. The dissolution of elements within the silicate phases could be the cause of the alkaline pH in the UAF ash samples. A model chemical equation for this dissolution could be $Ca_2SiO_{4\,(s)} + 2H_2O \rightarrow Ca^{2+}{}_{(aq)} + H_2SiO_4^{2-}{}_{(aq)} + 2OH^-$. Other metals within the silicate phases could take the place of Ca in the equation above, such as Mg, which was seen in **Figure 4.2 C**.

5.2.2 Total initial concentration

For several elements, unreacted FA contains a higher mass fraction than ESCA, which appears to partly explain some trends for Ca, Pb, Sb, and Zn (**Table 4.1**). This is most evident with Pb and Zn (**Figure 4.6** and **Figure 4.7**, respectively), where the unreacted fly ash contains *ca. 10x* more of each metal(loid) than ESCA, and leaching produces measurable leachate concentrations for FA, but were BDL for all ESCA samples. The trends are somewhat less clear for Ca and Sb. Calcium content of unreacted CCPs varies slightly (FA: 26.9 wt.% and ESCA: 21.6 wt.% CaO), thus initial concentration cannot explain all of the *ca.* 2x difference in leachate concentrations (**Figure 4.5**), but may still contribute to the differences observed in leachate concentration. The

Ca leaching trend is similar to that seen by Church et al. (1995) after two weeks of leaching. Church et al. (1995) describes the leaching of Ca as an initial increase in concentration followed by a gradual decrease. Differences in the time it took to see similar trends could be due to differences in leaching experiment set ups. Antimony FA leachate concentration is only somewhat higher than ESCA, despite a *ca*. 10x higher initial Sb content in the unreacted FA.

Both Pb and Zn exhibit an overall downward trend in leachate concentrations with increasing reaction time. Solid phase equilibrium modeling (**Figure 5.2**) shows that both Pb and Zn leached concentrations are undersaturated with respect to some common potential solid phases, indicating that the formation of these phases would not be thermodynamically favorable. The fact that they are undersaturated suggests that the observed decreases in leachate concentrations could be due to quick kinetic release from a labile solid phase followed by sorption to particle surfaces or co-precipitation with other neoformed phases. It has been suggested that Zn can be co-precipitated under high pH conditions due to the formation of Al and Fe hydroxides (Brownfield, 2002). It has also been shown that Pb can be readily removed from aqueous media due to the presence of calcite ($CaCO_3$) (Godelitsas et al., 2003).

On the other hand, solid phase equilibrium modeling for Ca (**Figure 5.1**) shows a supersaturation with respect to $CaCO_3$ and near saturation with respect to anhydrite ($CaSO_4$). This suggests that the decrease observed in Ca concentrations that initiates after 10 d reaction time is possibly due to the precipitation of $CaCO_3$ or $CaSO_4$. Indeed, when the filtered supernatants are exposed to air, a white precipitate likely calcite, has been observed to precipitate at the supernatant surface with *ca*. 30 minutes.

5.2.3 Dissolution reactions

There are several metal(loid)s (especially Al, Cr, and V) that increase in concentration with increasing reaction times, possibly due to dissolution reactions. All three metal(loid)s show a relatively consistent to slightly increasing leachate concentration prior to 28d and an increase in concentration from 28 d to 3 mo. The exception to this trend is ESCA V concentrations, which

increase steadily until 14 d, at which time the concentrations decreased. Solid phase equilibrium modeling was not performed for V.

Solid phase equilibrium modeling for Al (**Figure 5.1**) suggests a supersaturation with respect to gibbsite and diaspore, but an undersaturation with respect to amorphous $Al(OH)_3$. The slow increase in Al concentrations could be due to the slow dissolution of the aluminosilicate glass phase (Neupane and Donahoe, 2013). Aluminum concentrations and trends observed were similar to those seen by Church et al. (1995) after two weeks. However, Neupane and Donahoe (2013) never saw an increase in Al concentrations in later time points for alkaline ash samples, they observed a gradual decrease. Neupane and Donahoe (2013) attributed decreases in Al concentrations to the precipitation of secondary minerals. Differences in these leaching trends could be attributed to different source material and combustion processes that the fly ash is derived from.

Solid phase equilibrium modeling for Cr (**Figure 5.2**) suggests an undersaturation with respect to $Cr(OH)_{2\ (s)}$ in all leachates. It can be seen that the ESCA-RW samples become progressively more undersaturated and the FA experiments were more undersaturated than the ESCA-18 experiments. However, there are higher leached Cr concentrations in the ESCA experiments than the FA experiments. Chromium concentrations in solution are possibly due to the dissolution of chromite ($(Fe, Mg)Cr_2O_4$), Fe and Mg were both observed on the particles (**Figure 4.2**). Chromium speciation in fly ash is believed to be coal specific, with up to 30% of the total Cr in fly ash derived from western coal being Cr(VI) and 100% of the total Cr in Eastern Bituminous coal being Cr(III) (Neupane and Donahoe, 2013). Neupane et al. (2013) saw an increase in Cr concentrations for the alkaline FA sample, which is observed in the UAF FA and ESCA leachings, however, at significantly lower concentrations.

5.2.4 Higher early stage coal ash leached concentrations

For a few elements (Cr, Mo, and V), the ESCA leachate concentrations were higher than for FA despite very similar concentrations in the unreacted CCPs (**Figure 4.6** and **Figure 4.7**). Previous

work has indicated that Mo is usually volatilized to lesser extents than other metal(loid)s such as Cr and V (Iyer, 2002). The low volatility of Mo suggests that it could be concentrated on the interior of the FA particle, making it less readily available for leaching, as opposed to if it was concentrated on the surface (Neupane and Donahoe, 2013). Neupane and Donahoe (2013) observed an increase in Mo concentrations with time, however, at higher concentrations.

Unreacted ESCA and FA contained similar concentrations of Cr and V. It is possible that Cr and V are concentrated on the interior of the FA particles, causing a slow release, which would explain why there is no significant release of these metal(loid)s into solution until later time points. It has been suggested that Cr and V can be present as surface enrichment, impurities in crystalline components, or as discrete accessory crystalline phases in FA (Vassilev and Vasilleva, 1995). However, given the delayed release trend of Cr, it does not appear to be enriched on the surface of the particle. Church et al. (1995) determined that Cr and V were near or BDL in fly ash leachates. Neupane and Donahoe (2013) reported increased Cr and V concentrations with time in the leachates for their alkaline FA samples, however, concentrations were much higher. It is suggested that V concentrations in solution could be correlated with Mo concentrations (Neupane and Donahoe, 2013).

5.2.5 Particle size

Barium, Ca, Co, Cu, and Mn leached concentrations are higher for FA than for ESCA (**Figure 4.5, 4.7**, and **4.8**) despite having started with roughly the same concentrations (**Table 4.1**). It is possible that Ba, Co, and Mn are enriched on the surface of the FA particle because they are easily volatilized during the combustion process (Iyer, 2002). However, it is more likely that higher leachate concentrations are due to the smaller particle size of the FA. The smaller the particle size, the higher the surface area, and therefore, more contact with the solution for reactions to occur. Solid phase equilibrium modeling was performed for Ba (**Figure 5.1**) and indicated that both ESCA and FA were supersaturated with respect to witherite and undersaturated with respect to barite. Early stage coal ash is less supersaturated than FA and so one would expect to see lower concentrations of leached Ba from the FA. There is a constant

downward trend in leached Ba concentrations from FA with increased time, and this is possibly due to the precipitation of witherite. Barium trends observed are similar to those seen by Church et al. (1995)[9] after two weeks. However, the UAF FA and ESCA Ba concentrations leached were lower. Neupane and Donahoe (2013) reported decreasing Ba concentrations, however, UAF Ba concentrations were much lower. Neupane and Donahoe (2013) saw high concentrations of Ba in early leaching samples, similar to UAF fly ash samples, and hypothesize they were mobilized from surface bound highly soluble particles such as glass phases.

5.2.6 Possible equilibrium

Almost no metal(loid)s analyzed for reach an equilibrium. If equilibrium was reached, there would be a steady state concentration of metal(loid)s reached at the end of the experiment. In fact, it can take up to 140 days for equilibrium to be reached for many metal(loid)s (Roy and Griffin, 1984). However, As and Se appear to have reached a possible equilibrium (**Figure 4.8** and **Figure 4.9**). Despite differences in the CCP starting concentrations and the leachates, all experiment trends appear to be similar. The end concentrations also appear to not be very different from the starting concentrations. This suggests that only so much of these metal(loid)s can be leached into solution. Statistical analysis for the 1 hr, 7 d, and 3 mo time points for these elements do show that many of these experiments have statistically similar concentrations. While UAF samples appeared to reach an equilibrium, Neupane and Donahoe (2013) reported a decrease in Se and As concentrations. It is suggested that there are no Se-bearing phases oversaturated in alkaline CCP samples such as the UAF FA, and this is why there may be no observed decrease in Se concentrations (Neupane and Donahoe, 2013). Neupane and Donahoe (2013) also reported that their fly ash solutions were undersaturated with respect to ettringite, which is a secondary mineral that commonly sequesters Se, this may be why no decreasing trend was observed in UAF fly ash leachates.

5.2.7 Other metal(loid) trends

Iron exhibits leaching trends that are not similar to any other metal(loid) (**Figure 4.6**). Iron concentrations do not change very much until 10 d. The ESCA-RW and FA-RW exhibit similar

trends with an increase followed by a decrease. Solid phase equilibrium modeling for Fe (**Figure 5.1**) shows that the system is supersaturated with respect to magnetite, hematite, and siderite. It is possible that the decrease in Fe concentrations is due to the precipitation of one of these minerals. Iron leached concentrations is the only case where the leachate appeared to make a difference. >18 MΩ experiments exhibit different concentrations from the simulated rainwater experiments for both ESCA and FA. The differences between FA-18 and FA-RW experiment trends are possibly due to some time points for FA-18 being saturated/undersaturated with respect to siderite, while the FA-RW experiment is oversaturated for all time points. It is possible that the differing chemistry of the simulated rainwater played a roll in the different leaching concentrations and trends due to the addition of H_2SO_4 and also chloride salts that could possibly cause Fe to precipitate. Both Neupane and Donahoe (2013) and Church et al. (1995) observed low to near BDL concentrations of Fe in solution, which is inconsistent with what was observed in the UAF fly ash samples.

5.3 Synthetic leaching precipitation leaching procedure and other leaching comparisons

Synthetic precipitation leaching procedure results are plotted on the leaching graphs in **Figure 4.5**, **4.6**, **4.7**, **4.8**, and **4.9** if it was not BDL (**Table 4.4**). For Ca, Cu, and Pb, the FA SPLP leached concentrations appeared to be similar to the simulated rainwater leaching. In other elements, the FA SPLP leached concentrations were either higher, as is the case with Mn, or lower as is the case with Co, Mo, Se, and Zn. Early stage coal ash SPLP leached concentrations do not mimic the ESCA simulated rainwater experiments leached concentrations except for Mo. Early stage coal ash SPLP leached concentrations were either higher, as is the case with V, Cr, Se, and As, or lower as is the case with Ca, and Pb. It is difficult to say whether or not the simulated rainwater experiments were a harsher leaching method than the SPLP because of the high variability in similarities/differences between element and CCP. However, it can be observed that many transformations are still occurring in solution after the 18 hr leaching time for the SPLP. These transformations can cause significant changes in metal concentrations in solution (e.g. increases in Al and Cr and decreases in Ca and Ba). The long-term leaching performed in this thesis indicate that EPA standard leaching methods that are used to classify wastes, like the

SPLP, do not accurately represent metal concentrations in solution after extended periods of time.

5.4 Dissolved organic matter leaching trends

Similar to other leaching results reported in this thesis, the CCP metal(loid)-DOM leachings are complicated by many competing processes. Heterogeneity of metal(loid) concentration within the CCP particle, CCP particle surface area, total initial metal(loid) concentrations, and a closed system can complicate results. Dissolved organic matter can also undergo many different interactions with a particle surface, some of which include competition for sorption sites on the particle surface, dissolution and exposing new sites on the particle surface, and electron shuttling (Polubesova and Chefetz, 2013).

End point TOC analysis was not performed due to lack of sample volume. End point TOC values would have helped to quantify the amount of DOM remaining in solution vs. in the solid phase. Visual inspection of the solutions after filtration indicate that at least the colored fraction of DOM was adsorbed to the solid phase. Fly ash Ca is one of the only elements to exhibit very little DOC and DOM dependence.

One last factor that complicates the DOM leaching results is that both dissolved metal(loid) species and dissolved metal(loid)s bound to DOM are present in solution. Concentrations that are observed are a total metal(loid) concentration in solution and are not necessarily representative of metal(loid)s solely bound to the DOM.

5.4.1 Dissolved organic carbon independent metal(loid) mobility

Some metal(loid)s exhibited little to no change in concentration as DOC concentration increased, the prime example being Ca concentrations for ESCA SRFA and FA SRFA, PLFA, and GSE experiments (**Figure 4.10**). Calcium concentrations were effected very little by the DOC concentration, possibly due to the sorption of DOM to the solid phase instead of leaching metal(loid)s from the particle surface. Both SRFA and GSE concentrations were statistically

similar and PLFA, SRFA, and GSE concentrations were statistically similar for [DOC] ranging from 5-20 mg C L^{-1}. Slightly higher percentages of Ca were leached from FA-18 experiments than from the PLFA, SRFA, and GSE (**Table 4.5** and **4.7**). However, lower percentages of Ca were leached from ESCA-18 experiments than from the PLFA, SRFA, and GSE, suggesting that DOM does have some affect on Ca mobility from ESCA (**Table 4.5** and **4.7**).

5.4.2 Dissolved organic carbon dependent metal(loid) mobility

Metal(loid) concentrations that exhibit a decrease or increase as DOC concentrations increase suggest that the metal(loid)'s mobility is dependent upon the DOC concentration. A decrease in metal(loid) concentration can be seen for almost every metal(loid) depending on the CCP and DOM, for this reason, only a few metal(loid)s are discussed in detail.

For Fe, the decrease is only seen in the PLFA and GSE for the ESCA, and GSE for the FA (**Figure 4.10**). Humic substances contain a range of ligand functional groups that have free electron pairs that can be donated to Fe and other metal(loid)s to form coordination complexes (Yamashita and Jaffe, 2008). Carboxylic and phenolic functional groups, which are present in both the ESCA and FA samples (**Table 4.4**) commonly complex with Fe and other metal(loid)s in solution. Due to this, it would be expected that Fe concentrations would be higher in solution as the DOC concentration increases, however, this is only really the case for ESCA SRFA experiments and not until 50 mg C L^{-1}. A decrease in Fe concentrations could be a result of coprecipitated insoluble Fe^{3+}-organic complexes which can occur at high DOC/Fe ratios (Chen et al., 2014). For most experiments, the higher the DOC concentration, and therefore the higher the DOC/Fe ratio, less Fe is observed in solution. Higher percentages of Fe were leached from the PLFA, SRFA, and GSE solution for both FA and ESCA than in the either of the >18 MΩ experiments (**Table 4.5** and **4.7**). This confirms what many literature sources suggest, that DOM promotes the mobility of Fe.

Manganese concentrations decrease for all DOM experiments for the ESCA (**Figure 4.12**) more sharply than the decrease seen in Fe. However, for the FA, after the initial decrease form 0 mg

C L^{-1}, Mn concentrations increase and remain the same or decrease again. Manganese is known to strongly complex with dissolved organic carbon (Johnson et al., 2015). Decreases in Mn concentrations could be caused by the DOM adsorbing to the surface of the particle and inhibiting Mn leaching. Another possible reason for observed decreases is that there could be a secondary mineral precipitation occurring which would also decrease the DOC content of the solution, hence a change in color (Johnson et al., 2015). Fly ash Mn concentrations observed are higher than that of the ESCA concentrations which is consistent with what was observed in the >18 MΩ H_2O and simulated rainwater leachings (**Figure 4.8**). Higher percentages of Mn were leached during the FA PLFA leaching than the FA-18 experiment (**Table 4.5** and **4.7**). However, higher percentages of Mn were leached from the FA-18 experiment than both the FA SRFA and GSE leachings. Higher percentages of Mn were leached from the ESCA PLFA and SRFA leachings than in the ESCA-18 experiment. This suggests that SRFA is more likely to mobilize Mn from ESCA than from fly ash, while PLFA is just as likely to mobilize Mn from both FA and ESCA.

Arsenic and Zn follow similar leaching trends between the two CCPs (**Figure 4.11** and **4.13**, respectively). Early stage coal ash As and Zn concentrations decreased sharply regardless of DOM, while FA As and Zn concentrations decreased more steadily. It is possible that due to these metal(loid)s being enriched on the surface of the FA particle, that more is readily available for complexation with DOM compared to the ESCA (Iyer, 2002). Higher concentrations and slower decreases in As and Zn concentrations were seen for FA than ESCA. This difference in trends is also possibly due to As and Zn being *ca*. 10x higher in unreacted FA than the ESCA. It has been suggested that As mobility is dependent on DOM while Zn mobility is not (Kalbitz and Wenrich, 1998). For these leachings, Zn mobility does appear to be dependent on DOM, because Zn concentrations decrease differently for the GSE than SRFA or PLFA. Higher percentages of As were leached from FA-18 and ESCA-18 experiments than from PLFA, SRFA, and GSE (**Table 4.5** and **4.7**). Lower percentages of Zn were leached from FA-18 experiments than from PLFA and SRFA, but not GSE. Comparisons of percentages of Zn leached from PLFA, SRFA, GSE, and ESCA-18 experiments could not be made due to Zn being BDL (**Table 4.5** and **4.7**).

Some metal(loid) concentrations increase as DOC concentrations increase. This trend is most noticeable for Se, Mo, and V (**Figure 4.10**, **4.11**, and **4.12**). This increase in concentration would suggest that these metal(loid) are complexing with functional groups present in the DOM. Recently, it was found that Se exhibited a linear relationship with DOC concentration in permafrost regions and that DOM promoted the leaching of Se (Pokrovsky et al., 2018). While this result is seen for GSE and SRFA, it is not seen in the PLFA.

Due to the linearity of some of these graphs, a linear isotherm can be applied, the slope of which is a partition coefficient (**Table 5.1**) (Schwarzenbach et al., 2017). A trendline with an R^2 $\geq$0.8 was considered to be linear, while an R^2 <0.8 was considered not to have a partition coefficient. It is important to note that these linear isotherms are being applied with the assumption that all dissolved organic matter is in solution. However, from the color changes of the solutions, we know this is not exactly the case, so these partition coefficients are not necessarily the actual affinities of these DOM solutions for the particular metal. For the purposes of this discussion, these partition coefficients will be treated as the affinities of these DOM solutions for the particular metals. The first and most noticeable observation from this is that SRFA has a higher affinity for all three metal(loid)s from ESCA than from FA. This result is consistent with what was determined from the >18 MΩ H_2O and simulated rainwater leachings in that Mo and V appeared to be concentrated in the particle interior as opposed to the surface and not as readily available for leaching.

Comparing between the DOM solutions for the ESCA, SRFA has a higher affinity for Se than PLFA, PLFA has a higher affinity for Mo than SRFA, and PLFA and SRFA have similar affinities for V (**Table 5.1**). Differences in affinities is most likely due to differences in composition due to source materials for the DOMs (Guerard et al., 2009; Stevenson, 1982; Dittmar and Stubbins, 2014; Schwarzenbach et al., 2017) .

Table 5.1 Partition coefficients for linear CCP-DOM leaching trends.

Se	**PLFA**	**SRFA**	**GSE**
ESCA	N/A	0.0056	N/A
FA	N/A	N/A	N/A
Mo			
ESCA	0.29	0.10	N/A
FA	N/A	N/A	N/A
V			
ESCA	0.028	0.028	N/A
FA	N/A	N/A	N/A

Throughout almost every leaching experiment, at least one DOM solution behaved differently than the others. It is expected that the GSE and SRFA DOM solutions would behave similar due to source material of the DOM. Suwannee River fulvic acid is a terrestrial derived DOM while PLFA is a microbial derived DOM. Since GSE mainly has terrestrial inputs, which is evidenced by its aromaticity and fluorescence, it is expected to behave similarly to the SRFA (Gagne et al., In prep.). This trend is also seen for Co FA, Mn FA, Co ESCA and FA, Sb ESCA, Se ESCA and FA, and Mo ESCA (**Figure 4.11** and **4.12**). In some cases, these two DOM exhibit nearly opposite behavior from the PLFA solution (e.g. ESCA Co).

5.5 Unreacted coal combustion product metal(loid) bioaccessibility

Chromium, As, Se, Sb, and Pb, all commonly known toxic metal(loid)s were determined to be bioaccessible for SGF and SLF for both the ESCA and FA. The only exceptions being Pb in the SLF and Cr for ESCA in the SLF which were BDL. Both FA and ESCA consistently exceed EPA DW MCLs and EPA FW CMCs for the five metal(loid)s. There are many factors that can affect the bioaccessibility of metal(loid)s such as mineralogy, speciation, oxidation state, and particle size (Knight et al., 2017). Three important observations can be made for the bioaccessibility of the unreacted CCP samples.

The first is that much higher percentages of these metal(loid)s were leached in the SGF and SLF than the >18 MΩ H_2O, simulated rainwater, SPLP, and DOM leachings. This could be due to the presence of organic acids in SGF and SLF that promote the leaching of these metal(loid)s.

Secondly, it can be noted that the SGF was typically better at leaching the metal(loid)s from the CCPs than the SLF with the exception of Se. This could be due to the acidic nature of the SGF (pH 1.5) compared to the SLF (pH 7.4). Not only did the SGF start at more acidic conditions than the SLF, but it was also pH adjusted throughout the experiment with HCl to keep it at pH 1.5. This varies significantly from all other leaching experiments performed because other leaching experiments were under alkaline conditions regardless of starting pH due to the high alkalinity of the CCPs.

Lastly, metal(loid)s were consistently leached in higher concentrations, but not always higher percentages, from the FA than the ESCA. Consistently higher concentrations being leached regardless of leachate and metal(loid) suggest that the five metal(loid)s are more readily available for leaching than those in ESCA. Iyer (2002) reports that Cr, As, Se, Sb, and Pb are usually volatile to a significant extent during the combustion process, therefore, they would be concentrated on the surface of the FA particles and more bioaccessible. In addition, it has been suggested that smaller particle sizes tend to be more bioaccessible, and the FA has a smaller particle size relative to the ESCA (Knight et al., 2017).

5.5.1 Reacted early stage coal ash metal(loid) bioaccessibility

Reacted 1 hr, 1 d, and 3 mo ESCA samples also had bioaccessible metal(loid)s, despite already having metal(loid)s leached. There were some similarities to the unreacted CCP sample PBET results. Concentrations and percentages leached for these samples were typically similar to that of the unreacted ESCA sample. Higher concentrations and percentages were observed for the SGF solution compared to the SLF with the exception of Se concentrations. Bioaccessible concentrations were lower than those observed in the unreacted FA samples. Lastly, SLF concentrations were very low or BDL for Cr and Pb. It appears that Cr and Pb are not as

bioaccessible through lung fluid as they are gastric fluid. The highest percentages and concentrations of the five bioaccessible metal(loid)s were present in the SGF Pb PBETs. Regardless of the CCP or if the sample had been previously reacted, it appears that the acidic nature of the SGF caused significant amounts of Pb to be leached from the CCP samples. It has been previously reported that Pb has a higher bioaccessibility in SGF from particles (Knight et al., 2017). In addition, these results are consistent with those reported by Knight et al. (2017), who observed lower metal(loid) concentrations in SLF than in the SGF.

Chapter 6 Conclusions

A combination of WD-XRF and acid digestion showed the presence of several elements in both ESCA and FA samples. Some of the highest concentrations were observed in Ca, Fe, Mn, Al, Si, and Ba. Acid digestion also showed the presence of commonly known toxic metal(loid)s such as Cr, As, Se, Sb, Te, and Pb. Upon comparing the WD-XRF and acid digestion results to the average crustal abundances it was found that several metal(loid)s are enriched, some of which include Ca, Fe, Ba, Se, As, Sb, and Cu. Due to the presence of commonly known toxic metal(loid)s in both ESCA and FA, and enrichment of some of these metal(loid)s relative to the average crustal abundance, PBETs were performed.

It was found that Cr, As, Se, Sb, and Pb were all bioaccessible. Higher bioaccessible concentrations and percentages leached were seen for SGF as opposed to SLF with the exception of Se. The highest bioaccessible concentrations and percentages leached were seen for Pb. All bioaccessible concentrations of these metal(loid)s exceeded EPA contaminant levels. Environmental scanning electron microscopy showed that the ESCA particles primarily consisted of Ca, S, Si, Al, Fe, and Mg, were porous, and had a larger particle size than the FA. Through ESEM, it was found that FA contained two main particle types, a mineral aggregate with a similar composition as the ESCA, and a cenosphere that primarily consisted of Si, Al, and Mg, which is consistent with what is reported in literature. Fly ash having a smaller particle size than ESCA can cause it to be more reactive in solution and was suggested as one of the causes of some leaching trends observed.

Numerous trends were observed for >18 MΩ H_2O and simulated rainwater leachings. It was determined that total initial concentration, dissolution reactions, particle size, and particle metal(loid) heterogeneity all contributed to trends observed. Calcium, Pb, Sb, and Zn leaching appeared to be controlled in part by differences in total initial concentrations between the CCPs. Dissolution reactions appeared to occur for Al, Cr, and V. However, the dissolution did not occur until later time points for Al and Cr. Particle heterogeneity was also hypothesized to play

a role in the Cr, Mo, and V leaching trends. Barium, Ca, Co, and Cu leaching trends were controlled in part by the differences in particle sizes between the ESCA and FA. Se and As did not show significant changes in concentrations and appeared to be similar regardless of CCP or leachate. This suggested that Se and As are at a possible equilibrium in solution.
Similar to the other leachings, the CCP-DOM leaching had several competing processes occurring simultaneously. Trends varied depending on CCP, metal(loid), and DOM, therefore only a few results were discussed in detail. Solid-state cross-polarization magic angle spinning ^{13}Carbon nuclear magnetic resonance showed the presence of numerous functional in both ESCA and FA, some of which are known to complex with metal(loid)s in solution such as carboxylic acids and phenols. Some metal(loid) mobility did not appear to be controlled by the presence of DOM, the primary example being Ca. Calcium did not exhibit a significant change in concentration with an increasing DOC concentration for most DOM samples in both the ESCA and FA.

Other metal(loid) mobility did appear to be affected by the presence of DOM. This was observed in decreasing or increasing metal(loid) concentrations as DOC concentration increased. Some metal(loid)s that decreased in concentration as DOC concentration increased were Fe, Mn, As, and Zn. Decreases in concentration could be due co-precipitation with organic complexes, or the DOM binding to the CCP particle surface inhibiting the leaching of metal(loid)s.

Some metal(loid)s increased in concentration as the DOC concentration increased, these were Se, Mo, and V. By applying linear isotherms to these graphs, partition constants were determined, which allowed for the comparison of the affinities of the DOM samples for the metal(loid)s between the CCP samples. Suwannee River fulvic acid and PLFA appeared to have higher affinities for the three metal(loid)s from the ESCA whereas partition constants could not be determined for any DOM from the FA. Partition constants could also not be determined for and GSE samples.

One complication to the CCP-DOM leaching that could affect the results observed above, is that total dissolved metal(loid) concentrations in solution were measured, and not just concentrations of metal(loid) sorbed to DOM. A technique such as Field Flow Fractionation (FFF) combined with ICP-MS would be useful in this aspect. FFF would allow for the separation of dissolved metal(loid) species in solution from the DOM fraction. Upon collection of the DOM fraction, it could be analyzed on the ICP-MS and metal(loid) concentrations could be determined. This would allow for a more-clear picture of CCP metal(loid)-DOM interactions.

Experiments performed in this thesis not only indicate the presence of metal(loid)s of environmental and health concern in ESCA and FA, but also show that they do have the potential to leach into the environment. Once in the environment, these metal(loid)s do interact with DOM, which can both promote and inhibit the leaching of these metal(loid)s, which can affect their transportability and concentrations observed. Bioaccessibility experiments show that these CCPs do contain concentrations that exceed EPA regulations, even after they have been reacted. This study indicates there is a need for better short-term storage of FA and ESCA materials to help contain the leaching of metal(loid)s and prevent them from entering groundwater or surface water sources.

References

Aiken, G. R.; Hsu-Kim, H.; Ryan, J. N. Influence of Dissolved Organic Matter on the Environmental Fate of Metals, Nanoparticles, and Colloids. *Environmental Science and Technology*. **2011**, 45, 3196-3201.

Akar, G.;Polat, M.; Galecki, G.; Ipekoglu, U. Leaching Behavior of Selected Trace Elements in Coal Fly Ash Samples from Yenikoy Coal-Fired Power Plants. *Fuel Processing Technology*.
2012, 104, 50-56.

American Coal Ash Association. Coal Ash Recycling Reaches Record 56 Percent Amid Shifting Production and Use Patterns. [Press Release]. **2017**, https://www.acaa-usa.org/Portals/9/Files/PDFs/News-Release-Coal-Ash-Production-and-Use-2016.pdf (accessed October 24, 2018).

Bauer, J.; Mattson, S.; Eastes, W. In-Vitro Acellular Method for Determining Fiber Durability in Simulated Lung fluid. **2007**, 1-18.
https://dcpd6wotaa0mb.cloudfront.net/owenscorning.com/assets/sustainability/fiber-science/in-vitro-acellular-method-for-determining-fiber-durability-in-simulated-lung-fluid-1f30cd1be12fecdd25e19943aebb35f728872b1b88c7eab225beadc95b875983.pdf (accessed October 25, 2018).

Brownfield, M. E. Characterization and Modes of Occurrence of Elements in Feed Coal and Fly Ash; an Integrated Approach. *United States Geological Survey*. **2002**, Fact sheet: 038-02. https://pubs.usgs.gov/fs/2002/0038/report.pdf (accessed October 12, 2018).

Cawley, K. M.; McKnight, D. M.; Miller, P.; Cory, R.; Fimmen, R. L.; Guerard, J.; Dieser, M.; Jaros, C.; Chin, Y.; Foreman, C. Characterization of Fulvic Acid Fractions of Dissolved Organic Matter During Ice-Out in a Hyper-Eutrophic, Coastal Pond in Antarctica. *Environmental Research Letters*. **2013**, 8, 1-10.

Chancey, R. T.; Stutzman, P.; Juenger, M. C. G.; Fowler, D. W. Comprehensive Phase Characterization of Crystalline and Amorphous Phases of a Class F Fly Ash. *Cement and Concrete Research*. **2010**, 40, 146-156.

Chen, H.; Abdulla, H. A.; Sanders, R. L.; Myneni, S. C.; Mopper, K.; Hatcher, P.G. Production of Black Carbon-Like and Aliphatic Molecules from Terrestrial Dissolved Organic Matter in the Presence of Sunlight and Iron. *Environmental Science and Technology Letters*. **2014**, 1, 399-404.

Church, A.; Raad, L.; Tumeo, M. Experimental Study of Leaching of Fly Ash. *Transportation Research Record 1486*. **1995**, 3-12.

Davidson, E. A.; Chorover, J.; Dail, D. B. A. A Mechanism of Abiotic Immobilization of Nitrate in Forest Ecosystems: the Ferrous Wheel Hypothesis. *Global Change Biology*. **2003**, 9, 228-236.

Davidson, E. A.; Chorover, J.; Dail, D. B. A Mechanism of Abiotic Immobilization of Nitrate in Forest Ecosystems: the Ferrous Wheel Hypothesis. *Global Change Biology*. **2003**, 9, 228-236.

Dennis, L. Damage Cost of the Dan River Coal Ash Spill. *Environmental Pollution*. **2015**, 197, 55-61.

Dittmar, T.; Stubbins, A. Dissolved Organic Matter in Aquatic Systems. *Treatise of Geochemistry*. **2014**, 12, 125-156.

Dittmar, T.; Koch, B.; Hertkon, N.; Kattner, G. A Simple and Efficient Method for the Solid-Phase Extraction of Dissolved Organic Matter (SPE-DOM) from Seawater. *Limnology and Oceanography: Methods*. **2008**, 6, 230-235.

Ehlers, C. G. A.; Forrester, S. T.; Scherr, K. E.; Loibner, A. P.; Janik, L. J. Influence of the Nature of Soil Organic Matter on the Sorption Behavior of Pentadecane as Determined by PLS Analysis of Mid-Infrared DRIFT and Solid-State ^{13}C NMR spectra. *Environmental Pollution*. **2010**, 158, 285-291.

Environmental Protection Agency. National Recommended Water Quality Criteria – Aquatic Life Criteria Table. **2018**. https://www.epa.gov/wqc/national-recommended-water-quality- criteria-aquatic-life-criteria-table (accessed October 25, 2018).

Environmental Protection Agency. National Primary Drinking Water Regulations. **2018**. https://www.epa.gov/ground-water-and-drinking-water/national-primary-drinking-water- regulations (accessed October 25, 2018).

Environmental Protection Agency. EPA's Response to the Duke Energy Coal Ash Spill in Eden, NC. **2017**, https://www.epa.gov/dukeenergy-coalash (accessed October 25, 2018).

Environmental Protection Agency. History and Response Timeline. **2017**, https://www.epa.gov/dukeenergy-coalash/history-and-response-timeline (accessed October 25, 2018).

Environmental Protection Agency. SOP for In-Vitro Bioaccessibility for Lead and Arsenic in soil. **2017**. https://semspub.epa.gov/work/HQ/196750.pdf (accessed October 25, 2018).

Environmental Protection Agency. EPA Repsonse to Kingston TVA Coal Ash Spill. **2016**, https://www.epa.gov/tn/epa-response-kingston-tva-coal-ash-spill (accessed October 25, 2018).

Environmental Protection Agency. U.S. Environmental Protection Agency and Tennessee Valley Authority Kingston Coal Ash Release Site Project Completion Fact Sheet. **2014**, https://www.epa.gov/sites/production/files/201602/documents/projectcloseout_dec2014_ factsheet.pdf (accessed October 25, 2018).

Environmental Protection Agency. Surface Water Data - EPA Team 1 - July 2014. **2014**, https://www.epa.gov/sites/production/files/2014-08/documents/final-wmaps-2014-0710-surface-water-team1.pdf (accessed October 25, 2018).

Environmental Protection Agency. TVA Water Testing Results. **2009**, https://semspub.epa.gov/work/04/10644918.pdf (accessed October, 25, 2018).

Environmental Protection Agency. Bituminous and Subbituminous Coal Combustion: Final Section, 5th ed. *AP 42*. **1998**, 1, section 1.1.

Environmental Protection Agency. Method 1312: Synthetic Precipitation Leaching Procedure. **1994**, https://www.epa.gov/sites/production/files/2015-12/documents/1312.pdf (accessed Ocotber 25, 2018).

Environmental Protection Agency. Method 1311: Toxicity Characteristic Leaching Procedure. **1992**, https://www.epa.gov/sites/production/files/2015-12/documents/1311.pdf (accessed October 25, 2018).

Gagne, K.; Murphy, C.; Guerard, J. Method and Characterization of Permafrost Natural Organic Matter Leaching in Sub-Arctic Alaska. *Environmental Science and Technology*. In Preparation.

Georgakopoulos, A.; Filippidis, A.; Kassoli-Fournaraki, A. Leachability of Major and Trace Elements of Fly Ash from Ptolemais Power Station, Northern Greece. *Energy Sources*. **2002**, 24, 103-113.

Godelitsas, A.; Astilleros, J. M.; Hallam, K.; Harissopoulos, S.; Putnis, A. Interaction of Calcium Carbonates with Lead in Aqueous Solutions. *Environmental Science and Technology*. **2003**, 37 (15), 3351-3360.

Guerard, J. J.; Miller, P. L.; Trouts, T. D.; Chin, Y. The Role of Fulvic Acid Composition in the Photosensitized Degradation of Aquatic Contaminants. *Aquatic Sciences*. **2009**, 71, 160-169.

Hach Company. Phenolphthalein and Total Alkalinity: Method 8203. 9th ed.; Hach Company/Hach Lange GmbH: Loveland, CO, **2018**, https://www.hach.com/asset-get.download-en.jsa?code=56129 (accessed October 25, 2018).

Haque, S. E.; Tang, J.; Bounds, W. J.; Brudige, D. J.; Johannesson, K. H. Arsenic Geochemistry of the Great Dismal Swamp, Virginia, USA: Possible Organic Matter Controls. *Aquatic Geochemistry*. **2007**, 12, 289-308.

Hayes, M. H. B.; deAzevedo E. R.; Bonagamba, T. J. Characterisation of Black Carbon-Rich Samples by ^{13}C Solid-State Nuclear Magnetic Resonance. *The Science of Nature-Naturwissenschaften*. **2006**, 93 (9), 447-450.

Inyang, M. I.; Gao, B.; Yao, Y.; Xue, X.; Zimmerman, A.; Mosa, A.; Pullammanappallil, P.; Ok, Y. S.; Cao, X. A Review of Biochar as a low-cost Adsorbent for Aqueous Heavy Metal Removal. *Environmental Science and Technology*. **2015**, 46 (4), 406-433.

Iyer, R. The Surface Chemistry of Leaching Coal Fly Ash. *Journal of Hazardous Materials*. **2002**, B93, 321-329.

Izquierdo, M.; Querol, X. Leaching Behaviour of Elements from Coal Combustion Fly Ash: An Overview. *International Journal of Coal Geology*. **2012**, 94, 54-66.

Johnson, R. L.; Schmidt-Rohr, K. Quantitative Solid-State 13C NMR with Signal Enhancement by Multiple Cross Polarization. *Journal of Magnetic Resonance*. **2014**, 239, 44-49.

Johnson, K.; Purvis, G.; Lopez-Capel, E.; Peacock, C.; Gray, N.; Wagner, T.; März, C.; Bowen, L.; Ojeda, J.; Finlay, N.; Roberston, S.; Worrall, S.; and Greenwell, C. Towards a Mechanistic Understanding of Carbon Stabilization in Manganese Oxides. *Nature Communications*. **2015**, 6, Article #: 7628.

Kalbitz, K.; Wenrich, R. Mobilization of Heavy Metals and Arsenic in Polluted Wetland Soils and its Dependence on Dissolved Organic Matter. *Science of The Total Environment*. **1998**, 209, 27-39.

Kalyoncu, R. S. Coal Combustion Products. *United States Geological Survey Mineral Yearbook*. US Geological Survey: Washington, DC, **2001**; pp 113-127.

Khodadoust, A. P.; Naithani, P.; Theis, T. L.; Murarka, I. P. Leaching Characteristics of Arsenic from Aged Alkaline Coal Fly Ash Using Column and Sequential Batch Leaching. *Industrial and Engineering Chemistry Research*. **2011**, 50, 2204-2213.

Kim, A. G.; Hesbach, P. Comparison of Fly Ash Leaching Methods. *Fuel*. **2009**, 88, 926-937.
New Jersey Department of Environmental Protection. Development of Site-Specific Impact to Ground Water Soil Remediation Standards Using the Synthetic Precipitation Leaching Procedure. **2013**, https://www.nj.gov/dep/srp/guidance/rs/splp_guidance.pdf (accessed October 25, 2018).

Kimmell, T. A.; Williams, L. R.; Sorini, S. S. The RCRA Toxicity Characteristic Leaching Procedure (TCLP): A Concept for a New Method. *Federal Facilities Environmental Journal*. **2001**, 12, 7-24.

Knight, D. C.; Ramos, N. A.; Iceman, C. R.; Hayes, S. M. Is Unpaved Road Dust Near Fairbanks, Alaska a Health Concern? Examination of the Total and Bioaccessible Metal(loid)s. *Journal of Young Investigators*. **2017**, 33 (1), 8-18.

Koch, W. F.; Marinenko, G.; Paule, R. C. Development of a Standard Reference Material for Rainwater Analysis. *Journal of Research of the National Bureau of Standards*. **1986**, 91, 33-41.

Koukouzas, N.; Ketikidis, C.; Itskos, G. Heavy Metal Characterization of CFB-Derived Coal Fly Ash. *Fuel Processing Tehcnology*. **2011**, 92, 441-446.

Kutchko, B. G.; Kim, A. G. Fly Ash Characterization by SEM-EDS. *Fuel*. **2006**, 2537-2544.

Langmuir, D. *Aqueous Environmental Geochemistry*, 1st ed.; Prentice Hall: New Jersey, **1997**. Jegadeesan, G.; Al-Abed, S. R.; Pinto, P. X. Influence of Trace Metal Distribution on its Leachability from Coal Fly Ash. *Fuel*. **2007**, 87 (10-11), 1887-1893.

Maroto-Valer, M. M.; Lu, Z., Zhang, Y.; Tang, Z. Sorbents for CO2 Capture from High Carbon Fly Ashes. *PubMed*. **2008**, 28 (11), 2320-2328.

Mohebbi, M.; Rajabipour, F.; Scheetz, B. E. Reliability of Loss on Ignition (LOI) Test for Determining the Unburned Carbon Content in Fly Ash. *World of Coal Ash Conference*. Nashville, TN, **2015**. http://www.flyash.info/2015/141-mohebbi-2015.pdf (accessed October 25, 2018).

Mutschlecner, A.; Guerard, J. J.; and Harms, T. Regional and Intra-Annual Stability of Dissolved Organic Matter Composition and Biolability in High-Latitude Alaskan Rivers. *Limnology and Oceanography*. **2018**, 119, 17.

Neupane, G.; Donahoe, R. J. Leachability of Elements in Alkaline and Acidic Coal Fly Ash Samples During Batch and Column Leaching Tests. *Fuel*. **2013**, 104, 758-770.

O'Neil, C. Toxic Metal and Metalloid Liberation from Locally-Produced Coal Fly Ash Under Biological and Environmental Conditions. *Alaska Statewide High School Science Symposium*. **2015**. Unpublished.

Plumlee, G.; Morman, S.; Meeker, T.; Hagerman, P.; Wolf, R. The Environmental and Medical Geochemistry of Potentially Hazardous Materials Produced by Disasters. *Earth Systems and Environmental Sciences: Reference Module*. **2014**, 11, 257-304.

Pokrovsky, O. S.; Beuno, M.; Manasypov, R. M.; Shirokova, L. S.; Karlsson, J.; Amouroux, D. Dissolved Organic Matter Controls Seasonal and Spatial Selenium Concentration Variability in Thaw Lakes Across a Permafrost Gradient. *Environmental Science and Technology*. **2018**, 52, 10254-10262.

Polubesova, T.; Chefetz, B. DOM-Affected Transformation of Contaminants on Mineral Surfaces: A Review. *Environmental Science and Technology*. **2013**, 44, 223-254.

Poulin, B. A.; Ryan, J. A.; Aiken, G. R. Effects of Iron on Optical Properties of Dissolved Organic Matter. *Environmental Science and Technology*. **2014**, 48, 10098-10106.

Rivera, N.; Kaur, N.; Hesterberg, D.; Ward, C. R.; Austin, R. E.; Duckworth, O. W. Chemical Composition, Speciation, and Elemental Associations in Coal Fly Ash Samples Related to the Kingston Ash Spill. *Energy and Fuels*. **2015**, 29, 954-967.

Rodushkin, I.; Engström, E.; Baxter, D. C. Sources of Contamination and Remedial Strategies in the Multi-Elemental Trace Analysis Laboratory. *Analytical and Bioanalytical Chemistry*. **2010**, 396, 365-377.

Roy, W. R.; Griffin, R. A. Equilibria Relationships and Qualitative Modelling of Ash-Water Reactions. *Environmental Science and Technology*. **1984**, 18 (10), 739-742.

Rudnick, R. L.; Gao, S. Composition of the Continental Crust. *Treatise On Geochemistry*. **2003**, 3, 1-64.

Ruhl, L.; Vengosh, A.; Dwyer, G. S.; Hsu-Kim, H.; Deonarine, A. Environmental Impacts of the Coal Ash Spill in Kingston, Tennessee: An 18-Month Survey. *Environmental Science and Technology*. **2010**, 44, 9272-9278.

Ruhl, L.; Vengosh, A.; Dwyer, G. S.; Hsu-Kim, H.; Deonarine, A.; Bergin, M.; Kravchenko, J. Survey of the Potential Environmental and Health Impacts in the Immediate Aftermath of the Coal Ash Spill in Kingston, Tennessee. *Environmental Science and Technology*. **2009**, 43, 6326-6333.

Schaider, L. A.; Senn, D. B.; Brabander, D. J.; McCarthy, K. D.; Shine, J. P. Characterization of Zinc, Lead, and Cadmium in Mine Waste: Implications for Transport, Exposure, and Bioavailability. *Environmental Science and Technology*. **2007**, 41 (11), 4164-4171.

Schwarzenbach, R. P.; Gschwend, P. M.; Imboden, D. M. *Environmental Organic Chemistry*, 3rd ed.; John Wiley and Sons, Inc.: New Jersey, **2017**.

Schweinfurth, S. P. Coal-A Complex Natural Resource. *United States Geological Survey*. **2016**. https://pubs.usgs.gov/circ/c1143/html/text.html (accessed November 4, 2018).

Stevenson, F. J. Humus chemistry: Genesis, Composition, Reactions. *Environmental Science and Technology*. **1982**, 32, 2410-2416.

Strathmann, T. J. Redox Reactivity of Organically Complexed Iron(II) Species with Aquatic Contaminants. *Aquatic Redox Chemistry: ACS Symposium Series 1071*. **2011**, 283-313.

Temminghoff, E. J. M.; Van der Zee, S. E. A. T. M.; de Haan, F. A. M. Copper Mobility in a Copper-Contaminated Sandy Soil as Affected by pH and Solid and Dissolved Organic Matter. *Environmental Science and Technology*. **1997**, 31, 1109-1115.

U.S. Department of Transportation. User Guidelines for Waste and Byproduct Materials in Pavement Construction. **2016**, https://www.fhwa.dot.gov/publications/research/infrastructure/structures/97148/cfa53.cfm (accessed October, 25, 2018).

U.S. Energy Information Administration. Annual Coal Report 2016. **2017**, https://www.eia.gov/coal/annual/pdf/acr.pdf (accessed October 25, 2018).

U.S. Energy Information Administration. Subbituminous and bituminous coal dominate U.S. coal production. **2011**, https://www.eia.gov/todayinenergy/detail.php?id=2670 (accessed October 25, 2018).

United States Geological Survey. Humic Substances in the Suwannee River, Georgia: Interactions, Properties, and Proposed Structures. **1994**, https://pubs.usgs.gov/wsp/2373/report.pdf (accessed October 25, 2018).

Usibelli Coal Mine. Coal: Data Sheet. **2015**, http://www.usibelli.com/coal/data-sheet (accessed Ocotber 25, 2018).

Usibelli Coal Mine. UCM History: Key Dates. **2015**. http://www.usibelli.com/history/key-dates (accessed October 25, 2018).

Vassilev, S. V.; Vasilleva, C. G. Geochemistry of Coals, Coal Ashes and Combustion Wastes from Coal-Fired Power Stations. *Fuel Process Technology*. **1995**, 51, 19-45.

Waite, T.D.; Morel, F. M. M. Ligand Exchange and Fluorescence Quenching Studies of the Fulvic Acid-Iron Interaction: Effects of pH and Light. *Analaytica Chimica Acta*. **1984**, 162, 263-274.

Ward, C. [Personal communication]. **2018**.

Weng, L.; Temminghoff, E. J.M.; Lofts, S.; Tipping, E.; Van Riemsdijk, W. H. Complexation with Dissolved Organic Matter and Solubility Control of Heavy Metals in a Sandy Soil.

Wright, A. L.; Reddy, K. R. Dissolved Organic Matter in Wetlands. *University of Florida IFAS Extension*. **2009**, http://edis.ifas.ufl.edu/ss507 (accessed October 25, 2018).

Xiao, Y. H.; Sara-Aho, T.; Hartikainen, H.; Vahatalo, A. V. Contribution of Ferric Iron to Light Adsorption by Chromophoric Dissolved Organic Matter. *Limnology and Oceanography*. **2013**, 58, 653-662.

Yamashita, Y.; Jaffe, R. Characterizing the Interactions Between Trace Metals and Dissolved Organic Matter Using Excitation-Emission Matrix and Parallel Factor Analysis. *Environmental Science and Technology*. **2008**, 42, 7374-7379.

Żyrkowski, M. J. Characterisation of Fly-Ash Cenospheres from Coal-Fired Power Plant Unit. M.S. Thesis, Técnico Lisboa, Lisboa, Portugal, **2014**.